Investigating The Exergy Destruction Principle Applied to Precision Agriculture Using Thermal Remote Sensing

by

Heba AlZaben

A thesis
presented to the University of Waterloo
in fulfillment of the
thesis requirement for the degree of
Doctor of Philosophy
in
Mechanical and Mechatronics Engineering

Waterloo, Ontario, Canada, 2020

Examining Committee Membership

The following served on the examining committee for this thesis. The decision of the examining committee is by majority vote.

	Name	Title
External Examiner:	Jeffrey Luvall	Research Scientist at NASA
Supervisor:	Roydon Fraser	Professor
Co-Supervisor:	Clarence Swanton	Professor
Internal Member:	John Wen	Professor
Internal Member:	Kyle Daun	Professor
Internal-External Member:	Stephen Murphy	Professor

Author's Declaration

I hereby declare that I am the sole author of this thesis. This is a true copy of the thesis, including any required final revisions, as accepted by my examiners.

I understand that my thesis may be made electronically available to the public.

Abstract

Nitrogen is one of the most important yield-limiting nutrients for corn (Zea mays). In this research the exergy destruction principle (EDP) is applied as a theory to explain the expected inverse relationship between surface temperature and nitrogen stress. This is the first multi-year, greenhouse and field, study to systematically investigate thermal remote sensing for detecting nitrogen stress in field crops. Two hypotheses are developed as predicted by the EDP. It is hypothesized that agricultural crops experiencing greater *growth* and providing greater *yield* will have lower surface temperatures. The second hypothesis is that crops grown under optimum/higher rates of nitrogen will have lower surface temperatures compared to crops grown under *nitrogen stress* conditions. The two proposed hypotheses are tested under greenhouse and field conditions on corn plants at three different scales (i.e., leaf, canopy and over a plot area). Field studies were conducted during four summer seasons (2016, 2017, 2018 and 2019) on an established long-term field trial of corn yield response to varying rates of nitrogen. Greenhouse experiments were conducted at the University of Guelph and the University of Waterloo from Oct 2015 to May 2016 and from Apr 2019 to Feb 2020, respectively. Whorl temperatures were collected for continuous temperature measurements during the day and night cycle as a proxy for crop temperature to investigate if there is a variation in crop temperature with nitrogen stress. Canopy and leaf temperatures were collected using a high-resolution thermal camera, and an infrared hand-held point measurement gun, respectively. During the day, it is found that corn surface temperatures are lower for corn plants that received higher rates of nitrogen. A shallow but statistically significant negative slope is observed consistently with

increasing rates of nitrogen. An approximate 0.5-1°C average temperature variation between corn plants that experienced different levels of development (i.e., yield and leaf stage) due to nitrogen stress appears to be a reasonable magnitude given that ecosystems with a wider variation in development observed 5 °C average temperature variation. Surface temperature measurements, however, were highly variable. This variability is the result of many external and weather dependent variables that affect crop canopy temperature. Despite this variability, the exergy destruction principle (EDP) provides a theoretical background from which thermal remote sensing can be applied through surface temperature measurements to detect physiological stress in crop plants at early growth stages, before any visual indicators appear on plant surface. In addition, an average emissivity of 0.96 $\pm$0.006 for corn leaves over the 7.5-14 μm waveband is determined from multiple laboratory experiments measuring corn leaves spectral reflectance collected from corn plants grown under greenhouse and field conditions. This emissivity can be used as a reference value in future studies involving corn plants surface temperature measurements. Furthermore, it is concluded that whorl temperature measurement is not a good proxy of crop surface temperature and it can not be used to detect nitrogen stress. This research enhances the potential application of precision agriculture in the application of nutrients, herbicides, and pesticides to crop plants at an optimal time and location, which will subsequently increase production, reduce the cost of excessive input application, and reduce harmful impacts on the environment.

Acknowledgements

I would like to take this opportunity to first and foremost thank God for being my strength and guidance in the completion of this work. I thank him for the gift of life and health. Without him I would not have had the physical ability to complete this thesis.

I would like to express my deep and sincere gratitude to my supervisor, Prof. Roydon Fraser for the continuous and positive support during my PhD study. Also for his precious time that we spent on very long meetings especially in the past year. His patience, guidance and effort were very crucial to keep me focused and motivated. I attribute the level of my Doctoral degree to his encouragement, effort, and support. In addition, a huge thank you goes to my co-supervisor Prof. Clarence Swanton from the University of Guelph for his continuous support and help in arranging the experiments in the greenhouse and field and also for his guidance especially in the talk and type sessions for the research papers. Besides my advisors, I would also like to thank Prof. Kyle Daun and Prof. Michael Collins for helping me to setup and run the corn emissivity experiments in their labs many times at the University of Waterloo. In addition, I would like to thank Scott Liddycoat and Beverly Anne Raimbault staff members at the University of Waterloo for helping me to setup the greenhouse experiments and the soil nitrate testing, respectively. Finally, I would like to thank my committee members for reviewing and offering insightful comments to improve this research work.

A special thanks to my parents and two brothers for all the support and the amazing chances they gave me during my life and for always being there when I need their help. I would also like to thank my little daughter (Katya) that always put a smile on my face

even when she was away with my mom. I would not be where I am today and who I am today without their love, care, help and support. A special thanks goes also to my husband for being a great motivation to finish writing this thesis. Finally, I would like to thank my friends for their continuous support despite their busy life. You are all my inspiration, and I hope to make you all proud.

Dedication

I dedicate my dissertation work to my family. A special feeling of gratitude to my loving mom, dad, my brothers, my daughter, and my husband who have always supported me during my PhD. I hope that this accomplishment will make you all proud.

Table of Contents

List of Figures

List of Tables

Chapter 1

Introduction

1.1 Background

Crop stress is a serious problem that affects agricultural sector production [1, 2]. Minimizing crop stress is one of the major objectives for precision agriculture. Crop stress is caused by many abiotic and biotic variables such as: weed competition, insects, excess heat, water or nutrient deficiency [3, 4]. Crop plants are not passive to their environment, they are aggressive in responding to changes; a plant can rapidly change with a cue from its surroundings. Different methods have been used to detect crop stress such as: tissue analysis, transmittance, reflectance and florescence methods [5, 6, 7, 8]. All of these methods have limitations including: sensitivity to background noise, limited size or test area, and sensitivity to stress detection at early growth stages. Plant tissue analysis is considered a destructive and time consuming method [9, 10]. Alternatively, many non-destructive methods are used, such as leaf transmittance using a hand-held soil plant analyses devel-

opment (SPAD) chlorophyll meter, canopy spectral reflectance, and fluorescence methods [10, 11]. Studying leaf pigment reflectance as a crop stress indicator has proven to be less efficient for real time monitoring of plant photosynthesis and water status at plant level because the changes in leaf pigment concentrations are not rapid, therefore, it cannot be used as a direct indicator of plant physiological status [12]. In addition, the use of a non-destructive SPAD meter is found to be highly variable [13, 14] and is affected by leaf location, plant growth stage, solar irradiance and leaf water content [14, 15, 16]. The limitations of reflectance based methods include: sensitivity to high variations in sunlight and soil conditions, and the lack of sensitivity for stress detection at early growth stages [10, 17, 18, 19]. Chlorophyll fluorescence measurements are reported to be more accurate in nitrogen stress detection independently from soil background noise, leaf area, and biomass status [20, 21]. Hand-held versions such as Multiplex®, require a distance of approximately 10 cm between the sensor and the plant, therefore, limiting its usefulness at large field scales [10, 22]. As a result, accurately monitoring different inputs such as herbicides, pesticides, water and nitrogen fertilizer have attracted the attention of many researchers to enhance the precision agriculture by enabling the application of the right amount of inputs at the right time and place. The right amount represents a balance between yield production increase and harmful environmental impact decrease [23].

In this research, thermal remote sensing is proposed as a non-contact, non-destructive, rapid assessment capability, and easy to use method [24, 25, 26]. It has been used as a means of water stress detection in crop plants [27, 28, 29], which is based on the assumption that well-irrigated plants will transpire and cool crop surface temperature below the surrounding air temperature. Water stress reduces the transpiration rate [30] causing

plant canopies to reduce stomatal opening, thus increasing surface temperature above the surrounding air temperature. In addition, thermal remote sensing has been used to detect differences in canopy temperatures between nitrogen stressed and non-stressed plants [31, 32, 33]. Blad [31] observed a non-consistent relationship between nitrogen stress and canopy temperature across different years and locations in Canada. Carroll [32] studied the effect of varying nitrogen levels on leaf surface temperature for corn grown under different irrigation conditions. In his study, it is hypothesized that nitrogen deficient crops would have lower leaf temperatures due to lighter green leaf color and lower absorption of solar radiation. A non-significant difference was observed between nitrogen level and leaf surface temperature under two water stress conditions under greenhouse and field conditions despite the large differences observed in leaf chlorophyll concentration. Otherwise, a significant difference was observed between nitrogen rate and surface temperature associated with heat stress detection [34]. Ward [33] studied the effect of varying nitrogen and water stress levels on canopy temperature and found that both canopy temperature and canopy/air temperature difference provided an equally significant sensitivity to plant stress [34]. Akbari [35] in 1994 observed using a hand held infrared thermometer that field corn plants provided with higher levels of nitrogen were cooler compared to corn plants supplied with lower levels of nitrogen. This research work was motivated in part by these preliminary results of Akbari. Then in 1998 Luvall et al. [36] observed a strong correlation between canopy temperature and crop yield in results provided through personal communications providing additional motivation for this research work. There is no subsequent known investigation into the possible relationships between crop surface temperature and nitrogen stress or crop yield that were ever conducted until a first attempt by Lawrence [37]

in 2016. Lawrence's work focused on experiment development and formed the foundation for this thesis' experimental procedures.

Indications of crop stress is more quickly observed using thermal remote sensing data [27, 28, 29]. Observations of crop stress in the visible and near infrared (NIR) wavebands rely on a change in the spectral reflectance of various leaf chemical compounds and micro or macro nutrients, which take much longer time to manifest. One of the earliest indications of crop stress is reduced stomatal conductance and hence increased crop surface temperature [38].

In this research an approach is investigated for the purpose of precision agriculture to detect different types of crop stress including: weed competition, insects, water or nutrient deficiency as predicted by the exergy destruction principle (EDP). The main objective *is to determine if crop canopy temperature can be used as a measure of crop stress at early growth stages*. It is predicted that stressed plants are less able to maintain the same temperature differential between air and canopy compared to less stressed plants and this temperature differential can be used to estimate crop stress [27, 39]. In this study, two hypotheses are developed and tested under the greenhouse and field conditions on corn plants under variable nitrogen rates (e.g., high, medium, low and no nitrogen supply). The primary hypothesis states that agricultural crops experiencing greater growth and providing greater yield will have lower surface temperature. Given the primary hypothesis that crops experiencing greater growth and development will have lower surface temperature, and that crop stress affects growth and development [40, 41], the secondary hypothesis states that stressed plants will have higher temperatures compared to less stressed plants. This work is focused on nitrogen stress due to its strong correlation with yield [42], availability of the

experimental trials such as the Elora Research Station experiments, and due to the fact that it is relatively an easy variable to control under variable field conditions.

This research work can benefit the agricultural sector by maximizing the production (i.e., yield) and reducing the cost of input application to the soil including herbicides, pesticides and nutrients. Moreover, it can help farmers to control the level of nutrients being applied, which sequentially mitigates climate change, improves food products, and reduces contamination of the environment such as ground water pollution and greenhouse gas emissions, which became a serious problem.

1.2 Motivation

This research was motivated in part by some encouraging observations by Akbari [35] in 1994 who observed, using a hand held infrared thermometer, that field corn plants provided with higher levels of nitrogen were cooler. Akbari's limited observations are presented in his thesis but not in any Journal paper. Then in 1998 Luvall et al. [36] observed a strong correlation ($R^2 > 0.86$) between crop canopy temperature and crop yield providing further motivation for this research work. Since 1998, no subsequent known investigation into the possible relationships between crop surface temperature and nitrogen stress or crop yield were ever conducted until the attempt by Lawrence [37] in 2016. Lawrence's work focused on experiment development and formed the foundation for this thesis' experimental procedures.

This research investigates an approach to detect relative levels of crop stress in order to selectively apply nutrients under variable field conditions. Different methods have been

used to detect crop stress, as discussed in detail in chapter 2, which have different limitations including sensitivity to solar radiation variation, sensitivity to soil background noise, and study area limitation. In this research, thermal remote sensing is proposed through crop surface temperature measurements to detect crop stress at early growth stages for the purpose of precision agriculture as predicted by the exergy destruction principle discussed in more detail in chapter 3. The potential exists to take the advantage of the inverse correlation between surface temperature and crop stress for dynamically and precisely varying the amount of nutrients, herbicide, or pesticide by a spatial location in the field to sustainably increase the crop production while decreasing the input costs and reducing the environmental losses.

1.3 Research objective

The main objective in this research is *to determine if surface temperature can be used to predict crop stress at early growth stages.* More specifically is to determine if there is a correlation between surface temperature and nitrogen stress, and between surface temperature and yield as predicted by the exergy destruction principle (EDP). This main objective is accomplished by fulfilling the following research sub-objectives:

- To test and justify the two proposed hypotheses:

  Hypothesis #1: It is hypothesized that agricultural crops experiencing greater *growth* and providing greater *yield* will have lower surface temperature.

  Hypothesis #2: It is hypothesized that *stressed crop plants* will have higher surface temperatures compared to non-stressed plants.

- To conduct experiments on corn plants grown under different supplied nitrogen rates in greenhouse and field conditions in order to test the two proposed hypotheses and to investigate the difference in crop surface temperature and spectral emissivity among supplied nitrogen treatments.

- To investigate the difference in leaf thermal emissivity for the selected infrared (IR) waveband (7.5-14 μm) among nitrogen treatments.

- To investigate the potential use of thermal remote sensing in precision agriculture applications.

1.4 Thesis contributions

In this research two hypotheses were developed based on previous studies investigated the inverse correlation between ecosystem development and surface temperature on a large ecosystem scale. The two hypotheses (Section 1.3) were proposed and tested under greenhouse and field conditions, more specific research contributions are listed below:

- To determine the relationship between nitrogen stress and crop canopy temperature under controlled experiments as predicted by the exergy destruction principle.
- To determine the feasibility and effectiveness of the exergy destruction principle as a theory to identify crop stress for the purpose of precision agriculture.
- To investigate the spectral thermal emissivity difference among nitrogen treatments.
- To investigate the temperature temporal variation.

1.5 Thesis outline

This thesis is divided into seven chapters and five appendices, where Appendices B, C, and D describe the ongoing work that still needs to be further investigated in order to draw more solid conclusions. This thesis is structured as follows:

- Chapter 1 presents a research overview through the use of thermal remote sensing to detect crop stress as predicted by the exergy destruction principle (EDP).
- Chapter 2 provides an overview on different available methods that are used to detect crop stress with their corresponding limitations. This chapter starts with a definition of precision agriculture and crop stress in general.
- Chapter 3 provides information about the exergy destruction principle theory in general and more specifically applied to corn plants. In addition, it describes the two

research hypotheses from a previously known relationship between ecosystem development and surface temperature. It also discusses the energy and exergy balances for a corn plant system.

- Chapter 4 presents the overall temperature data acquisition and analysis including thermal image acquisition, processing and overall data analysis.

- Chapter 5 presents the greenhouse experiments conducted at the University of Guelph and the University of Waterloo.

- Chapter 6 presents the experiments conducted under field conditions at the Elora Research Station, ON, Canada over 4 years period and one experiment conducted at the Woodstock Research Station, ON under variable nitrogen and weed competition conditions. In addition, a discussion of the proposed sources of error in temperature measurements with suggested error minimization methods. The two chapters (5 and 6) cover materials, methods, results and discussions to make it easier to follow the research experiments conducted to test and justify the two research hypotheses under the greenhouse and field conditions, respectively.

- Chapter 7 presents the thesis summary, recommendations, future work and potential research applications.

- Appendix A discusses the canopy temperature sensitivity analysis including the different variables that affect crop temperature directly or indirectly with an example of nitrogen rate variation effect on surface temperature.

- Appendix B describes corn leaf thermal emissivity experiments conducted through spectral reflectance measurements. An average leaf thermal emissivity for corn plants over the 7.5- 14 μm waveband is proposed based on multiple laboratories experiments, which can be used as an emissivity user input reference value in a thermal camera.

- Appendix C presents the observations of whorl temperature measurements conducted using type t thermocouples attached to a temperature recording device under growth chamber conditions.

- Appendix D describes the observations from the field experiment conducted at the Elora Research Station in the summer of 2019 to measure canopy temperatures over a plot area scale using a high resolution thermal camera attached to a drone.

- Appendix E describes the order of magnitude estimates for energy equation terms discussed in Section 3.6.

- Appendix F describes the order of magnitude estimates for exergy terms compared to the incoming solar exergy discussed in Section 3.10.

Chapter 2

Precision agriculture and crop stress detection

Precision agriculture describes the agricultural information that is collected with regards to its geographical position, some examples of precision agriculture include: yield mapping, monitoring the application of herbicides, pesticides, and irrigation. The objective of this chapter is to identify precision agriculture, remote sensing, crop stress, and additionally discuss different methods that are used to detect various types of crop stress such as weed competition and water stress with a focus on nitrogen stress, and finally, summarize the advantages and disadvantages of different existing methods used to detect nitrogen stress.

2.1 Precision agriculture

Precision agriculture concerns optimizing farming practices to increase yield production and decrease the cost of different inputs such as nitrogen (N) fertilizer, pesticides and herbicides [43], which requires an efficient application of water and nutrients to crops at the right time and location. The technologies used in precision agriculture include geographic information system (GIS), global position system (GPS), remote sensing and variable rate technology [44]. Precision agriculture is defined as a crop management technique that enables the application of different tools and analysis to conduct accurate agricultural decisions to increase yield production [45] through applying the right rates of inputs in a controlled way to reduce harmful environmental impact[46]. As an example, one of the latest technologies in precision agriculture is the automated robotic field phenotyping platform[47]. The platform has a highly capable framework that enables to carry 500 kg payload in the camera bay. The platform includes a visible and thermal camera for water stress detection, and a chlorophyll fluorescence imagery (70 cm above the canopy level) to detect nitrogen stress. All the equipment is mounted on a field scanalyzer to scan the farm field on an average height of 2-3 m above the crop canopy and the soil compaction is reduced due to rail utilization [48]. The height of the platform is 6 m, but there are still some restrictions on farming equipment such as sowing and harvesting operations to minimize the soil compaction that could change data output. In this research, the potential exists to take advantage of the relationship between canopy temperature and crop stress for dynamically and precisely varying the amount of fertilizer, herbicide, or pesticide by spatial location in the field.

2.2 Remote sensing

Remote sensing has many applications in precision agriculture [49]. It is defined as the extraction of information without any physical contact with the object under study[50]. Remote sensing permits a large amount of data to be collected either by ground using hand held or tractor mounted sensors or by air using drones and satellite imagery. Remote sensing is divided into two types: active and passive remote sensing[51]; in active remote sensing, a signal is emitted by a satellite or aircraft and the reflected radiation from the object will be measured by the sensor. On the other hand, in passive remote sensing, the reflection of sunlight will be measured by the sensor.

There are four terms that are widely used in agricultural remote sensing including: spatial resolution, spectral resolution, radiometric resolution, and temporal resolution. In spatial resolution, the data are collected to identify crop physical features such as size and height, which help farmers to capture precise and high resolution images that will show specific areas in the field and give a small map-to-ground ratio, where the low resolution images can capture the entire field. In spectral resolution, the data are collected based on different wavelength bands. For example, to determine the normalized difference vegetation index (NDVI), the reflectance in the red visible and near-infrared bands need to be determined. The radiometric resolution involves different levels of brightness that can be detected by a sensor[52]. The radiometric resolution ranges from 8 to 14 bit and 256 levels of grey scale to 16,384 diverse shades of colors. The temporal resolution is the time period over which the data are collected. In longer time duration, more data will be collected compared to short period of time. Vegetation measurement requires fine spatial scale to

sufficiently resolve all of the plant components. Therefore, conducting analysis of satellite images can be inefficient due to its limited wavelength bands and low spatial resolution where the whole field can appear in 1 to 3 pixels of an image.

Thermal remote sensing is a branch of remote sensing that is concerned with surface emitted radiation, not surface reflected radiation in the thermal infrared (TIR) region of the electromagnetic spectrum [53]. Thermal remote sensing is non-destructive, non-contact, and easy to use method, which has many applications in detection, study, and management of vegetation fires and water stress detection [54, 27]. In this research, thermal remote sensing is used through surface temperature measurements to detect crop stress at early growth stages as predicted by the exergy destruction principle (EDP).

2.3 Introduction to crop stress

Crop stress is defined as any unfavorable condition or substance that affects the plant's metabolism, growth and development [55, 56]. Crop stress is also defined as an external factor that exerts a disadvantageous influence on crop plants [57]; it is a significant deviation from the optimal conditions for plant life [58]. Environmental stressors considerably affect crop production. Crop stressors are classified into biotic and abiotic stress factors. Abiotic stress includes the non-living components such as water, nutrients deficiency, radiation, and salinity [4]. Biotic stress includes the living components that cause disease or damage to plants including insects, bacteria and weed competition [59].

There are two types of nutrients that are essential for plant growth and development; micro and macro nutrients. The micro-nutrients includes: iron, copper, boron, zinc and

manganese, which are required by plants in small amounts for growth and development compared to macro-nutrients. The macro-nutrients are required in large amounts including: potassium (K), phosphorus (P), magnesium (Mg), calcium (Ca), and nitrogen (N), which are generally applied to increase crop production and quality [60]. Nutrient deficiency affects the plant's growth processes such as photosynthesis, respiration, transpiration and enzyme activities.

2.4 Crop stress detection methods

In this section crop stress detection methods will be discussed in general for different stress factors, but the focus will be on nitrogen stress because the two proposed research hypotheses were tested on corn plants grown under different supplied nitrogen rates. The traditional methods of crop stress detection are based on the observation of plant physical changes such as color or turgidity [61], with the risk of being detected after a critical damage point is reached. Other detection methods use the biochemical and biophysical techniques such as leaf water potential and stomatal conductance, which are time consuming, expensive and not efficient for large areas [61].

For nitrogen stress detection, tissue analysis was extensively used in the past to determine nitrogen status in plants, but it is a time consuming and destructive method that causes damage to plant tissues [62, 9]. Therefore, non-destructive methods were utilized for nitrogen stress detection such as canopy reflectance, leaf transmittance, and chlorophyll fluorescence [10]. The Soil-Plant Analyses Development (SPAD) chlorophyll meter is one of the most commonly used devices to detect nitrogen status in plants [63, 64], but

N content in leaves can be under or over estimated due to sieve effects [13] and light-dependent chloroplast movements [13], respectively. SPAD measurements fail to detect over-fertilized plants due to chlorophyll saturation [10]. The second method used to detect nitrogen stress is through investigating the electrical properties of plant tissues used to estimate water status and nutrient deficiency in crop plants [10]. Sap and electrical meters are used for crop nitrogen stress detection. Sap nitrate test is a potential tool for nitrogen fertilizer management and nitrogen losses reduction to groundwater [65], it is more rapid to distinguish between different nitrogen treatments as compared to SPAD chlorophyll meter measurements [66]. The limitations of sap nitrate testing include its destructive properties that causes damage to plant tissues and requires long sampling and processing times [67].

Leaf and canopy reflectance based methods are used through satellite data analysis and digital image processing [16] in the visible and near-infrared (NIR) spectrum to detect nitrogen status in crops. A spectral region of considerable interest called the “red edge" is the region between the red and NIR where the light is not absorbed by the plant[5, 68]. This method has some limitations including lack of sensitivity for nitrogen stress detection in early growth stages [17], sensitivity to sunlight variation and soil conditions [10, 69]. Chlorophyll fluorescence is another method that is used to detect nitrogen stress. This method allows for a high sensitive stress detection independently from soil background noise [20], leaf area, and biomass status [21]. Laser induced fluorescence (LIF) methods producing chlorophyll fluorescence emission are more applicable for use in large field areas compared to variable chlorophyll fluorescence measurements [69, 21]. The LIF method measures the chlorophyll fluorescence induced by red laser light at 0.63 μm. The ratio of the 0.69 and 0.73 μm fluorescence wavelengths highly correlates with N content [70].

The potential of fluorescence imaging in crops is limited for field phenotyping applications [71] due to power requirements that are widely utilized for disease monitoring in trees and plants[72]. Most of the methods used for nitrogen stress crop detection are dependent on chlorophyll content. Therefore, these methods fail to detect over-fertilized crops due to chlorophyll saturation [10]. Table 2.1 summarize the most commonly used methods to detect nitrogen stress in crop plants.

Furthermore, reflectance and chlorophyll fluorescence methods are used to detect water stress in crop plants. The chlorophyll content in leaves decreases with crop stress [73], thereby changing the proportion of light-absorbing pigments, leading to a reduction in the overall light absorption [74], therefore, the spectral reflectance pattern changes with stress in the visible (e.g., red, green and blue) and NIR regions of the electromagnetic spectrum. The strong absorption features of water in the shortwave infrared (SWIR) have been used as a water stress assessment tool [61]. Leaf chlorophyll fluorescence is measured using portable optical system and compact chlorophyll fluorescence meter, which depend on photosynthesis process. Chlorophyll fluorescence may occur before any physical signs appears on a plant surface, where crop stress can be detected before any damage to plants appears []. The photochemical efficiency of Photosystem II (PSII) is estimated by Fv/Fm, which is the ratio of variable fluorescence (Fv) to maximum fluorescence (Fm), where non-stressed plants have a ratio (Fv/Fm) of 0.8. This ratio is used as an indicator of water stress. Thermal remote sensing has been used since the 1960s as an indicator of water stress, which depends on the sensitivity of leaf temperature to evaporation rate and hence to stomatal opening [75, 76, 77, 78]. Well-irrigated crop plants will transpire and cool leaf temperature below the surrounding air temperature. Otherwise, water stressed plants

will exhibit lower transpiration rates and leaves will become warmer than the surrounding air due to the absorbed solar radiation[39]. Crop water stress index (CWSI) is widely used as an indicator of water stress in crops [28, 79]. Different researchers were interested in studying the effect of heat stress on crop development and yield [80, 81]. Canopy temperature is used as an indicator to reduce the error associated in estimating heat stress effect on crop yield. As an example, in Siebert et al. [80], two infrared radiometers were fixed to a carrier at 0.5 m above the canopy and air temperature was measured using a band-gap temperature sensor at 2.5 m above the canopy. Air temperature measurements were verified using a weather station at 2 m height. It was found that increasing the soil moisture through proper irrigation decreases heat and water stress[39].

Another example of crop stress that affects plant growth and development is weed stress. Weeds will take most of the nutrients from a plant, and thus, leave a plant nutrient deficient. Different methods are used to detect weed stress including spectral reflectance measurements though aerial imagery, which has different limitations such as the absence of quantitative data, high cost of color-infrared film, the image processing is time consuming, and requiring variable interpretation [82]. Therefore, hyperspectral sensors are used to detect different invasive weeds. As an example, Lass and his colleagues [83] utilized a 2 m spatial resolution sensor with 12 nm spectral resolution to identify weed locations in Swan Valley near Idaho Falls, ID and the spectral reflectance was measured between 415 and 953 nm.

Therefore, due to the previously mentioned limitations of different methods that are used to detect nitrogen stress before any visual indicators appear on a plant surface, this research proposes the use of *thermal remote sensing through surface temperature measure-*

ments to detect crop stress as predicted by the exergy destruction principle.

Table 2.1: A summary of nitrogen stress detection methods

Method	**Advantages**	**Disadvantages**
Tissue analysis	No nitrate reduction, Good estimation of chlorophyll content [10]	Destructive, Requires a lot of sampling and processing time [10]
Electrical meters	High correlation between N status and plant sap nitrate concentration, Quick response as compared to optical measurements [66], Direct measurement of plant electrical properties	Invasive, Does not measure total N in plant tissue, Destructive, Sensitive to other ions [10]
SPAD meter	Portable device, High correlation between N status and leaf chlorophyll content [10]	Require many measurement points, Dependent on leaf location [70], Incapable of detecting over-fertilized crops due to chlorophyll saturation, Low sensitivity of detecting N stress at early growth stages [10], N can be underestimated due to sieve effects, N can be overestimated due to chloroplast movements [13]
Reflectance	Applicable for large field areas, High correlation between N status and leaf chlorophyll [5]	Delayed sensitivity, Need for specific chlorophyll, Requires biomass or cover fraction [21], lack of sensitivity for nitrogen detection in early growth stages [17], Affected by background noise, affected by leaf area index (LAI) variability [84]
Florescence	Highly sensitive to plant N status independently from soil interference, leaf area, and biomass status [10, 21], Suitable for early growth stages and widely spaced crops [20]	Power requirement is a limiting factor for field phenotyping applications [71], Challenge of laser induced fluorescence (LIF) measurements is to separate the apparent reflectance spectra from LIF in leaves [85]

2.5 Surface temperature measurements

Many prior studies have noted the importance of measuring canopy and leaf temperatures to monitor different physiological processes in crop plants such as evapotranspiration [27, 86]. Monitoring the reduction in canopy temperature relative to air temperature is considered as an indicator of transpiration effectiveness in leaf cooling under different environmental conditions [75]. Ecosystem surface temperature has also been proposed to capture a spatial integrated response of thermal buffer capacity [87].

More closely related to the research conducted in this thesis is the work of Holbo and Luvall [88], and Quattrochi and Luvall [89]. Holbo and Luvall [88] investigated the frequency distribution of a spatial surface temperature variation in forests. Quattrochi and Luvall [89] introduced three different indicators for ecosystem development including beta index, thermal response number (TRN) and the ratio of net radiation to incident radiation due to energy partition variation for different land covers. Beta index is utilized to assess an ecosystem spatial temperature variability. TRN is the ratio between the total net radiation to the difference in surface temperature over a time period as described in Equation 2.1. It resents the amount of energy required to change one unit of temperature [90]. It is used to distinguish between different land covers, for example, it can distinguish an artificial tropical rain forest from a primary tropical forest [90].

$$TRN = \frac{\sum_{t_1}^{t_2} R_n \Delta t}{\Delta T} \tag{2.1}$$

where R_n is the total net radiation of the site over the time period between flights t_1

and t_2 in Jm^{-2}, Δt is the time between flights, ΔT is the change in the mean surface temperature (spatially averaged) [91].

In 1989, Luvall et al. [91] used a thermal infrared multispectral scanner (TIMS) to measure the thermal infrared radiation emitted (8.2 - 12.2 μm) over a 400 m transact with different land covers in Costa Rica. It was noticed that different land covers have a significant difference in surface temperature, and that more developed ecosystems (e.g., a tree island) has lower surface temperature compared to less developed ecosystem (e.g., a pasture). Further experiments [92] using the TIMS were conducted in the H.J. Andrews Experimental Forest using a similar setup with an aircraft [91]. The aircraft flew over a 1000 m transact measuring the surface temperature of different land covers (e.g., a narrow road, a wide road, an edge of a forest, a pond, a shelter wood, and a trail). Two flights were conducted over the transact, one around noon and the other post sunset. In addition, as an example of a possible precision agriculture application for crop surface temperature measurements, Rickman et al., [36] observed that crop surface temperature months prior harvest (June) is highly correlated with crop yield at harvest (September).

Chapter 3

The exergy destruction principle

Given the overall objective of this research is to investigate the application of the exergy destruction principle applied to precision agriculture, it is necessary to first identify exergy as a thermodynamic pseudo property with its corresponding properties, and thus provide the foundation for a thermodynamic link of an ecosystem to its environment [37], by following the exergy destruction principle via discussion. This chapter discusses the formulation of the two proposed research hypotheses, the exergy destruction principle applied to crop plants, the exergy and energy balances for crop plant system, and finally the importance of black box consideration for a crop plant system, which is a complex open thermodynamic system that exchanges energy and matter with the surroundings. This chapter will help to answer the question of how exergy can be utilized to monitor health and development of a crop system over time.

3.1 Exergy

Energy has both magnitude and quality. The quality of energy is defined as exergy. Exergy is the maximum useful to the dead-state work for a system moving from a given state to a state of equilibrium with its surroundings [93]. Exergy is the maximum useful work involved in many process [94]. Exergy is the available energy to be used [95] and it is also the driving force for most biological and thermodynamic processes on earth [37]. The incoming solar exergy is very large in magnitude compared to the amount of exergy being consumed. Wall and Gong [96] mentioned that the sun maintains 13,000 times more exergy compared to what human beings consume. The solar exergy that reaches the earth surface sustains life on earth, which is related to the photosynthesis process of crop plants that converts solar energy into chemical energy. Exergy is context sensitive because it is formulated with respect to a reference environment; that is, if the environment temperature and pressure change then the exergy changes [97, 98]. In addition, it can be used as a decision making tool in many engineering and non-engineering applications, it is used as optimization tool in power plant design and operation specifications [99]. Exergy is also used in life cycle assessment [100, 101], resource accounting [98, 102, 103] and as an ecological indicator of ecosystem development, complexity and integrity [104, 105, 106, 107, 108]. Exergy is not conserved, unlike energy, it can be destroyed but not created [98, 109].

3.2 The exergy destruction principle (EDP) overview

In non-equilibrium thermodynamics for complex systems such as ecosystems, exergy can be used to measure the distance with which the system and the environment are kept away from the equilibrium state due to an external applied gradient such as temperature or pressure. Therefore, it requires that both system and environment are well defined. Exergy is a useful tool to study non-equilibrium thermodynamic systems; the larger the value of exergy the more out of equilibrium the situation is[110]. The exergy destruction principle applied to non-equilibrium thermodynamics as discussed by James Kay [110] states that "A system exposed to a flow of exergy from outside will be displaced from the equilibrium state. The response of the system will be to re-organize itself so as to degrade exergy as thoroughly as circumstances permit, thus limiting the degree to which the system is moved from thermodynamic equilibrium. Furthermore, the further the system is moved away from the equilibrium state, the larger the number of organizational (i.e. dissipational) opportunities will become accessible to it and consequently, the more efficient it will be at exergy destruction". The further the system is moved away from the equilibrium state the more exergy will be destroyed and the system produces more entropy, thus more work will be required to maintain the system in its non-equilibrium state [104]. This principle is also called the restated Second Law of thermodynamics to include non-equilibrium systems [111] where it is no longer a simple statement about entropy production, but states that systems can be moved away from the equilibrium state by an external applied gradient. As the external applied gradient increases, the system's resistance of being moved away from the equilibrium state increases. Destroyed exergy ($\dot{X}_{destroyed}$) or work lost in the

system is directly related to entropy production ($\dot{S}_P$) through the environment reference temperature ($T_\circ$) as described in the Guoy-Stodola theorem Equation 3.1 for a fixed environment temperature [112, 113].

$$\dot{X}_{destroyed} = T_\circ \times \dot{S}_P \tag{3.1}$$

Exergy destruction and energy degradation are related directly. Energy degradation occurs when the quality of energy decreases. It is not referred as reduction in quality (energy dissipation), because the concept of energy quality involves not only entropy, where entropy production is often referred to as dissipation [114, 115], but also environment consideration. The exergy destruction principle existing hypothesis states that ecosystem development is associated with maximizing the amount of work available for the purpose of structural organization, function, and survival [104, 105, 110]. Ecosystems are complex, non-equilibrium self-organizing dissipative thermodynamic systems [116] that are open to energy and mass flows, which maintain their organization and structure through continuous energy dissipation [117, 118, 91, 119]. As ecosystems develop and mature they increase their total energy dissipation and the use of available exergy, thus, they develop more complex structures with greater diversity [116, 110]. Ecosystems develop in a way that enables them to survive in the environment while increasing their ability to extract solar exergy from the incoming solar radiation and use it to maintain their organization. The more exergy the ecosystem captures the greater its ability to support organizational processes. Thus, ecosystem development is measurable in terms of its use of exergy rate[116, 110]. Furthermore, the organization and complexity of an ecosystem increases with increase in

ecosystem development [104, 105, 120].

Ecosystem development has been measured using surface temperature [119, 118, 91, 104, 105]. Schneider and Kay [104, 105] suggested that more developed ecosystems are more efficient at energy dissipation compared to less developed ecosystems, thus their surface temperature is lower compared to less developed ecosystems. Luvall and Holbo [91] used a thermal infrared multispectral scanner over a 400 m transact with different land covers. A significant difference of 10°C was observed in surface temperature among varying land covers. The more developed the land cover, the cooler its surface temperature and the more degraded its emitted energy.

More developed ecosystems have larger biomass to accommodate the increase in complexity, which is correlated with development. Lin et al [121] showed a theoretical relationship between entropy production/exergy destruction, and forest canopy temperature. Entropy production and exergy destruction are directly related through the Gouy-Stodola theorem [97]. However, the exergy destruction gives an additional information about the system's environment [122]. It was found that entropy production increases with ecosystem development [121, 123], thus surface temperature decreases. It has been found that more developed ecosystems tend to utilize more exergy from incoming solar radiation enabling them to be more efficient in exergy destruction compared to less developed ecosystems [35, 110, 37].

3.3 The two research hypotheses

The exergy destruction principle states that ecosystems will develop in a way to maximize the amount of work available to them for the purpose of structural organization, function and survival [104, 105, 110, 34], which systematically increase their ability to destroy the incoming exergy [122, 89]. Ecosystem organization increases with ecosystem development [105, 124]. Therefore, maximizing organization corresponds to maximizing development. A general trend in ecological science exists where more developed ecosystems have larger biomass to accommodate the increase in complexity that is correlated with development [105]. Crop development is also referred to as growth, which for agriculture crops generally correlates with yield [125, 126]. Furthermore, it was shown that the maximum work available to an ecosystem exists for the lowest surface temperature given within a local ecosystem or crop. Therefore, given the existing hypothesis as predicted by the EDP [110] that ecosystem organization can be measured using surface temperature, and that increasing ecosystem organization corresponds to increasing ecosystem development, growth and yield. The primary hypothesis for this research is as follows:

HYPOTHESIS #1: It is hypothesized that agricultural crops experiencing greater growth and providing greater yield will have lower surface temperature.

In addition, it is known that crop stress affects plant growth and development [40, 41]. When a crop plant is stressed with an external stress factor (e.g., excess heat, pests, or nutrient deficiency), its functions and processes (e.g., stomatal conductance, transpiration, respiration, and photosynthesis) are all affected. Highly stressed crops experience less growth and development. Therefore, given Hypothesis #1 that a crop experiencing greater

growth and development will have lower surface temperature, and given that crop stress affects growth and development, a corollary hypothesis exists as follows:

HYPOTHESIS #2: It is hypothesized that stressed crop plants will have higher surface temperature compared to non-stressed plants.

The two proposed hypotheses have been tested under greenhouse and field conditions. In order to be able to use the two hypotheses for the purpose of precision agriculture, crop plants need to be compared under the same environmental conditions.

3.4 The exergy destruction principle applied to corn plants

This research applies the exergy destruction principle as a theory to explain the inverse correlation between crop canopy temperature and crop stress. During the day, the amount of exergy input (from solar radiation) is much greater than exergy output. Given that solar exergy available to an ecosystem is maximized when surface temperatures are the lowest, and based on the exergy balance for an ecosystem [104, 105, 37] that ecosystem's development and organization can be measured using surface temperature [116, 110], as more developed and complex ecosystems have lower surface temperatures compared to less developed ecosystems as predicted by the exergy destruction principle (EDP).

More developed ecosystems have larger biomass to accommodate the increase in complexity and development [125, 126]. The exergy destruction principle considers crop development directly, not crop stress, hence any link between stress and development requires

an additional hypothesis. It is well known that stress affects crop growth and development thereby altering the ability of the plant to exchange energy and matter with its surroundings [86, 127]. Given this link, it is hypothesized that corn plants supplied with optimum/higher rates of nitrogen will have lower surface temperatures compared to corn grown under nitrogen stressed conditions.

Crop plant systems develop so as to degrade exergy more effectively, as revealed by surface temperature measurements predicted from the exergy destruction principle [110, 120, 104, 105, 110, 116]. The EDP states that ecosystem development is associated with maximizing the amount of work available for the purpose of structural organization, function, and survival [104, 105, 116, 110]. It is expected that more developed ecosystems degrade the exergy content of the energy they capture more completely compared to less developed ecosystem. It is found that the energy dissipation across an ecosystem is a function of the temperature difference between the captured solar energy and the energy emitted by the ecosystem. As an example, "if a group of ecosystems are bathed by the same amount of incoming solar energy, the most mature ecosystem would have the coldest surface temperature," that is re-radiate at the lowest energy level [116]. Besides the temperature expectation, a key point was made by Kay et al.[116] in the EDP expectation is that there will be the "same amount of incoming solar energy". This condition recognizes that for quantitative surface temperature comparisons between ecosystems their environment must be the same. Therefore, in order to quantitatively compare different nitrogen supplied corn plants using the EDP, the environment must be the same for all the crops being compared as exemplified by the experiment that was conducted by Allen and Norman [128] in a wind tunnel for the same type of crop under two different environments (high and low wind

speed conditions) [116], where it is found that crops in a wind tunnel is cooler at wind speeds that it had acclimated and crops are able to use exergy more efficiently in conditions that are less stressful. The inverse correlation between ecosystem development and surface temperature in plant communities was discussed by Allen and Norman [129, 130]. It is suggested that surface temperature of plant communities tend to increase when they move from their normal living conditions. It is found that plant communities are cooler and degrade more exergy when they are in their normal living conditions, which they are adapted to.

For the purpose of this research, the relevant plant system is not an individual corn plant, but a crop of plants. With the crop plant system selected, the nitrogen rate is an internal variable for the black box assumption, the same as a difference in DNA/genes between corn hybrids as reported in Feng, et al.[131], which is an internal variable to the crop plant system. The key to the crop of plants viewpoint is that what should be measured is the crop canopy temperature. Figure 3.1 represents the system boundaries for corn crops grown under field and greenhouse conditions. In this research corn plants grown under greenhouse conditions were used as a proxy for corn plants grown under field conditions. The greenhouse environment can be used as a proxy for the field environment because of the (i) similarities in air temperature, humidity, and incoming solar radiation, and (ii) the nitrogen rate supplied can be similarly controlled in the field and the greenhouse.

(a) Field

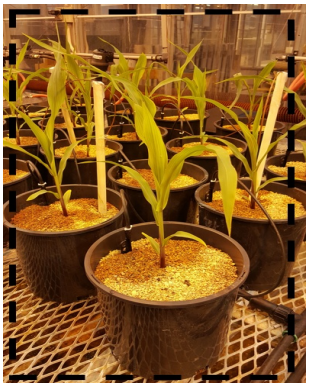

(b) Greenhouse

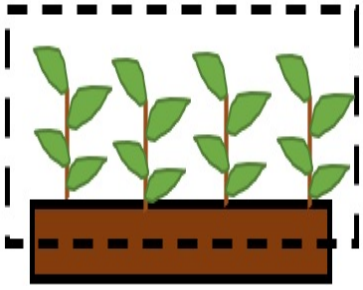

(c) Crop system boundary surrounds multiple plants, roots, encompassing soil and surrounding air

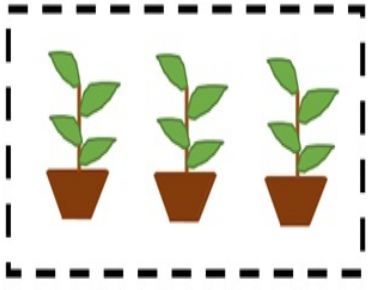

(d) Proxy of crop system boundary surrounds multiple plants, roots, pots, encompassing soil and surrounding air in the greenhouse

Figure 3.1: The selected system boundary for corn plants grown in the field and greenhouse.

As a summary, the exergy destruction across a crop plant system is a function of the difference between incoming and outgoing exergy flows. The exergy of incoming solar energy and the exergy of outgoing surface radiation emissions dominates the exergy flows [122], assuming that a crop plant system is bathed by the same amount of incoming solar energy (i.e., under the same field conditions/same environment), then less stressed crops, which are more developed and mature, will re-radiate its energy at the lowest exergy level, thus will have the lowest surface temperature compared to stressed crops.

3.5 Physiological, ecological and black-box crop plant system consideration

This research, does not attempt to explain "the physiological and ecological" considerations because the applied exergy destruction principle (EDP) excludes the internal system functions, and is only concerned with energy and mass flows at the system boundary. The EDP is a "black-box" theory, therefore, understanding the internal mechanisms is not part of applying EDP thermodynamics once a system boundary has been identified.

From an engineering thermodynamic perspective, a crop plant system can be modelled as a black-box with input and output energy and mass flows [37, 34], therefore, all physiological processes and mechanisms used to raise or lower surface temperature such as stomatal conductance, transpiration, respiration and photosynthesis are implicitly taken into account and are not directly considered in this work. Furthermore, the nutrition supply is considered within the black-box definition of a crop plant system and is not part of a different environment.

In the greenhouse experiments, leaf surface temperature has been measured as a proxy for canopy temperature because this work investigates early growth stages (e.g., V2 stage) where canopy temperature (defined as the spatial average temperature of a grouping of multiple plants + soil) would be dominated by soil temperature. This significantly increases the noise-to-signal ratio when studying the temperature differences between stressed and less stressed crop plants. In contrast, surface temperature differences predicted by the exergy destruction principle (EDP) should be dominated by development/growth which is

concentrated in early growth stage corn plants. In order to compare crop plants supplied with different nitrogen rates using the EDP, the environment needs to be the same between systems. That is, by looking at canopy temperature, nitrogen availability is internalized inside a "black-box", thus enabling an EDP consistent comparison between crops supplied with different nitrogen rates.

3.6 Energy analysis applied to a corn plant system

The exergy destruction principle depends upon a black-box concept of engineering thermodynamics to asses how surface temperature can be used to characterized the energy flow of a crop plant system. A crop plant system is a complex open thermodynamic system that exchanges energy and matter with its surroundings. From an engineering thermodynamic perspective, a crop plant system can be modeled as a thermodynamic black-box with input, output energy, and mass flows [37] as presented in Figure 3.2. For the mass flow, the input water is through the soil and rain/watering, the output water is through evaporation from the soil and evapotranspiration from the corn plant surface, the fertilizer input is through discrete applications at specified times, and the mass outputs as a biomass. Air flowing in and out of the system will carry with it water vapor in the form of humidity, while the soil may conduct thermal energy into or out of the system. When solar radiation reaches the crop surface it will be absorbed or reflected. The background radiation comes from radiation emitted from particles and molecules in the atmosphere and surrounding objects.

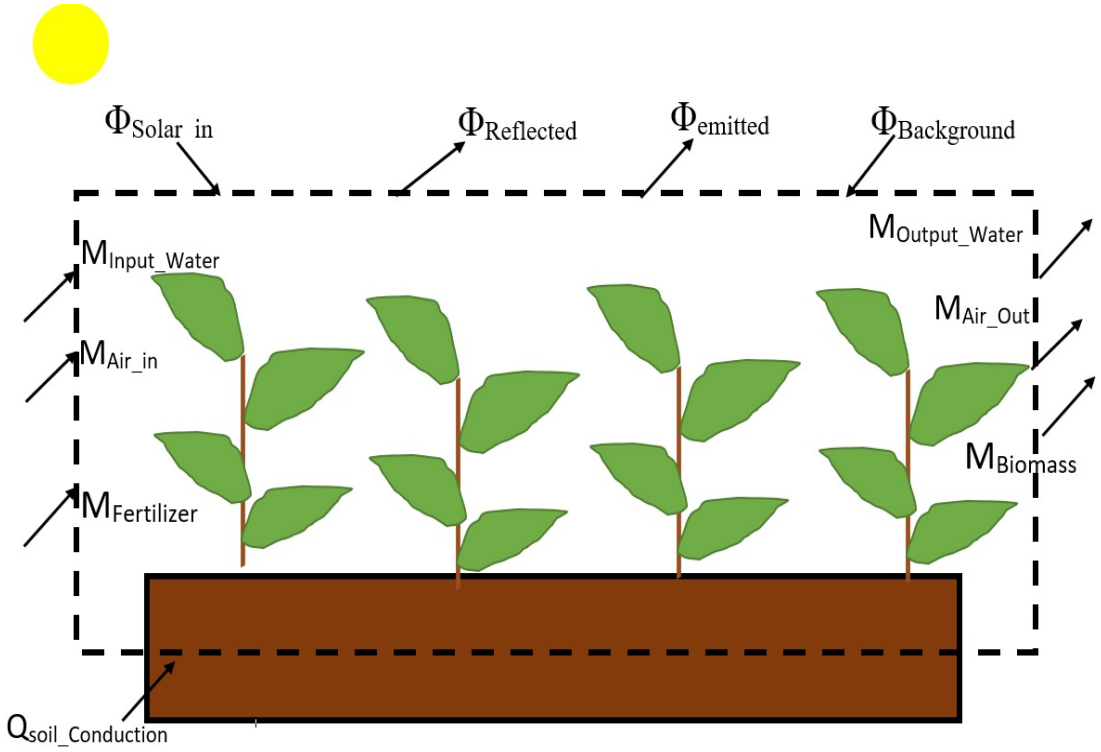

Figure 3.2: Mass and energy flows of a crop plant system

Referring to Figure 3.2, the First Law of energy balance for a crop plant system is described by Equation 3.2.

$$\frac{dE}{dt} = \dot{E}_{in} - \dot{E}_{out} \tag{3.2}$$

=(net radiation input)+(net thermal energy input)+(work transfer input)
+(net transport energy input)

$$\frac{dE}{dt} = \dot{\phi}_{Solar\_in} + \dot{\phi}_{Background} + \dot{Q}_{Soil\_conduction} + \int PdV + \dot{m}_{input}(u + \frac{v^2}{2} + gz)_{input} - \dot{\phi}_{Reflected} - \dot{\phi}_{Emitted} - \dot{m}_{output}(u + \frac{v^2}{2} + gz)_{output} \quad (3.3)$$

where $\frac{dE}{dt}$ is the change of system energy with respect to time, $\dot{E}_{in}$ is the input energy to the system and $\dot{E}_{out}$ is the output energy from the system. $\dot{\phi}_{Solar\_in}$ is input solar radiation, $\dot{\phi}_{Reflected}$ is reflected radiation, $\dot{\phi}_{Background}$ is background radiation, $\dot{\phi}_{Emitted}$ is emitted radiation, $\dot{Q}_{soil\_Conduction}$ is soil conduction heat flux, P is the atmospheric pressure, V is the system volume, u is the specific internal energy of the system, v is the velocity of the system in m/s, g is gravitational acceleration in m/s^2, z is the system height in m, and $\dot{m}_{input(output)}$ is the mass flow input (output) to (from) a crop plant system.

Now, not all the terms presented in Equation 3.3 are significant for thermal remote sensing measurements collected during mid-day conditions. A summary of the energy components and their significance is presented in Table 3.1.

Table 3.1: The energy components for a crop plant system

Energy term	**Approximate energy term magnitude compared to radiation inputs/outputs**	**Assumptions/comments**
Work term $\int PdV$	Zero. By definition, there is no change in the system volume (V), therefore $dV = 0$ at all times, and the work transfer is necessarily always zero.	Since $dV = 0$, pressure changes are irrelevant.
Air and water transport via expansion	Negligible, for more details please refer to Appendix E.	Assumptions: Ideal gas; minimum 4 hours of heating from coolest to warmest plant temperature (i.e, morning to afternoon).
Fertilizer input	zero	Fertilizer is only added once or periodically, it is not added the day of temperature measurements so the "rate" of energy flow from fertilizer on the day of measurement is zero. Note, Equation 3.3 is a rate equation.
Water transport due to transpiration	Order of 102 W/m^2,for more details please refer to Appendix E.	Assumptions: T_{soil_in}=10 °C, $T_{leaf\_surface}$=25 °C, $T_{Environment\_temperature}$=30 °C, output mass flow of 3.7 $L/day/m^2$ [132]. The energy water output is 102 W.
Biomass output	Zero.	It is zero before harvest, when temperature measurements were conducted.

Continued on next page

Table 3.1 – The energy components for a crop plant system

Energy term	**Approximate energy term magnitude compared to radiation inputs/outputs**	**Assumptions/comments**
Soil conduction heat flux	Small	Assumptions: 1 m depth below ground; area of 1 m^2 change in temperature between soil surface of 35 °C and soil temperature of 10 °C; thermal conductivity (k) of the soil= 0.5 W/mK [133]; conduction heat flux $=Q_{soilflux} = \frac{-k\Delta T}{Distance}$=$-0.5W/mK \times 1m^2 \times (10-35)/1m$=7.5 W/m^2.
Emitted radiation	[400-700 W/m^2]	Observed during mid-day measurements.
Reflected radiation	[80-120 W/m^2]	Observed during mid-day measurements.
Background radiation (5-30 μm)	[350-500 W/m^2]	Observed during mid-day measurements.
Incoming solar radiation (0.3-2μm)	[400-900 W/m^2]	Observed during mid-day measurements.

From Table 3.1, it is concluded that the radiation terms (i.e., incoming solar, reflected, background, and emitted radiation) and the transpiration term, in Equation 3.3, dominate the other energy balance terms.

3.7 Remote sensing energy balance

The energy balance given by Equation 3.3, is expressed in another form by many researchers in the environmental and remote sensing fields of study [121, 134, 135, 91, 136, 137]. The alternate form of Equation 3.3 is given by Equation 3.4, which will be referred to as the remote sensing energy balance equation that include both radiation and non-radiation energy terms. Equation 3.4 is provided to permit the current research work to be related to previous remote sensing work. The remote sensing energy balance equation is given by

$$R_n = H + LE + G \tag{3.4}$$

where R_n, is the net input radiation energy defined below in Equation 3.5. It is the amount of radiation energy transformed at the surface into non-radiative processes [91]. H is the sensible heat flux to the air, LE is the latent heat flux to the water through evotranspiration, and G is the energy flux into the soil. The sensible heat flux (H) in Equation 3.3 is calculated through air mass flow multiplied by specific heat and enthalpy $(\dot{E}_{out}) = \dot{m}_{out} C_p \Delta T$ (Appendix E), the latent heat flux (LE) is calculated as described in section E.3 for the net water transpiration through mass flow output [138], and the energy flux into the soil (G) is the same calculation as $\dot{Q}_{Soil\_conduction}$ described in Table 3.1. The net input radiation energy is given by Equation 3.5.

$$R_n = (\phi_{Solar\_in} + \phi_{Background}) - (\phi_{Reflected} + \phi_{Emitted}) \tag{3.5}$$

where, from Section 3.6, ϕ_{Solar_in} is the input solar radiation, $\phi_{Reflected}$ is the reflected

radiation, $\phi_{Background}$ is the background radiation, $\phi_{Emitted}$ is the emitted radiation.

It is also common for the remote sensing energy balance Equation 3.4 to split the electromagnetic radiation spectrum into shortwave and longwave radiation [91, 118]. This split is performed because solar energy dominates the shortwave electromagnetic spectrum while the longwave corresponds to thermal radiation. For example, [139] classifies shortwave radiation to be in the 0.3-3 μm range, and longwave radiation to be in the 3-50 μm range. The alternative form of Equation 3.5 is given as follows [121]

$$R_n = K_{in} - K_{out} + L_{in} - L_{out} \tag{3.6}$$

where, K_{in} is the incoming shortwave radiation, K_{out} is the outgoing shortwave radiation, L_{in} is the incoming longwave radiation, and L_{out} is the outgoing longwave radiation.

3.8 The Second Law of thermodynamics: Entropy analysis

Based on the Second Law of thermodynamics, the rate of entropy change in the system equals the rate of entropy input minus the rate of entropy output plus the rate of entropy produced due to system irreversibilites as described by the following equations [121]:

$$\frac{dS}{dt} = \dot{S}_{in} - \dot{S}_{out} + \dot{S}_p \tag{3.7}$$

$$\frac{dS}{dt} = (\frac{\dot{Q}_{in}}{T_0} - \frac{\dot{Q}_{out}}{T_0}) + (\dot{m}_{in}S_{in} - \dot{m}_{out}S_{out}) + \dot{S}_p \tag{3.8}$$

where $\frac{dS}{dt}$ is the change of entropy in the system, $\dot{S}_{in}$, $\dot{S}_{out}$ is the input and output entropy to the system, and $\dot{S}_p$ is the entropy produced in the system. $\dot{Q}_{in}$, $\dot{Q}_{out}$ is the input and output rate of heat transfer to the system in $W.m^{-2}$, and T_0 is the environment reference temperature.

There is a controversy between researchers on how to calculate the entropy flow associated with radiation energy transfer [93, 140, 141, 142]. The controversy concerns whether or not there is a $\frac{4}{3}$ term. The entropy S of an equilibrium photon gas at a black-body temperature T is related to its internal energy E as follows [143]

$$S = \frac{4}{3}\frac{E}{T} \tag{3.9}$$

Solar radiation is a non-equilibrium beam radiation, the related photon gas is no longer isotropic, and the validity of a relationship between energy and entropy flux similar to Equation 3.9 is no longer clear. Some researchers argued that the radiative entropy flux is related to energy or heat flux in the same manner as in the case of heat conduction (i.e., $S = \frac{Q}{T}$) [143, 144, 145, 146]. Other researchers suggest that the Planck factor of $\frac{4}{3}$ need to be maintained even in that case (i.e., $S = \frac{4}{3}\frac{Q}{T}$) [145, 147, 140]. Wright [140] showed that using the $\frac{Q}{T_0}$ relationship for calculating the entropy of thermal radiation heat transfer may have a significant error and cause the irreversibility of the energy conversion device to be underestimated. When solar radiation energy crosses a system boundary it can carry more entropy across a boundary than conduction or convection entropy flux for the same energy flux and source temperature [93, 141, 148, 149, 147]. A detailed analysis of the radiation entropy is presented in the work of Kabelac [150, 145]. In contrast, there is a group of researchers who do not include the $\frac{4}{3}$ term in the entropy flow associated with radiation energy transfer calculation [121, 151, 142]. As an example, Ozawa et al., [151], argued that the $\frac{4}{3}$ term is only needed if the emitted radiation is absorbed, scattered, and changed into isotropic radiation in thermodynamic equilibrium, which is not the case for solar radiation

as it is a non-equilibrium beam of radiation lying in a specific solid angle and possessing the brightness temperature of T_{Sun}. In order to calculate the exergy associated with solar radiation for this work, the three models proposed by Kabelac [150, 145] were considered. Each model involved different assumptions, but all three models incorporated the $\frac{4}{3}$ term. It is beyond the scope of this work to resolve the $\frac{4}{3}$ controversy, however, it will be noted that regardless the controversy surface temperature would still be a characterizing factor for the solar exergy. In addition, from previous thermal remote sensing and solar exergy work [145, 93, 148, 152, 153] that assumed the existence of the $\frac{4}{3}$ term, so this research is consistent with previous work. The model of Kabelac [150, 145] that is used in this work to explain the relationship between solar exergy and surface temperature is identified in the next section (Section 3.9).

The rate of entropy flux ($\dot{S}_{flux}$) as used by many researchers in the field of environmental, thermal, and remote sensing studies which is calculated as follows [121]

$$\dot{S}_{flux} = \dot{S}_{\phi_{Solar\_in}} - \dot{S}_{\phi_{Reflected}} + \dot{S}_{\phi_{Background}} - \dot{S}_{\phi_{Emitted}} - \dot{S}_H - \dot{S}_{LE} - \dot{S}_G \tag{3.10}$$

where $\dot{S}_{\phi_{Solar\_in}}$ is the entropy associated with input solar radiation, $\dot{S}_{\phi_{Reflected}}$ is the entropy associated with reflected radiation, $\dot{S}_{\phi_{Background}}$ is the entropy associated with background radiation, $\dot{S}_{\phi_{Emitted}}$ is the entropy associated with emitted radiation, $\dot{S}_H$ is the entropy associated with sensible heat transfer,$\dot{S}_{LE}$ is the entropy associated with latent heat transfer and $\dot{S}_G$ is the entropy associated with soil heat flux. In addition, there is no need to include the $\frac{4}{3}$ factor for radiation heat transfer terms described in Equation 3.10 because

it expresses the radiation terms in general entropy terms (e.g., $\dot{S}_{\phi_{Solar\_in}}$), which does not specify how to calculate the radiation entropy terms. Finally, the entropy balance equation in this section is only presented for completeness of the thermodynamic balances; it is not directly used in this research.

For this work, the interest is in exergy, not entropy, though both are related to each other as follows: For a fixed environment temperature, the rate of exergy destruction ($\dot{X}_d$) is proportional to the rate of entropy production through the Guoy-Stodola theorem [97] which is discussed in Section 3.2 from this chapter.

3.9 Solar exergy

Solar exergy (or low entropy radiation input to the earth relative to earth's output radiation) is essential to the existence of life on earth as it provides the potential to organize earth's elements into more complex structures. This organization potential is primarily captured via photosynthesis process that converts solar energy into chemical energy for the purpose of sustaining life on earth [104]. When solar radiation that carries high exergy content comes into contact with the earth, it will interact with matter and biological processes, and start to degrade [37].

Now, there are three different models that exist to calculate the solar exergy, each of which is based on different assumptions [150, 145, 93]. The three models are discussed next, and only one model is identified for the use in this work.

Model 1: Zero entropy production, finite area

Model 1 assumes zero entropy production and a finite system area. Kabelac [150] then derives the following equation for the solar radiation exergy, where the surface temperature ($T_{Surface}$) is equal to the environment reference temperature (T_0), so that there is no entropy production for radiation energy transfer from the surface to the background:

$$X_{Solar,Model1} = \Phi_{T,Solar}(1 - \frac{4}{3}\frac{T_{Surface}}{T_{Solar}} + \frac{1}{3}\frac{T^4_{Surface}}{T^4_{Solar}}) \tag{3.11}$$

where $X_{Solar,Model1}$ is the solar exergy for model 1, $\phi_{T,Solar}$ is the solar radiation energy which is calculated using Stefan-Boltzmann law, $T_{Surface}$ is the surface temperature in K, and T_{Solar} is the sun temperature in K. This model is chosen for the solar exergy discussion in this work because real systems are of finite area, and the zero entropy production assumption is consistent with the zero entropy production Carnot engine assumption.

Model 2: Non-zero entropy production, finite area

Model 2 assumes a non-zero entropy production and a finite area system. Although, Model 1 is used in this work for solar exergy calculation, the second model is provided to reveal that it also yields to an increasing exergy with decreasing surface temperature. The resulting solar exergy equation derived by Kabelac [145] is as follows:

$$X_{Solar,Model2} = \Phi_{T,Solar}(1 - \frac{T^4{}_{Optimum}}{T^4{}_{Solar}})(1 - \frac{T_o}{T_{Optimum}}) = \Phi_{T,Net}(1 - \frac{T_o}{T_{Optimum}}) \tag{3.12}$$

where $T_{Optimum}$ is the surface temperature, that is defined by the solution to the following Equation 3.13

$$4T^5{}_{Surface} - 3T_0T^4{}_{Surface} - T^4{}_{Solar}T_0 = 0 \tag{3.13}$$

The other variables described in Equation 3.12 are also found in Equation 3.11. Where $X_{Solar,Model2}$ is the solar exergy for model 2, $\phi_{T,Solar}$ is the solar radiation energy, and T_0 is the environment temperature.

Model 3: Zero entropy production, infinite area

Model 3 assumes zero entropy production and infinite area system. In addition, the third model is provided to reveal that it also yields to an increasing exergy with decreasing surface temperature. The resulting solar exergy equation is as follows:

$$X_{Solar,Model3} = \Phi_{T,Net}(1 - \frac{T_o}{T_{Solar}}) \tag{3.14}$$

For this model it is assumed that surface temperature will approach solar temperature. Since infinite area is assumed for this model, Kabelac [150] pointed out that model 3 can be used as the maximum theoretical efficiency of solar radiation, but not for solar exergy calculation.

3.10 Exergy analysis applied to a corn plant system

Now applying the black-box concept to exergy analysis using the same approach discussed previously and presented in Figure 3.2. It shows that surface temperature can be used as a sole measurement for the net exergy available to a crop plant system. From the general balance equation, the rate of exergy change in the system equals the rate of exergy input minus the rate of exergy output minus the rate of exergy destroyed.

$$\frac{dX}{dt} = \dot{X}_{in} - \dot{X}_{out} - \dot{X}_{des} \tag{3.15}$$

Now, Equation 3.15 can be expanded as in the case of the energy flows into and out of the crop plant system, shown in Figure 3.2, as follows

$$\frac{dX}{dt} = \dot{X}_{Solar\_in} + \dot{X}_{Background} + \left(1 - \frac{T_0}{T_{Soil}}\right)\dot{Q}_{Soil\_conduction} + \int PdV + \dot{m}_{in}\psi_{in} - \dot{X}_{Reflected} - \dot{X}_{Emitted} - \dot{m}_{out}\psi_{out} - \dot{X}_{des} \tag{3.16}$$

where $\frac{dX}{dt}$ is the change of system exergy with respect to time, $\dot{X}_{in}$ is the input exergy to the system, $\dot{X}_{out}$ is the output exergy from the system, and $\dot{X}_{des}$ is the exergy destroyed due to reversibilities. $\dot{X}_{Solar\_in}$ is the exergy associated with input solar radiation, $\dot{X}_{Reflected}$ is the exergy associated with reflected radiation, $\dot{X}_{Background}$ is the exergy associated with background radiation, $\dot{X}_{Emitted}$ is the exergy associated with emitted radiation. $\left(1 - \frac{T_0}{T_{Soil}}\right)\dot{Q}_{Soil\_conduction}$ is the exergy associated with soil heat conduction where

$\dot{Q}_{soil\_Conduction}$ is soil conduction heat flux, T_0 is the reference environment temperature and T_{Soil} is the soil temperature. P is the atmospheric pressure, V is the system volume, and $\dot{m}_{in(out)}$ is the mass flow input (output) to (from) a crop plant system. $\psi_{in(out)}$ is the specific exergy input (output) to (from) a crop plant system.

The specific flow exergy is calculated as follows [93, 97]

$$\psi_{in\ (out)} = (h_{in\ (out)} - h_0) - T_0(S_{in\ (out)} - S_0) \tag{3.17}$$

where h_{in}, h_{out} are the specific input and output enthalpy in and out of the system measured in kJ/kg. T_0 is the reference environment temperature, which is assumed of 30 °C for exergy calculations. S_{in}, S_{output} are the input and output entropy in and out of the system measured in $kJ/kg.K$. h_0, S_0 are the enthalpy and entropy at the reference environment temperature.

Now, not all the terms presented in Equation 3.16 are significant for thermal remote sensing measurements collected during mid-day conditions. A summary of the exergy components with their corresponding significance is presented in Table 3.2.

Table 3.2: The exergy components for a crop plant system

Exergy term	**Approximate exergy term magnitude compared to incoming solar exergy**	**Assumptions/comments**
Work term $\int PdV$	Zero. By definition, there is no change in the system volume (V), therefore $dV = 0$ at all times, and the work transfer, or exergy transfer, is always zero.	Since $dV = 0$, pressure changes are irrelevant.
Air and water transport via expansion	Negligible,for more details please refer to Appendix F.	Assumptions: $T_{Environment\_reference}$=30°$C$, and T_{Soil_input}=10°C.
Fertilizer input	Negligible,for more details please refer to Appendix F.	Assumptions: Average solar plus background flux in Elora Ontario is 1325 $W/m2$, 1 m^2 surface area, 3 months growing season, 10 hours sunlight per day, and the fertilizer is Ammonium Nitrate.
Water transport due to transpiration	Small order of 0.012% of the solar exergy, for more details please refer to Appendix F.	Assumptions: $T_{Environment\_reference}$=30°$C$, and T_{Soil_input}=10°C.
Biomass output	Zero	It is zero before harvest, when temperature measurements were conducted.

Continued on next page

Table 3.2 –The exergy components for a crop plant system

Exergy term	**Approximate exergy term magnitude compared to incoming solar exergy**	**Assumptions/comments**
Soil conduction heat flux	Small order of 0.088% of the solar exergy.	The exergy associated with soil heat transfer is given by $\dot{X}_{soil\_conduction} = \left(1 - \frac{T_0}{T_{soil}}\right) \times \dot{Q}_{soil\_conduction}$, where T_{Soil}=10 °C (283 K) and T_0=30 °C (303 K), so the Soil conduction exergy is 0.53 W. Then, the relative soil heat transfer exergy ($\frac{X_{Soil\_conduction}}{\bar{X}_{solar}}$) is $\frac{X_{Soil\_conduction}}{\bar{X}_{Solar}} = \frac{0.53\ W/m^2}{604\ W/m^2} = 8.77 \times 10^{-4} \approx 0$
Background radiation	The background exergy ratio ($\frac{X_{Background}}{\phi_{Background}}$) is 0.0163 and 1.17×10^{-3} for $T_{Background}$=1°C and 18°C, respectively, for more details please refer to Appendix F.	The exergy contribution from background radiation for assumed background temperatures of $T_{Background}$=1°C and 18°C is small (1.2 %) to negligible (0.0828 %), respectively.
Solar radiation	The solar exergy ($\frac{X_{Solar}}{\phi_{Solar}}$) is 0.931, for more details please refer to Appendix F.	by definition, the relative exergy is 1 $\frac{X_{solar}}{X_{solar}} \left(\frac{kJ_{solarexergy}}{kJ_{solarexergy}}\right)$

As a conclusion from Table 3.2, the solar exergy dominates all other exergy input and output terms, with most of the solar exergy being destroyed or used by the system in one manner or another. For example, for photosynthesis and transpiration processes.

Furthermore, from Equation 3.11 the solar exergy can only be changed by changing the surface temperature assuming a constant solar temperature.

Chapter 4

Overall data analysis

This chapter discusses the overall thermal image acquisition and processing that were conducted during temperature data collection under the greenhouse and field conditions.

4.1 Thermal image acquisition

Temperature measurements were initiated at the three leaf tip stage (V1 stage) of corn seedling growth using a high resolution research thermal camera (T620 series, FLIR Systems, Canada). The thermal camera specifications are described in Table 4.1. The camera has a precision of 0.1°C. FLIR T620 thermal camera has an uncooled microbolometer that is very sensitive to temperature drift of the camera housing. The thermal camera was powered on for at least 10 minutes prior to thermal image acquisition to minimize the effect of vignetting [154]. In addition, a manual non-uniformity correction (NUC) was performed before taking every image to reduce the fixed pattern noise [155, 156] and maintain a good

image quality. The manual NUC involves the selection of a calibration function to force the thermal detector to re-calibrate the location of every pixel in the image.

Table 4.1: FLIR T620 thermal camera specifications

Resolution	640 × 480
Accuracy	±2°C
Temperature range	-40–650°C
Spectral range	7.5 –14 μm
Field of view	25° × 19°

The canopy thermal images were consistently taken perpendicular to the plant surface (in the nadir direction). The thermal camera calculated surface temperature from the incident thermal radiation on the thermal detector. Different parameters are required as a user input to the camera including surface emissivity, distance from the camera lens to the object, reflected apparent temperature, atmospheric temperature, and relative humidity, prior to thermal image acquisition to obtain an accurate estimate of surface temperature. The thermal camera corrected the object temperature for atmospheric and sky background variation.

Prior to crop temperature measurements, an average emissivity of 0.96 was determined under multiple laboratory experiments, based over the 7.5 to 14 μm waveband for corn leaf thermal emissivity measurements. The reflected apparent temperature was measured each time prior to surface temperature measurements using the procedures described in the thermal camera's user manual and the guidance of ISO18434–1. The thermal camera was calibrated using a blackbody source (463 Cavity black-body, Infrared Industries, Hayward, USA). The difference between the thermal camera measurement and the standard reference temperature was no more than the accuracy of the thermal camera (± 2°C). The thermal

camera was calibrated before every measurement using the Programmable NUC set in the camera. The reflected apparent temperature was estimated using a crumpled aluminum foil to reduce the specular reflection. The aluminum foil was placed in front of a canopy surface and the emissivity was set to 1 [157, 158].

4.2 Processing of thermal images

Surface temperatures were extracted from the collected thermal images using FLIR ResearchIR (FLIR Systems Inc., Boston, MA, version 3.5) and Matlab R2018B (Mathworks Inc., Natick, MA) software. Multiple thermal images were collected to calculate the error in temperature measurement. The pixel value in each thermal image represents the temperature of that pixel since a radiometric thermal camera was used. Thermal images were converted to 'csv' file format using ResearchIR, then imported into Matlab. In addition, thermal images were analyzed in Matlab using the image processing toolbox. The average and maximum temperatures were extracted from each selected region of interest (ROI).

In the greenhouse experiments leaf surface temperatures were collected from the middle two rows to avoid any border effects from the neighboring corn plants and due to size limitations the ROI over a leaf surface was defined as a rectangular box of approximately 2000 pixels (0.03 m^2), when calculating leaf surface temperature. Furthermore, the ROI was defined over multiple plants as a rectangular box with 100,000 pixels(1.5 m^2), for canopy temperature measurements. The raw data, metadata of a thermal image, and calibration constants were obtained using an Exiftool program (Harvey, 2016). The maximum standard deviation of temperature values measured within the selected ROIs was 2 °C at

the canopy level and 7 °C at soil level.

The measured leaf and canopy temperatures are affected by the variations in soil and air temperatures. Air temperature was measured using a type T thermocouple attached to a corn plant at 2 m height, where the tip of the thermocouple was exposed and measured the surrounding air canopy temperature. Soil temperatures were extracted from thermal images. The following two equations 4.1, and 4.2 represent the corrections that were applied to leaf and canopy temperatures for the temperature data collected from the field experiments.

$$T_{\mathrm{cc}} = T_{\mathrm{c}} - T_{\mathrm{air}} + T_{\mathrm{air\_mean}} \tag{4.1}$$

$$T_{\mathrm{cc}} = T_{\mathrm{c}} - T_{\mathrm{soil}} + T_{\mathrm{soil\_mean}} \tag{4.2}$$

Where T_{cc} is the corrected canopy temperature, T_{c} is the measured canopy temperature (°C), T_{air} is the air temperature (°C), T_{air_mean} is the mean air temperature (°C), T_{soil} is the soil temperature (°C), and T_{soil_mean} is the soil mean temperature (°C).

Thermal images were obtained in a standard JPEG format. The images were decomposed into: raw data, metadata, FLIR logo and calibration constants for a specific camera model using the Exiftool program (Harvey, 2016). The raw images in TIFF format were processed in Matlab software and converted to radiometric temperatures using equations described in Di Felice et al. [159] after applying the thermal camera calibration constants obtained from the thermal image metadata.

4.3 Data analysis

Statistical data analysis was conducted on the collected leaf, whorl and canopy temperatures using Matlab software. Analysis of variance (ANOVA) and F-test were applied to investigate the significance of the difference in surface temperature across nitrogen treatments. Statistical significance was determined using a p-value < 0.05. In addition, linear regression models were used to test the relationship between temperature, nitrogen rate and yield. Pearson correlation analysis was used to investigate the relationship between yield and surface temperature. A paired t-test with an equal variance assumption was used to compare temperatures associated with the two nitrogen extremes (i.e., high and low nitrogen supply). Tukey's post hoc test was used to investigate which specific treatment means (compared with each other) are different. T testing at $P < 0.05$ was used to test the significance of the difference between low and high nitrogen treatments across the experiments. Finally, the errors in the trends are explained in more detail in Appendix A.

Chapter 5

Greenhouse experiments

5.1 Introduction

Nitrogen (N) is one of the most important yield-limiting nutrients for corn (Zea mays) production worldwide [160]. The exergy destruction principle was refined to provide two directly related research hypotheses. The first hypothesis describes the relationship between plant development and crop temperature, and the second hypothesis suggests an inverse correlation between crop stress and crop surface temperature. The first hypothesis states that agricultural crops experiencing greater growth and providing greater yield will have lower surface temperature and the second hypothesis states that stressed crop plants will have higher surface temperature compared to less stressed plants. The two hypotheses were tested under the greenhouse conditions. Different experiments were conducted at the University of Guelph and University of Waterloo greenhouses under different set conditions from the period of Oct 2015 to Apr 2016 and Apr 2019 to Feb 2020, respectively.

For the experiments conducted at the University of Guelph greenhouse, the main objective was to investigate whether there is a difference in surface temperature between corn plants supplied with three different rates of nitrogen (high, medium and low rates) in the first two experiments, and for the last two experiments the main objective was to determine whether surface temperature decreases with supplying N rate for nitrogen stressed corn plants. For the other set of experiments conducted in the University of Waterloo greenhouse the main objective was to investigate whether there is a difference in leaf thermal emissivity for corn plants supplied with four nitrogen rates (high, medium, low and no nitrogen supply).

5.1.1 The environment consideration for greenhouse experiments

Greenhouse leaf surface temperatures were measured and averaged as a proxy for canopy temperature that inherently averaged over multiple plants and soil. The first part of establishing this proxy between leaf surface temperature and crop temperature was to report averages of leaf temperatures taken from multiple greenhouse plants (e.g. 20 plants per each N treatment), measured at the same time ($\pm$30 minutes), from within the same greenhouse. In order to complete the establishment of leaf surface temperature measurements as a proxy for crop surface temperature measurements, consideration must be given to soil temperature impacts; specifically, (i) potted soil versus field soil impacts, and to (ii) why soil temperatures were not averaged with leaf temperatures.

(i) Potted soil versus field soil temperature: leaf surface temperature measurements were conducted around solar noon. At this time of the day soil temperature at depth,

(e.g., 15 cm) would be lower than the surrounding environment air temperature, whether the plants were growing in the greenhouse or in the field. However, there will be a difference in field versus greenhouse soil temperature for a given air temperature due to the lower thermal mass of the greenhouse soil, and due to a larger contact surface area with air. More specifically, the greenhouse soil for a given air temperature at noon hour will be warmer than the field soil. The first reason because the greenhouse does not experience as cold temperatures as the soil in the field, assuming that night temperatures are cooler than the day, therefore, the greenhouse soil is warmer in the morning. The second reason because the thermal mass in the greenhouse soil per plant is less so it will warm up more quickly for a given energy input.

(ii) Potted soil versus field soil canopy temperature impact: With the greenhouse soil being warmer than the field soil, there are two possible scenarios for the plant temperature, either the greenhouse plants will be at the same temperature as the field plants or they will be warmer. Near the noon hour greenhouse plant temperatures may be the same as field plant temperatures if the plant biology manages, possibly through changes in transpiration rate, to operate in a manner that stabilizes plant temperature for the possible purpose of optimizing photosynthesis. Or, near the noon hour greenhouse plant temperatures may be shifted to a higher temperature due to the warmer greenhouse soil. Either way, there is no known plant cooling mechanism that would change the relative order of plant temperature. Therefore, any difference between greenhouse and field soil temperatures is not expected to change the trend for plant surface temperature measurements, and therefore, the potted plants and soil surface temperatures in the greenhouse can be used as a proxy for field crop surface temperatures.

(iii) The exclusion of soil temperature from average crop temperature: whether the crop temperature measurements are conducted in the greenhouse or the field, it is desirable to only measure plant surface temperature to improve the signal-to-noise ratio. For early growth crops, canopy temperature (defined as the spatial average temperature of a grouping of multiple plants + soil) would be dominated by soil temperature. However, the temperature differences between stressed and less stressed corn plants, predicted by the EDP, should be dominated by development/growth, with the soil acting as a noisy and large background signal that would swamp early growth averages of canopy temperature, thus possibly obscuring in the noise EDP predicted temperature trends between stressed and non-stressed crops. Therefore, for signal-to-noise purposes it was desirable to exclude soil surface temperatures when measuring crop average temperature, provided this exclusion would affect observed temperature trends between stressed and non-stressed crops. If one considers that the non-stressed plants are predicted to develop and grow faster, the effect is to shade more soil more quickly which can only serve to magnify the expected EDP cooling trend, not to change the trend. Soil surface temperature measurements confirmed this expected cooling. Therefore, it was concluded that soil surface temperature could be excluded from the measured canopy temperature, with only averages of plant surface temperatures being used in order to improve signal-to-noise ratio. As a corollary, in the late growth stage, the soil becomes obscured, therefore only measuring plant surface temperature for late growth stages (assuming a typical corn crop planting that seeks to optimize the land use). Lastly plant surface temperatures that cannot be viewed from the top are, by definition, not part of the crop canopy temperature.

Finally, given that the greenhouse is a good proxy for the field environment, and given

to improve the signal-to-noise ratio, only plant surface temperatures need be averaged. In addition, given that leaf surface temperatures are a good proxy for plant surface temperatures when viewed from the top, it was concluded that averages of leaf surface temperatures from multiple potted plants serves as a good proxy for field crop canopy temperatures.

5.2 University of Guelph experiments

5.2.1 Materials and methods

Greenhouse experiments were conducted at the University of Guelph, Ontario, Canada from Oct 2015 to Apr 2016. A single seed of corn hybrid Pioneer P8906AM was planted at a depth of 2 cm in the center of 180 individual pots (22.86 cm width, 22.54 cm depth) of 5.62 Liters in volume. It took the corn seed approximately one week to emerge. The soil mixture was Turface ®MVP (Profile Products LLC Buffalo Grove, USA). The pots were placed onto six separate benches, each bench consisting of 30 pots (i.e., 6 pots wide $\times$ 5 pots in length) as presented in Figure 5.1. The experimental design was a randomized complete block.Two benches were assigned as independent individual replicates per nitrogen treatment. The pots had holes at the bottom to allow for adequate drainage.

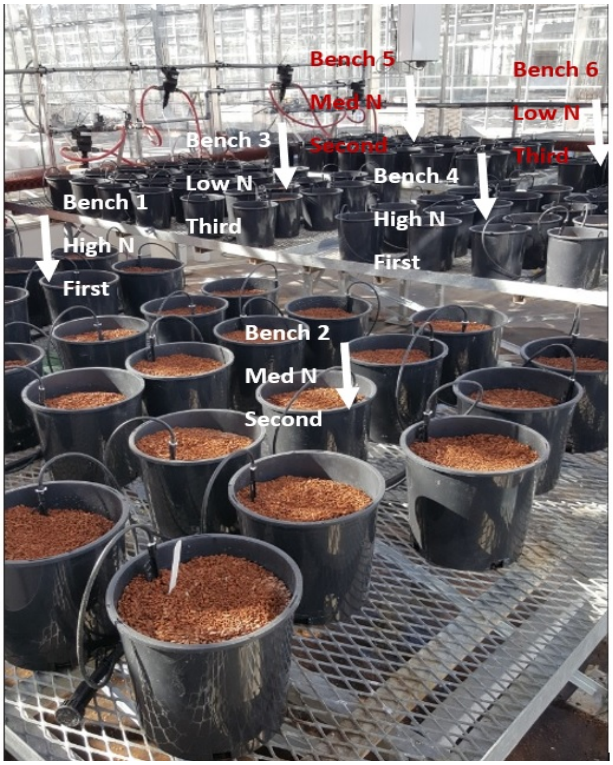

Figure 5.1: The University of Guelph greenhouse experimental design

Nutrients were mixed with water and supplied automatically right after seed emergence to each bench separately using a miniDos pump (Hydro systems, Cincinnati, USA) connected to a timer. The nutrients mixture was supplied to each pot individually using a drip irrigation system. Each pot was supplied with an average of 2.5 cm water per week and weeds were manually removed from pots at the time of seed emergence to ensure that corn plants are only under nitrogen stress. The light source in the greenhouse was set to supply a 16 hour photoperiod. Two types of non-dimmable lamps were used; a 1000 Watt Metal Hallide lamp (SYLVANIA 64469-3, Gerrie Electric, Hamilton, Canada) and 1000 Watt High pressure sodium lamps (SYLVANIA 64469-3, Gerrie Electric, Canada). There

were 18 lamps of each type alternating in 6 rows of 6. The light intensity at bench level was between 575 to 780 umol.m^2s. Lights were controlled with an ARGUS Control System. Two fans were used for air circulation inside the experimental room.

Two experiments were conducted to study the effect of varying nitrogen rate on surface temperature. The first experiment (Expt 1) utilized three rates of nitrogen (N); high (20 mM), medium (12 mM), and low (4 mM) N rates applied to individual pots right after the emergence of a corn seed as described in [161]. Experiment 1 included two tests, one conducted in October 2015 (test 1) and one in January 2016 (test 2). In each test, two benches were assigned as independent individual replicates per treatment for a total of four replications (two tests $\times$ two benches). The second experiment (Expt 2) utilized the high rate of nitrogen (20 mM N) applied to individual pots at different timings; benches 1 and 4 were supplied with nitrogen at the beginning of the experiment (after one week of seed planting), benches 2 and 5 were supplied with N after two weeks of seed planting, and benches 3 and 6 were supplied with N closer to the end of the experiment (after three weeks of seed planting). In experiment 2, two tests were conducted; one in February 2016 (test 1) and one in April 2016 (test 2). Expt 1 and Expt 2 setups are shown in Figure 5.2. Temperature data were collected from the middle two rows to avoid any border effects, 10 measurements per bench were conducted with a total of 20 measurements per N treatment. The mean leaf surface temperature reported in this section and following sections are an average of 20 measurements per nitrogen treatment.

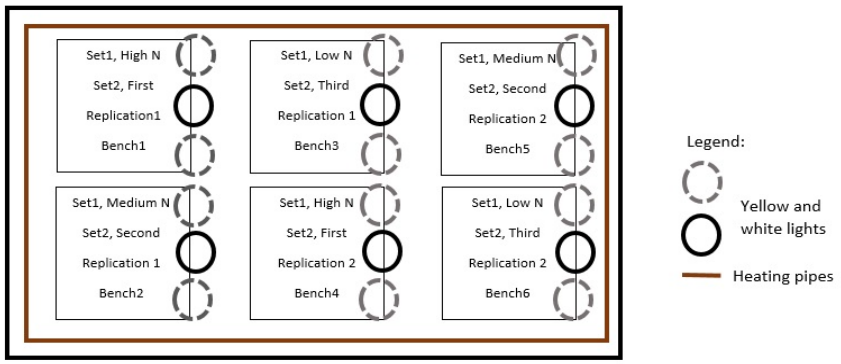

Figure 5.2: The two Experimental setups conducted at the University of Guelph greenhouse

Corn plants were hand harvested at V7 growth stage and dried in an oven for 5 days at 80 $^{\circ}C$ set temperature. The biomass of dried corn (stem, leaves and root) was measured using a digital scale, which needed to be calibrated manually before every measurement. Visual differences were observed across nitrogen treatments in corn plant height, leaf color, and root configuration. Corn leaf stage and plant height were recorded 2 to 3 times per week to ensure that corn plants were growing and developing properly with respect to applied nitrogen rates (Figure 5.3).

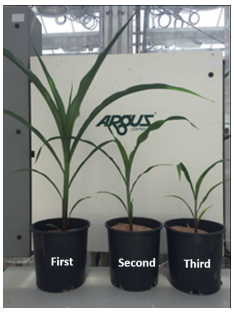

(a) Different heights of corn due to different N supplied timings (Expt 2)

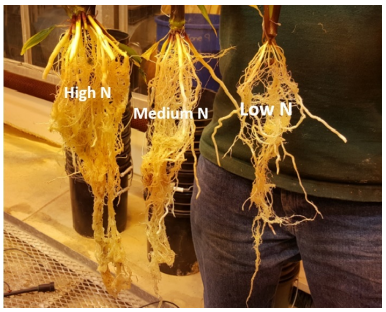

(b) Different root configuration for high, medium and low N rates (Expt 1)

Figure 5.3: Corn plants grown at the University of Guelph greenhouse from Expts 1 and 2.

5.2.2 Results and Discussion

In the first experiment conducted in the greenhouse to investigate the supplied nitrogen rate variation on surface temperature, an approximate difference of 1 °C was observed in leaf surface temperature between corn plants supplied with high and low nitrogen rates, which supports the hypothesis that stressed plants will have higher temperatures compared to less stressed plants at a 0.05 significance level (Table 5.1 and 5.2).In both tables the last column contains a, b beside each p-value number, which represents a statistical significance at $P \leq 0.05$. In addition, leaf tip stage is the average leaf stage for high nitrogen rate corn plants on a specific day. Leaf surface temperature decreased with increasing supplied nitrogen rate (Figure 5.4). As an example, the average leaf surface temperatures using an IR hand-held gun for corn supplied high, medium, and low nitrogen rates on Nov 9^{th}, 2015 were 25.48±2.59 °C, 25.55±1.94 °C and 28.74±3.43 °C, respectively, with a corresponding statistically significant difference among nitrogen treatments (Table 5.1), where the data is presented as mean± SD. The mean leaf surface temperature using a thermal camera for corn receiving high, medium and low nitrogen rates on Jan 29^{th}, 2016 were 23.82±1.75 °C, 24.44±0.96 °C, and 24.08±1.2 °C, respectively (Table 5.2).

Table 5.1: The mean leaf surface temperature decreases with increasing supplied nitrogen rate using IR hand-held gun data

Date	Leaf tip stage	High N (°C)	Medium N (°C)	Low N (°C)	p-value
Nov, 3	2	29.63± 2.76	26.82± 3.1	29.13± 2.06	0.003a
Nov, 5	3	27.89± 1.82	27.59± 2.37	28.96± 2.09	0.057b
Nov, 6	3	26.11± 1.41	25.10±1.71	29.19± 3.25	<0.001a
Nov, 9	4	25.48± 2.59	25.55± 1.94	28.74± 3.43	<0.001a
Nov, 10	4	29.61± 3.48	30.63± 2.45	33.81± 3.31	<0.001a
Nov, 12	5	23.10± 1.85	24.38± 2.32	25.92± 2.07	<0.001a
Nov, 13	5	23.33± 1.25	23.44± 1.87	26.83± 1.76	<0.001a
Nov, 16	6	31.03± 2.27	27.88± 3.04	32.25± 3.05	<0.001a
Nov, 17	7	26.10± 0.95	22.65± 2.09	25.23± 2.93	<0.001a

Table 5.2: The mean leaf surface temperature decreases with increasing supplied nitrogen rate using the thermal camera data

Date	Leaf tip stage	High N (°C)	Medium N (°C)	Low N (°C)	p-value
2015 Nov, 5	3	30.41± 0.68	30.08± 0.6	31.88± 0.52	<0.001a
Nov, 11	4	30.43± 0.45	30.82± 0.41	32.19± 0.73	0.005a
Nov, 18	7	25.885± 1.46	24.33± 1.11	27.13± 1.83	<0.001a
Nov, 22	7	25.61± 1.06	25.69± 0.73	26.16± 0.71	0.39b
Nov, 24	8	27.02± 1.31	27.28± 0.88	27.82± 1.33	0.1b
2016 Jan, 19	3	24.45± 3.49	24.29± 2.07	25.46± 2.06	0.13b
Jan, 23	4	24.93± 2.04	24.52± 1.12	24.51± 1.71	0.35b
Jan, 29	6	23.82± 1.75	24.44± 0.96	24.08± 1.2	0.3b

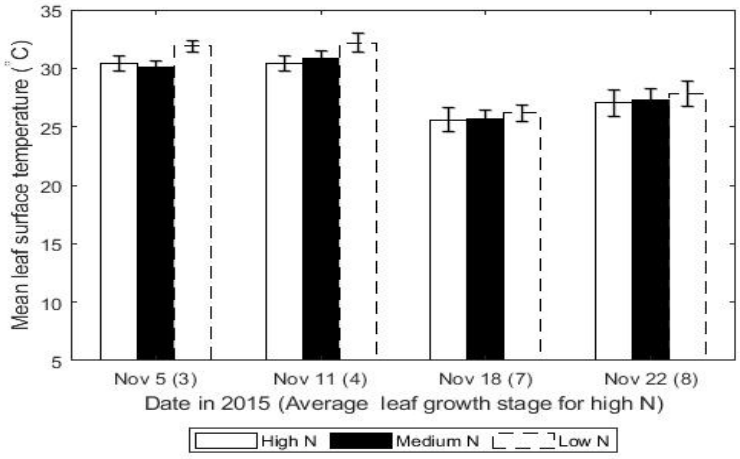

Figure 5.4: The average leaf surface temperature decreases with increasing nitrogen rate from a thermal camera data (Expt 1, test 1). The error bars represent standard errors.

In experiment 2, the high rate of nitrogen (20 mM N) was supplied to plants based on different timings; benches 1 and 4 were supplied with nitrogen (N) after one week of seed planting, benches 2 and 5 were supplied with N after two weeks of seed planting and benches 3 and 6 were supplied with nitrogen (N) after three weeks of seed planting. It was observed that even after nitrogen is added to previously stressed plants (i.e., benches 3 and 6 supplied after three weeks of planting) surface temperature remains higher compared to plants that received nitrogen from the beginning of the experiment. It was observed that corn received a high rate of nitrogen after one week of seed planting (First application) had consistently lower surface temperatures compared to corn that received nitrogen after two weeks of seed planting (second application) or after three weeks of seed planting (third application) (Figure 5.5), which supported the hypothesis that stressed plants have higher surface temperatures compared to less stressed plants as predicted by the exergy destruc-

tion principle (EDP). As an example, on Mar 7th, 2016 the average leaf surface temperature for corn that received nitrogen after one week of seed planting (First N application) was 27.73± 1.7 °C compared to 31.25± 2.8 °C for corn that received nitrogen after two weeks of seed planting (Second N application) as presented in Table 5.3.

Table 5.3: The mean leaf surface temperature increases with increasing nitrogen stress (Expt 2, test 1)

Date	Leaf tip stage	First N (°C)	Second N (°C)	Third/last N (°C)	p-value
Mar, 1	2	26.15±1.8	29.705±4.2	29.55±3.4	0.001a
Mar,3	3	27.68±2.7	28.405±3.4	28.01±3.6	0.78b
Mar, 7	4	27.73±1.7	31.25±2.8	31.97±3.6	<0.001a
Mar,8	5	30.285±1.7	33.585±3.1	33.955±2.8	<0.001a
Mar, 10	5	22.515±1.2	24.51±1.5	26.12±1.4	<0.001a
Mar, 11	6	24.01±2.1	26.705±2.9	28.675±3.7	<0.001a
Mar, 14	6	24.965±1.7	23.52±1.53	28.845±2.38	<0.001a
Mar, 15	7	26.6±2.1	26.515±2.5	29.08±3.4	0.005a
Mar,17	7	22.725±1.6	22.015±0.9	25.445±2.1	<0.001a

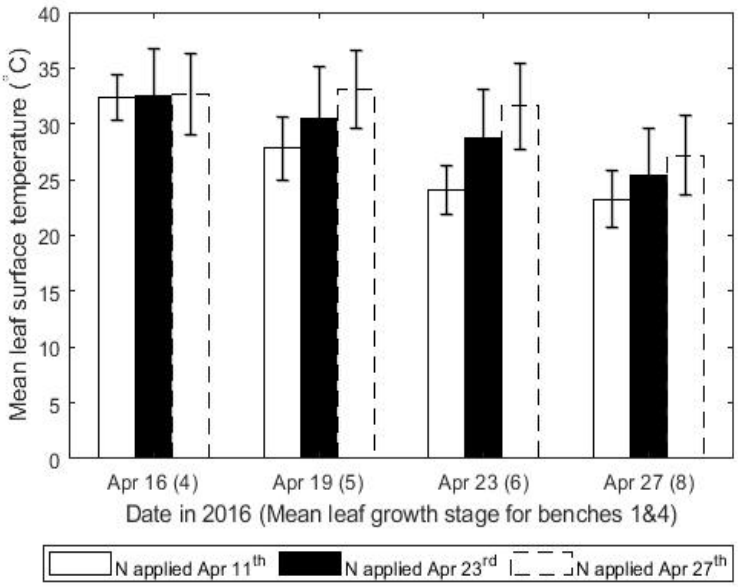

Figure 5.5: The effect of applying high rate of nitrogen at different timings on average leaf surface temperature from the IR hand-held gun data (Expt 2, test 1). The error bars represent standard errors.

The total biomass for corn plants increased with increasing nitrogen rates and leaf surface temperature decreased as observed in Expt 1. The mean total biomass including leaves, stem and roots for 20 corn plants per N treatment was higher in corn that received high rates of nitrogen, or supplied with the high nitrogen rate after one week of seed planting compared to corn that received low nitrogen rate or supplied with the high nitrogen rate after three weeks of planting (Table 5.4). In Expt 1, test 1, the mean total biomass for corn receiving high, medium and low rates of nitrogen were 18.9 ±3.49 g, 11.1 ±1.92 g, and 6.5±1.34 g, respectively. For Expt 1, test 2 the mean total biomass for corn receiving high, medium and low rates of nitrogen were 4.4 ± 0.97 g, 4.2 ±1.17 g, and 3.3±0.61 g,

respectively. There was a substantial difference in the two tests conducted in experiment 1 due to the growth stage difference at the harvest time. As an example, on Nov 27th, 2015 (Expt 1, test 1) corn that received high, medium and low rates of nitrogen were in 11, 9 and 9 average leaf tip stage, respectively, at harvest time. For Expt 1, test 2, as an example, on Feb 2nd, 2016 corn that received high, medium and low rates of nitrogen were in 8, 7 and 7 average leaf tip stage, respectively, at harvest time. Furthermore, a negative correlation was observed between leaf surface temperature and total biomass across corn plants grown under different crop stress conditions (Figure 5.6), where each data point represents an average of 10 measurements for the two experiments conducted. Stressed plants will have lower biomass and higher temperatures compared to less stressed plants, this negative correlation between temperature and biomass was also confirmed in previous studies involving crop plants[162].

Table 5.4: The mean total biomass increases with increasing supplied nitrogen rate

Expt no.	Test no.	Time period	High N (g)	Medium N (g)	Low N (g)
1	1	Oct-Dec 2015	18.9± 3.49	11.1± 1.92	6.5± 1.34
	2	Jan-Feb 2016	4.4± 0.97	4.2± 1.17	3.3± 0.61
			First N applied (g)	Second N applied (g)	Third N applied (g)
2	1	Feb-Mar 2016	7.5± 1.16	1.9± 0.35	0.88± 0.17
	2	Apr-May 2016	13.8± 1.69	2.1± 0.46	0.71± 0.18

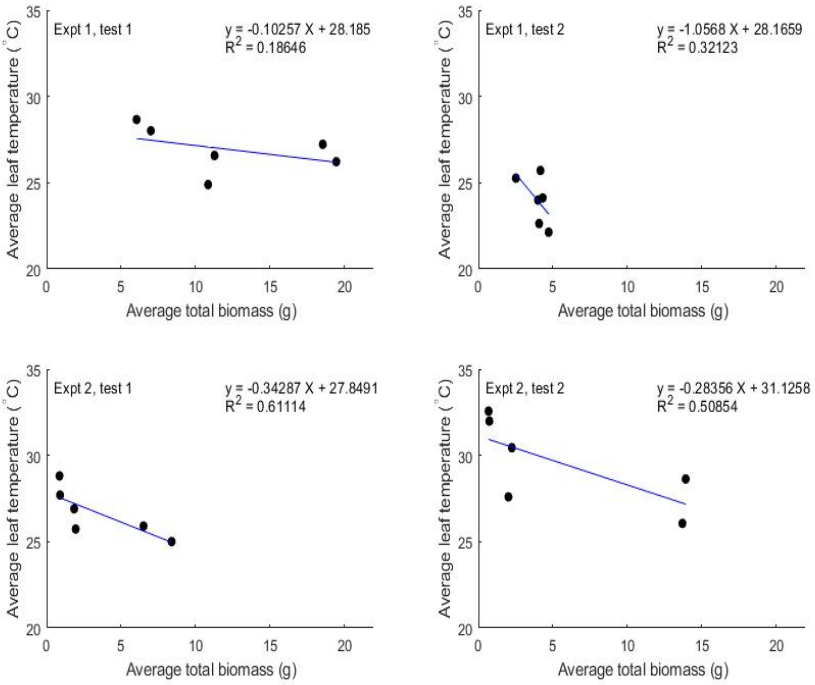

Figure 5.6: Decreasing leaf surface temperature with biomass increase due to nitrogen stress decrease

5.2.3 Whorl temperatures decrease with increasing rates of nitrogen

Whorl temperatures were measured for stressed and less stressed corn plants during the day and night to investigate if there is a significant difference between them. It was observed that stressed corn plants during the day have higher whorl temperatures compared to less stressed plants (Figure 5.7). During the night, nitrogen stressed plants were cooler compared to less stressed plants. Whorl temperatures were measured using type T

thermocouples and air temperatures were measured using type k thermocouples with an approximate ± 2 ° accuracy.

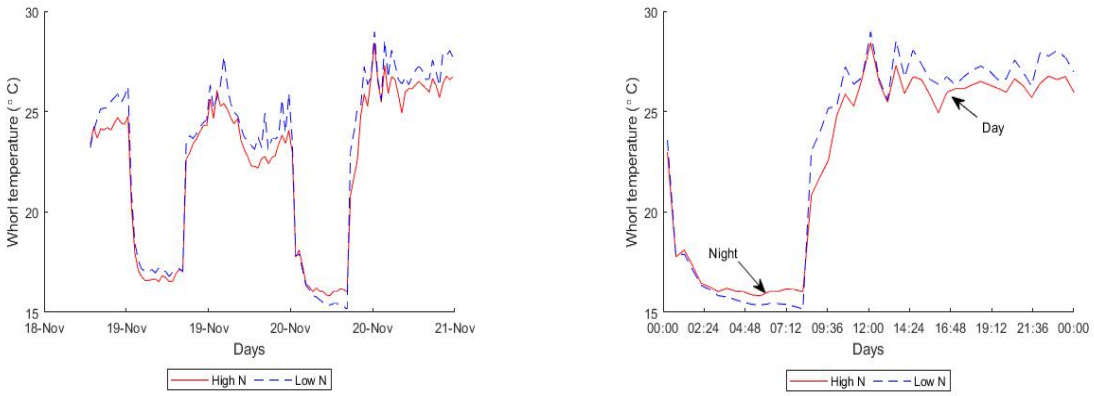

(a) Three days period **(b)** One day period

Figure 5.7: Whorl temperature variation between day and night in November 2015.

It was observed that air temperature was warmer relative to whorl temperature at night, which was not unexpected given that temperature measurements were collected under greenhouse conditions in fall, November 2015, where the air temperature in the room was heated while the greenhouse walls and ceiling were cold due to the colder outdoor temperature. That is, a cooler whorl temperature confirms the heat loss to the background controls the energy balance at the plant surface, similar to when a background radiation controls the formation of frost on lawns at night. When analysing whorl temperatures at night, if temperature difference trends between plants under different nitrogen stress levels are the result of nitrogen stress, or because of changes in energy balance given there is no solar radiation input at night, while the warmer nitrogen stressed plants will initially cool faster compared to less stressed plants due to the large temperature difference between

plant surface temperature and background radiation temperature. The physics of radiation heat transfer dictates, that for the stressed plants to cool to a lower temperature compared to the less stressed plants at night, stressed plants must have properties or mechanisms unrelated to the incoming background radiation that differ from the non-stressed plants. One possible reason mirrors what happens in a desert where temperatures fluctuate widely between day and night [163, 164] due to low "effective" thermal mass.

5.3 University of Waterloo experiments

5.3.1 Materials and methods

Three seeds of corn hybrid Pioneer P9188AM were planted at a depth of 2 cm in the center of each pot which took approximately one week to emerge. After the seed emergence, corn plants were thinned to one plant per pot (22 cm width, 22 cm depth) of 5 Liters in volume. The soil that was used in the pot is an equal mixture of Turface MVP (Profile Products LLC Buffalo Grove, USA) and a commercial potting medium (Sun Gro Professional Growing Mix, Sun Gro Horticulture, Agawam, MA) to allow for an adequate drainage. The pots were organized in a randomized design placed onto two separate benches, 4 to 5 pots were assigned per nitrogen treatment.

Five experiments were conducted at the University of Waterloo, Ontario, Canada from Apr 2019 to Feb 2020 to investigate whether there is a difference in leaf thermal emissivity between corn plants supplied with different Nitrogen rates. Experiment 1 (Expt 1) was conducted in April until mid-June 2019, Experiment 2 (Expt 2) was conducted in mid- June

until mid- August, Experiment 3 (Expt 3) started in mid-August to the end of September, Experiment 4 (Expt 4) started in October to mid- November 2019, and Experiment 5 (Expt 5) started in January to mid- February 2020. Each experiment took approximately 5 weeks under semi-controlled conditions of air temperature, humidity, lighting and water supply.

In Expt 1, corn plants were supplied with three rates of nitrogen (N): high, medium and low nitrogen rates. The high rate is 1 g/L, medium rate is $0.5g/L$ and the low nitrogen rate is $0.15g/L$. The fertilizer mixture for the high nitrogen rate is obtained after dissolving 6 grams of Plant Prod fertilizer 21-7-7 Acid in 6 liters of tap water with $pH = 7.04$.The water pH was measured using the Seven Easy pH meter (Mettler Toledo, ON, Canada). Expt 1 was a pilot experiment used to determine what nitrogen rates need to be applied to establish a difference across treatments. In Expt 2 four rates of nitrogen were supplied: high N of 1.2 g/L, medium N of 0.6 g/L, low N of 0.2 g/L and no nitrogen supply. In Expts 3, and 4, four nitrogen rates were supplied to corn plants: high N of 1.4 g/L, medium N of 0.8 g/L, low N of 0.3 g/L, and no nitrogen supply to create different degrees of nitrogen stress. The nitrogen fertilizer was supplied to each pot manually using a graduated cylinder, the fertilizer mixture was supplied manually once every week right after corn seed emergence.. The no nitrogen supply represents corn plants that are not supplied with nitrogen from the beginning to the end of the experiment, which was supplied with tap water and iron nutrient. Corn plants were watered once every 2-3 days. Three grams of Iron nutrient (plant prod, 7% of actual iron mixture) were dissolved in 6 liters of tap water and supplied to corn plants at 3 and 5 leaf growth stages.Corn plants were sprayed for thrips control at 6 leaf growth stages using Success 480 SC (Dow AgroScience Canada Inc., Calgary, Alberta).

Visual differences in plant height, leaf color, and root configuration were observed across nitrogen rates.

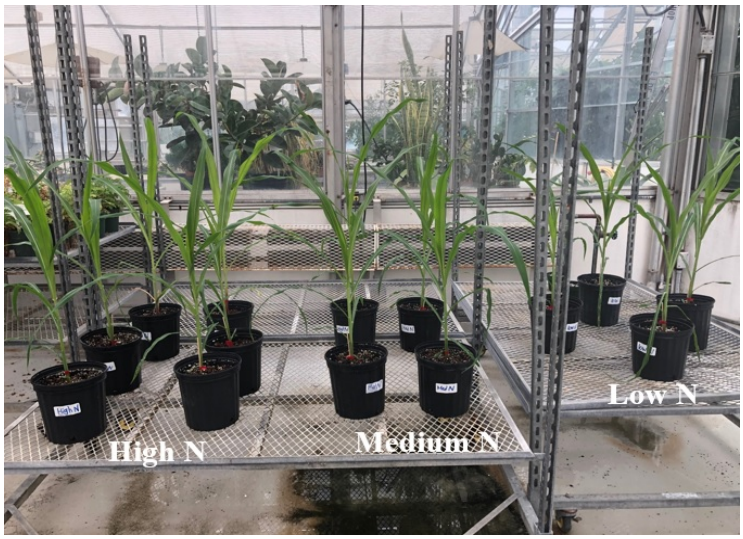

Figure 5.8: Greenhouse experiments conducted at the University of Waterloo

5.3.2 Leaves nitrogen content and soil nitrate analyses

Soil nitrate and leaves nitrogen content analyses were utilized to assess soil and plant nitrogen status, and also to investigate if there is a difference in supplied nitrogen rate across the nitrogen treatments. Plant tissue analyses were conducted in Expt 1 at V10 and Expt 3 at V7 growth stage. In addition, soil nitrate analysis was conducted for Expts 1 and 2 at V10 and for Expt 3 at V7 growth stage. Plant tissue analysis was conducted at a commercial laboratory (SGS Agri-Food Laboratories, Guelph, Canada), the total nitrogen percent (%) of the sample on a dry basis is determined by combustion using the Dumas method (J. Legg, personal communication, SGS Agrifood Laboratories). The results obtained were compared to a critical value, which is related to the amount of

nutrients required to achieve a theoretical yield that is generally 90-95% of the maximum yield obtained under optimal nutrient conditions at a given sampling growth stage[165, 166]. It was observed that corn plants with no nitrogen supply from the beginning of the experiment (highly stressed plants) had a nitrogen content below the critical level of 2.5 % based on ear leaves (J. Legg, personal communication, SGS Agrifood Laboratories) compared to the other three rates of nitrogen supplied (i.e., high, medium and low N rate) which were higher than the critical level as presented in Figure 5.9 for Expt 3, where two corn plants were selected per N treatment. One possible explanation for the difference between the two corn samples is due to a non-consistent application of nitrogen fertilizer mixture to the same spot every time it was applied.

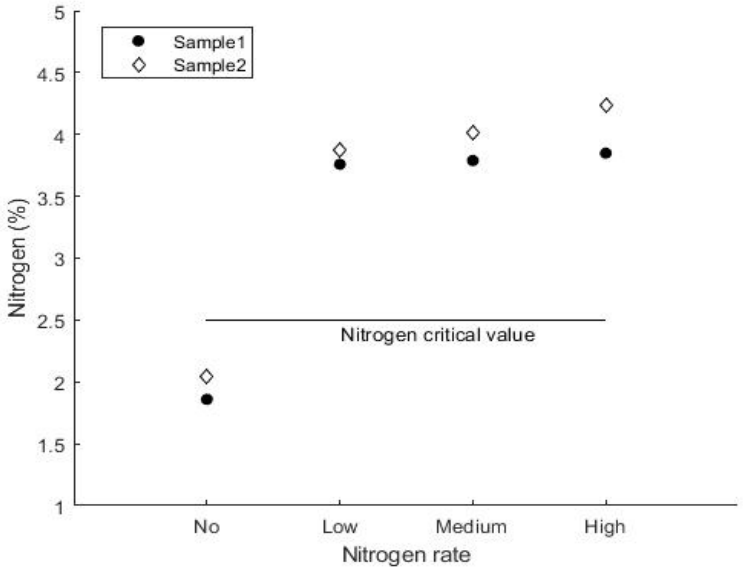

Figure 5.9: Nitrogen content for two corn samples from Expt 3 compared to the critical nitrogen value of 2.5% (J. Legg, personal communication, SGS Agrifood Laboratories).

The soil nitrate test and pH analyses were conducted on soil samples extracted from

the greenhouse experiments. Soil pH is essential to be monitored because it affects crop nutrient availability. Soil pH was measured using a Hanna pH meter (Hanna HI-9321, Woonsocket, RI, USA) after mixing 10 g of soil with 100 ml distilled water. Soil pH results were within the corn acceptable range of 5.5-6.5 for different N treatments[167]. It was observed that the soil sample with high nitrate content had a lower pH value compared to the soil sample with low nitrate content, which is consistent with previous studies [168]. The soil nitrate was measured using a colorimeter (smart 3 soil, LaMott, MD, USA) as described in the LaMotte instruction manual.

The soil extracts were prepared with the soil mixed with distilled water to prepare the blank, then the soil was mixed with an acidic reagent followed by a nitrate reducing agent to prepare the sample. Finally, after waiting 10 minutes for color development, the blank and the sample were placed in the colorimeter while choosing the 64-Nitrate N LR test. Nitrate concentrations were measured in units of ppm. Visual differences in color were as shown in Figure 5.10; the more pinkish color indicates the higher nitrate content. It was found that soil nitrate content increases with nitrogen rate supply (Figure 5.11), however, a difference across the samples for the same N rate was observed due to non-consistent nitrogen concentration applied on the same spot.

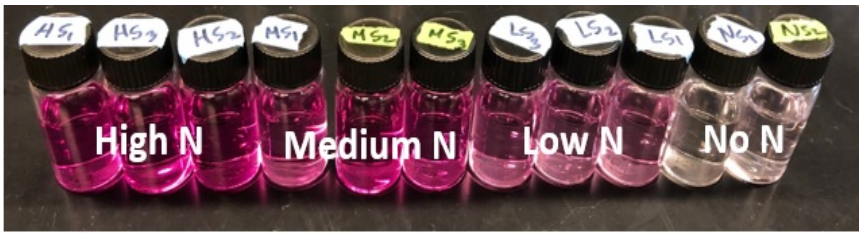

Figure 5.10: Nitrate content difference in soil samples from Expt 3

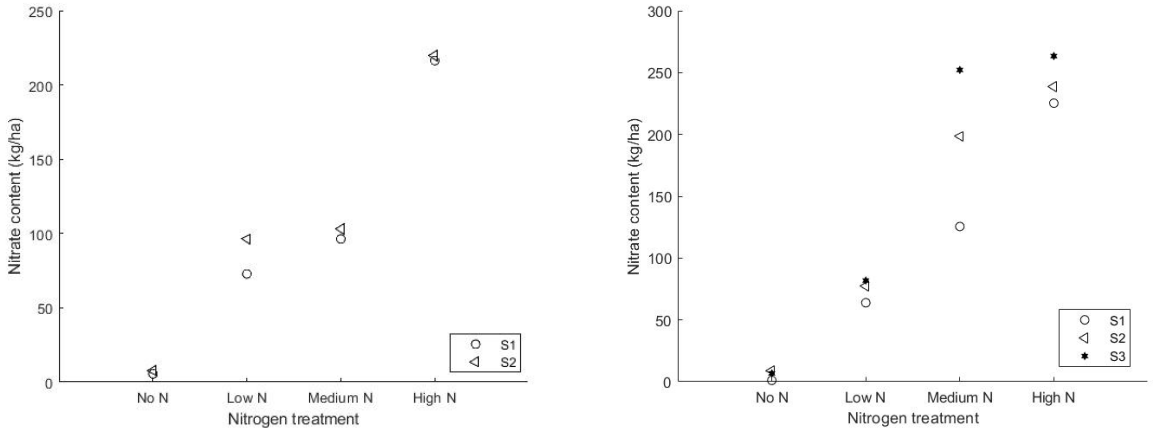

(a) Experiment #2 **(b)** Experiment #3

Figure 5.11: Soil nitrate for the two experiments conducted at the University of Waterloo greenhouse

5.3.3 Results and Discussion

University of Waterloo experiments were conducted to support the effect of decreasing surface temperature with increasing nitrogen rate, and to study the effect of supplied nitrogen rate variation on leaf thermal emissivity and whorl temperature for corn plants grown under greenhouse conditions. Leaf thermal emissivity results can be found in Appendix B and whorl temperature results can be found in Appendix C. Temperature data were collected twice during the first two experiments at 3 and 7 leaf tip stages, crop surface temperature is proposed as a relative measure for nitrogen stress. It was observed that surface temperature decreased with increasing supplied rates of nitrogen as predicted by the exergy destruction principle [34]. A shallow but statistically significant negative slope was observed for increasing rates of nitrogen (Figure 5.12). A statistically significant

difference, at 0.05 significance level, was observed in leaf surface temperatures between nitrogen stressed and less stressed corn plants as predicted by the EDP with 95 % confidence hypothesis testing.

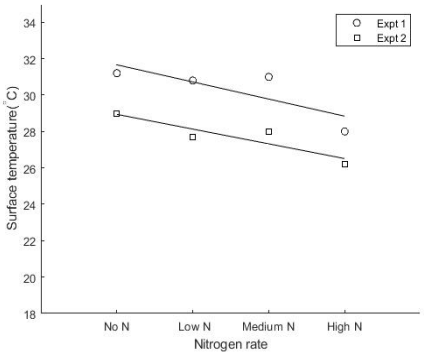

Figure 5.12: Surface temperature decreased with increasing supplied nitrogen rate at the University of Waterloo greenhouse

5.3.4 Variations in soil and air temperatures and net radiation components at the University of Waterloo greenhouse

Net radiation, incoming and outgoing shortwave and longwave radiation data were measured at the University of Waterloo greenhouse from experiment 4 using a net radiometer(Apogee instrument SN-500-SS, Logan, USA). The radiometer was mounted overtop a two meter tripod facing the north direction, and placed very close to the corn plants. The net radiometer was attached to a data logger (Sutron XLink 100, VA, USA) calibrated for one minute sampling time, while the LinkComm app was used to view, monitor, and download the radiation energy transfer data. This data was used to investigate the variation in the incoming shortwave radiation and outgoing longwave radiation, which affect

surface temperature estimation. It was observed that the outgoing longwave radiation had a range of [441- 483] $W.m^{-2}$ on Oct 24^{th} and [449- 494] $W.m^{-2}$ on Oct 25^{th}, while the incoming shortwave radiation from the solar radiation was more variable at [26- 426] $W.m^{-2}$ on Oct 24^{th} and [17- 272] $W.m^{-2}$ on Oct 25^{th} and due the time of the day the radiation measurements were taken including the highest radiation value around solar noon (Figure 5.13).

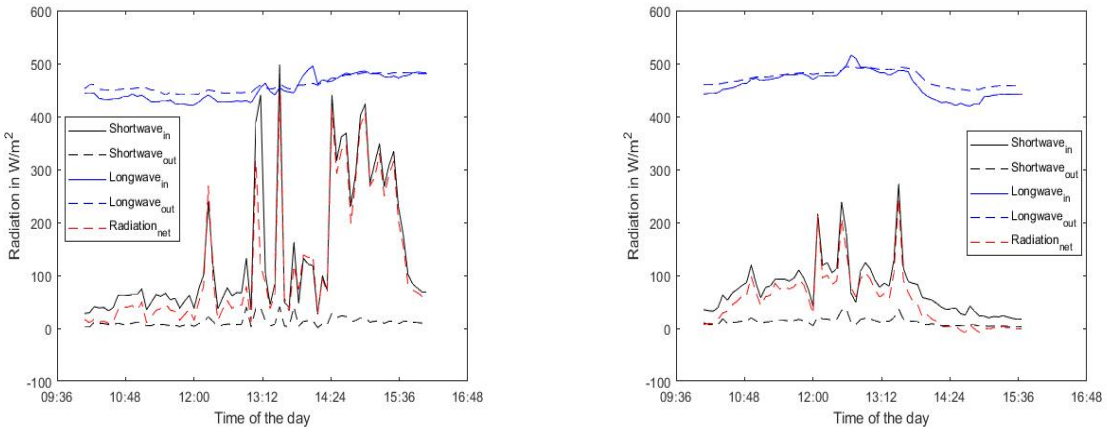

(a) Oct 24^{th}, 2019 **(b)** Oct 25^{th}, 2019

Figure 5.13: The net radiation measured at the University of Waterloo greenhouse on two days in 2019.

In addition, soil and air temperatures were measured using type T thermocouples with FEP-insulated probe; the specifications of the thermocouples used are described in Table 5.5. Air temperatures were measured at 2 m height, and soil temperatures were measured at soil surface and 10 cm underground soil depth (Figure 5.14). It was observed that soil temperature measured at 10 cm underground depth had generally higher temperatures compared to soil measured at surface level. Therefore, due to the variation in soil

temperature, air temperature and net radiation within one day and between days due to many factors including cloud cover, a consistency in surface temperature and leaf thermal emissivity data collection is required to minimize the effect of environmental condition variation.

Table 5.5: Thermocouple specifications

Max temperature	200°C
Min temperature	-200°C
Wire diameter (mm)	0.51
Length (m)	3
Sheath material	FEP insulated wire
Junction	Un-grounded
Accuracy	±0.5°C

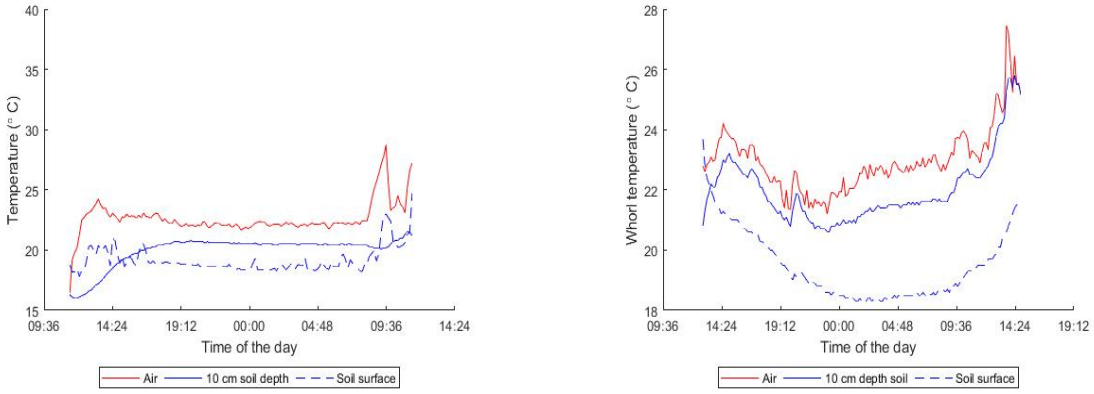

(a) On Oct 18th, 2019 **(b)** On Nov 2nd, 2019

Figure 5.14: Soil and air temperatures variation at the University of Waterloo greenhouse on two days in 2019.

Chapter 6

Field experiments

Field studies were conducted during four summer seasons (2016, 2017, 2018 and 2019) on an established long-term field trial of corn yield response to varying rates of nitrogen at the Elora Research Station, ON, Canada. In addition, two experiments were conducted in the summer of 2016 at the Woodstock Research Station, ON, Canada to investigate the effect of varying supplied nitrogen rate and weed competition on surface temperature. Field experiments were conducted using a randomized block design with 4 replications to enable a mathematical separation between true treatment effects from the background noise.

6.1 Woodstock Research Station

6.1.1 Materials and methods

Two experiments were conducted in the summer season of 2016 at the Woodstock Research Station, ON, Canada for the first time under three applied nitrogen rates (0,80, 160 kg.ha^{-1}), which were applied to the soil for the first time. In addition, five weed conditions (untreated, weed removed at 4 leaf stage (LS), weed removed at 7 LS, weed removed at 10 LS, and weed free) corn plants, respectively. A corn seed of Pioneer P38N94 was planted on May 17$^{\text{th}}$, 2016 using a finger pickup planter at a planting rate of 74900 S/H, 3 cm depth and 76 cm row spacing on a silty loam soil. It took approximately 10 days for the corn seed to emerge. Each plot consisted of 4 rows of 15 m^2 in area (3 m in length $\times$ 5 m in width). The herbicide mixture was Callisto (Mesotrione, Syngenta) at 0.3 L/ha along with Primextra II Magnum (S-metolachlor and atrazine, Syngenta) at 4 L/ha.

For the nitrogen stress experiment, nitrogen fertilizer was supplied using a 'Planet Jr' set at 248 grams of 34-0-0 (ammonium nitrate) per 7 m distance of every row at a normal walking speed of 5 Kph. Weed stress experiment utilized the presence of weed planted in close proximity to corn plants to induce crop stress. Weeds were removed at different corn plants growth stages to investigate weeds effect on crop surface temperature. Figure 6.1 shows the visual difference between stressed and less stressed corn plants with weeds. A temperature difference was observed between stressed (untreated plots) and non-stressed corn plants (weed free plots) of an average 2 °C. Corn plants were hand harvested on Nov 1$^{\text{st}}$, 2016.

(a) Corn plants free from weeds

(b) Corn plants stressed with weed

Figure 6.1: Treated and untreated corn plants of invasive weeds (pictures were taken on July 20^{th}, 2016).

6.1.2 Results and Discussion

The collected temperature data were statistically analyzed and the trends between the variables (surface temperature, crop stress, and grain yield) were investigated. It was found that increasing crop stress, either nitrogen or weed stress, will increase surface temperature. For the weed stress experiment, it was observed that surface temperature decreases and yield increases with weed stress decrease, as an example for the temperature data recorded on June 22^{nd}, 2016 (Figure 6.2), which supports the two proposed hypotheses. The yield data are represented from two corn rows (2.4m $\times$ 1.5 m).The numbers on the x-axis describe when the weeds are removed with a reference to corn plants growth stage; for example, 10 LS means that weeds are removed when corn plants were at 10 leaf growth stage.

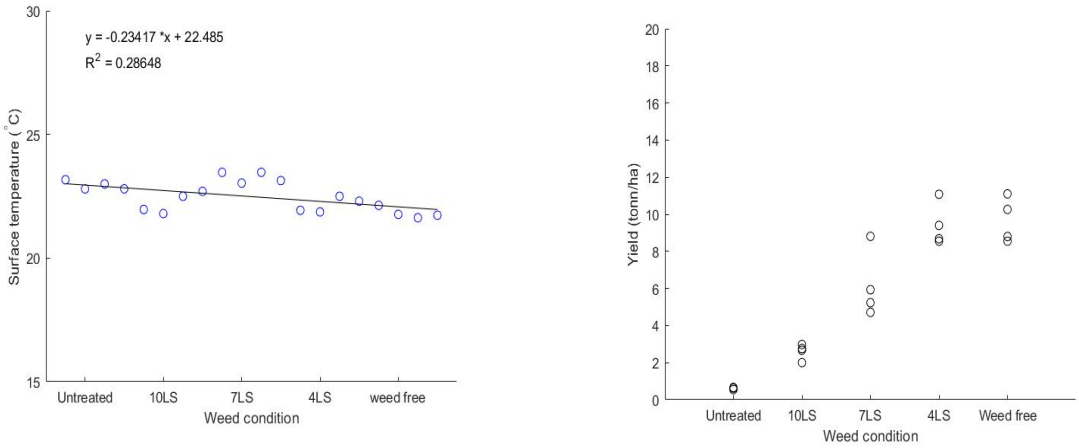

(a) Surface temperature decreases with weed stress decrease

(b) Yield increases with weed stress decrease

Figure 6.2: Woodstock Research Station data under different weed conditions in 2016.

For nitrogen stress experiment, it was observed that corn surface temperatures are correlated negatively with yield, as an example for the surface temperature data recorded on July 7$^{\text{th}}$, 2016 at the Woodstock Research Station (Figure 6.3b), the higher the yield, the lower the surface temperature, which supports the primary hypothesis of this research that agricultural crops experiencing greater growth and providing greater yield will have lower surface temperatures. This is explained by the fact that less stressed plants generate more pathways for exergy destruction and energy degradation, thus it becomes a more complex system that discloses itself as an increase in yield [104, 105]. In addition, surface temperature decrease with increasing nitrogen rate applied and yield increases (Figure 6.3). The average difference between nitrogen stressed and less stressed corn plants was 0.5 °C.

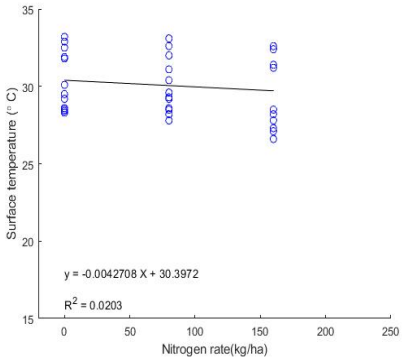

(a) Decreasing surface temperature with increasing nitrogen rate

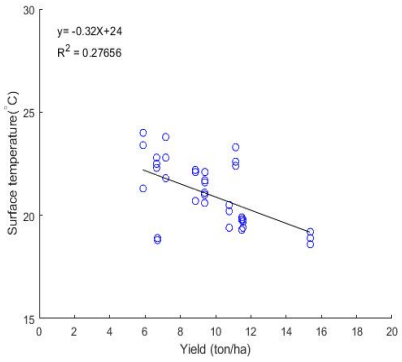

(b) Decreasing surface temperature with increasing yield

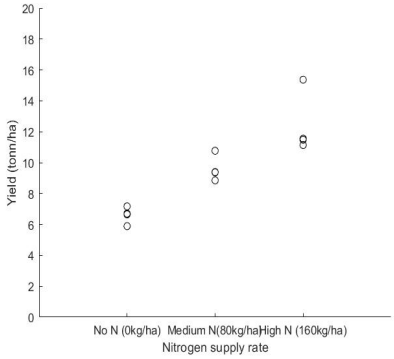

(c) Increasing yield with increasing nitrogen rate

Figure 6.3: Decreasing surface temperature with nitrogen rate increase and yield increase for weed stress experiment in 2016

6.2 Elora Research Station

6.2.1 Materials and methods

A long-term field trial was established at the Elora Research Station, ON, Canada since 2008 to investigate the response of corn yield to varying rates of nitrogen. This experimental study was conducted on a silt clay loam soil (pH 7.7, organic matter of 3.5%). The total test area is 1.72 hectare. The average distance between corn plants was 20 cm and the average distance between the plot rows was 80 cm with a total of 600 corn plants per plot, which includes around 100 plants per row. Four experiments were conducted each summer season (2016, 2017, 2018 and 2019), which utilized leaf, whorl and canopy temperature measurements, leaf thermal emissivity, and SPAD measurements across different treatments.

Corn hybrid DeKalb DKC 3987 (DEKALB Canada, Chatham, ON, Canada) was planted in May each year at a seeding rate of 79000 seeds per hectare. The selected corn hybrid requires 2700 heat units with 2000 growing degree days to mature. Individual plots consisted of 6 rows of corn plants, 76 cm row spacing and approximately 15 m length $\times$ 4.5 m width. A starter fertilizer of 19-19-19 (P-K-N), applied at the time of seed planting in a band at a distance of 5 cm from the row at a depth of 5 cm, was used at 30 $kg.ha^{-1}$ rate and the remaining nitrogen was knifed into inter-rows with Urea Ammonium Nitrate (UAN)-28%. The UAN was injected between rows every year. Nitrogen rates of 0, 28, 57, 115, 188, and 230 $kgN.ha^{-1}$ were applied at planting. Weeds were controlled prior to corn planting using the herbicide Callisto (Mesotrione, Syngenta) at 0.3 L/ha along with

Primextra II Magnum (S-metolachlor and atrazine, Syngenta) at 3.5 L/ha [34]. Standard agronomic practices were applied to optimize corn growth and development. Conventional fall tillage with a plow was used. The average rainfall was approximately 75 mm per month. Each individual plot was machine harvested in November each year. Yield was reported at 15% moisture level. Temperature measurements were recorded twice a week around noon time over approximately 2-hrs period under clear sky or uniform overcast conditions for a uniform sky background radiation assumption. Surface temperature measurements continued on a weekly basis until the corn silking stage.

6.2.2 Weather conditions

The meteorological data, including relative humidity, air temperature, and wind speed, were collected through a nearby weather station (Elora Research weather station) that is approximately 1.5 km from the study site operated by the University of Guelph. In addition, a mobile Vantage Vue weather station (Davis Instrument, Hayward, CA) was installed in the field during surface temperature measurements.The sampling rate was set to 1 Hz, and 15-min averages of data were recorded. Wind speed, relative humidity, and solar radiation were compensated through conditional sampling, and days with low wind speed in the range of 0.3 to 1.3 m.s^{-1} were selected for temperature data acquisition.

Furthermore, in 2019 during temperature data collection a net radiometer (Apogee instrument SN-500-SS, Logan, USA) was used to measure the incoming shortwave radiation (K_{in}), the outgoing shortwave radiation (K_{out}), the incoming longwave radiation (L_{in}), the outgoing longwave radiation (L_{out}), and the net radiation (R_n) in W/m^2. The radiometer

was mounted on a two meter tripod facing the north direction. The radiometer was attached to a data logger (Sutron XLink 100, VA, USA) calibrated for one minute sampling time, while the LinkComm mobile application was used to view, monitor, and download the radiation energy transfer data. The data were used to investigate the variation in the incoming shortwave radiation and outgoing longwave radiation. The radiation components in W/m^2 on different days is summarized in Table 6.1. The time duration in the Table is in hours, which represent the time duration when the radiation data were collected. All the presented data are an average over the specified time period.

Table 6.1: Net radiation variation in the summer of 2019 at the Elora field

Date	time (hrs)	K_{in}	K_{out}	L_{in}	L_{out}	R_n
July,18	1	497.35±216.5	84.6±35.66	413.94±11.82	470.35±5.77	351.9±163.95
July, 26	4	890.59±208.85	127.14±36.22	370.54±15.2	493.53±11.05	636.01±168.51
Aug, 9	3	482.26±260.8	76.75±33.2	359.47±21.2	443.59±8.86	361.86±199.4
Aug, 15	2	653.16±132.6	88.15±20.64	332.54±10.5	455.53±11.8	441.22±107.12
Aug, 23	3	700.96±363.43	90.27±48.5	343.79±21.5	442.95±11.4	502.75±300

6.2.3 SPAD measurements

A hand-held soil plant analyses development (SPAD) chlorophyll meter was used to monitor leaf N status in crop plants. SPAD meter is highly affected by different environmental variables, crop hybrid, growth stage, and leaf features [13], however, SPAD measurements cannot be used for accurate predictions of how much N is required to be applied during the growing season [169]. SPAD measurements were collected only from 2019 experiments using a Minolta SPAD-502 (Minolta Corp., Ramsey, NJ) to estimate the chlorophyll concentration that is directly correlated to leaf nitrogen content [170]. SPAD measurements were conducted on the uppermost and fully expanded leaves at multiple leaf locations starting from the base to the tip of a corn leaf, measurements were made consistently at noon time. A summary of SPAD measurements are described in Table 6.2, where each data point represents an average of 15 measurement points (5 leaves $\times$ 3 points per leaf). For the p-value column, (a) represent a significant difference between N treatments and (b) represent a non-significant difference between N treatments at 0.05 significance level. For higher growth stages a significant difference was observed in SPAD units (around 15 unit difference) between the two nitrogen extremes (0 and 230 $kgN.ha^{-1}$), so corn plants supplied with a high rate of nitrogen had higher SPAD unit compared to plants supplied with a lower nitrogen rate. To minimize the SPAD unit variation for the same rate of nitrogen it is recommended to be consistent with SPAD measurements, therefore, using ear leaf for corn plant and the same leaf position is more accurate late in the growing season [171].

Table 6.2: A summary of SPAD measurements in the summer of 2019 experiments

Date	Leaf stage	0 N	28 N	57 N	115 N	230 N	p value
July, 7	8	38.28±5.1	40.06±5.8	38.85±5.8	39.02±4.9	39.82±5.6	0.068b
July, 16	10	31.54±5.4	31.86±5.4	33.42±4.2	36.37±4.1	34.95±5.1	<0.001a
July, 18	11	34.09±4.3	33.35±4.9	33.24±5.5	37.3±5.3	38.47±3.46	<0.001a
July, 27	12	23.97±4.68	32.54±5.3	34.61±4.6	43.06±1.82	41.03±3.87	<0.001a
Aug, 9	Tasseling	37.17±2.2	41.98±5	47±3.22	48.92±4.3	51.99±3.2	<0.001a
Aug,10	Tasseling	35.2±2.3	41.05±4.9	45.27±4.54	50.44±3.85	51.88±4.1	<0.001a

6.2.4 Soil nitrate, plant nitrogen and water stress detection

Soil nitrate samples are collected twice a year at the Elora field to a depth of 30 cm prior to seed planting in May and the second time after harvesting the field in November each year where the same plots are chosen to study the level of nitrate variation in the soil, five cores per plot are taken and mixed. In the year of 2016, soil nitrate levels ranged between 4.5-7 ppm in May. A non-significant difference among nitrogen treatments within the field was observed in soil nitrate levels prior to fertilizer application each year. This implies that the amount of nitrogen added in the previous year does not impact the following year. One of the major advantages for soil nitrate sampling prior to seed planting is to determine the nitrogen residual content in the soil from the previous year.

In the year of 2016, the average soil moisture for two nitrogen rates of 0 and 188 $kgN.ha^{-1}$ was 26.07±0.062 and 24.06±0.056, respectively (Personal communications, H. Wichers). In addition, the soil volumetric water content ($\frac{volume of water}{volume of soil}$) was measured over different plots within the field using an EC5 soil moisture sensor (Decagon Devices, Inc., Pullman, WA, US), which was inserted into 10 cm depth below ground.

Corn plants were checked for water stress conditions during the growing season in 2016, 2017, 2018 and 2019, where the soil volumetric water content and precipitation rate were monitored. In 2016, the average soil volumetric water content during the growing season (June–August) for plots supplied with 0 and 188 $kgN.ha^{-1}$ were $26.07\% \pm 0.062$ and $24.06\% \pm 0.056$ ($m^3.m^{-3}$), respectively (Personal communications, H. Wishers). In 2017, the volumetric water contents for plots supplied with 0 and 188 $kgN.ha^{-1}$ were $25.07\% \pm 0.074$ and $22.0\% \pm 0.048$ ($m^3.m^{-3}$), respectively, with the averages extracted over 12 days for 12 plots per N rate. In 2018, the volumetric water contents for plots supplied with 0 and 188 $kgN.ha^{-1}$ were $18.46\% \pm 0.058$ and $16.33\% \pm 0.038$ ($m^3.m^{-3}$), respectively, with the averages extracted over 10 days for 4 plots per N rate (Personal communications, R. Eerpina). These results are within the field capacity range of 22% to 28% of silt clay loam soil [172], and, when coupled with visual observations of no wilting, they indicate that corn plants did not experience significant water stress [34]. For the precipitation rates; in 2016, the average rate per day during the growing season was 5.76 ± 8.59 mm, in 2017 was 4.19 ± 6.17 mm, and in 2018 was 5.62 ± 7.1 mm. However, even if corn plants were stressed with water in some periods of time, it was effectively uniform across plots, as ensured by the randomized block design of the plots. Therefore, even if water stress did affect the corn surface temperature, it would only shift the temperature and not affect the temperature difference trends induced by the nitrogen differential stressor.

The total plant N taken in selective plots at the silking stage over three years period (2016, 2017 and 2018) is presented in Figure 6.4 for plots supplied with 0 kg.ha^{-1} (personal communications, R. Eerpina). Five corn plants were collected from the second row in each reported plot. Rep in Figure 6.4 represents the replication number, for example, Rep 1 is

the plots selected from the first replication. The zero nitrogen plot does not represent the true zero since the whole field was supplied with 30 kg of nitrogen using a planter while planting, so it is 30 Kg N.

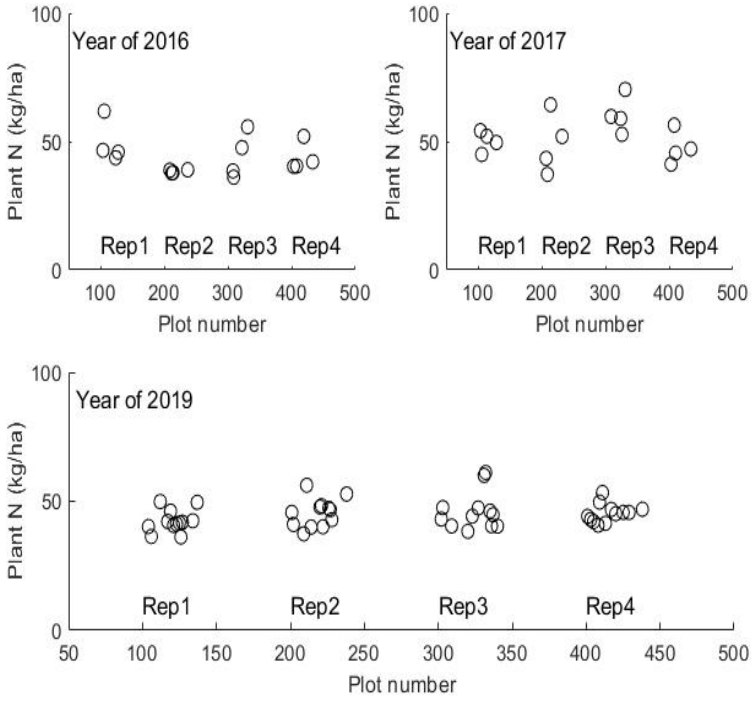

Figure 6.4: The total nitrogen content variation among plots over three years period at the Elora field

6.2.5 Results and Discussion

Surface temperature decreases with increasing nitrogen rate

Corn surface temperature decreases as the rate of nitrogen increases. A shallow but statistically significant negative slope was observed consistently with increasing rates of nitrogen

(Figures 6.5 and 6.6)[34]. For example, on July 7th and August 10th in 2019 , the 0 nitrogen rate had a mean leaf surface temperature of 27.2 $\pm$ 0.73°C and 20 $\pm$ 0.37 °C, compared to 25.57 $\pm$ 0.85 °C and 18.89$\pm$ 0.37°C, respectively, for corn that received 230 $kgN.ha^{-1}$ nitrogen. A similar response was observed in previous years. The temperature data presented on a single graph are an average of the four replications per nitrogen treatment for a given day. Despite the large temperature variability between corn plants within and between the four replications, the regression analysis consistently identified a negative slope (Figures 6.5 and 6.6), supportive of the hypothesis that crop stress affects surface temperature. It was observed that a consistent difference in leaf surface temperature between nitrogen stressed and non-stressed corn plants started to appear when corn plants were at V3 stage, at which stage the plants were no longer provided with nutrients from the seed [173, 174].

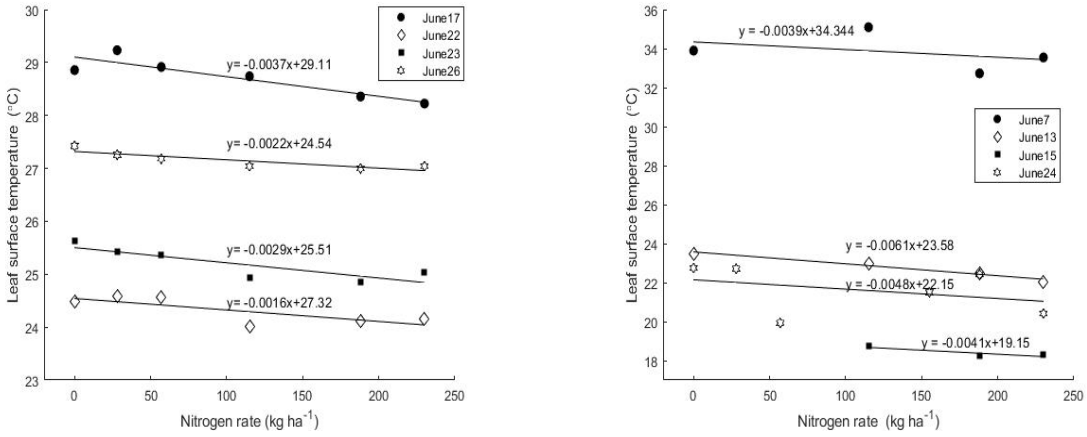

(a) 2016 **(b)** 2017

Figure 6.5: The mean leaf surface temperature decreased with increasing nitrogen rate in June 2016 and 2017.

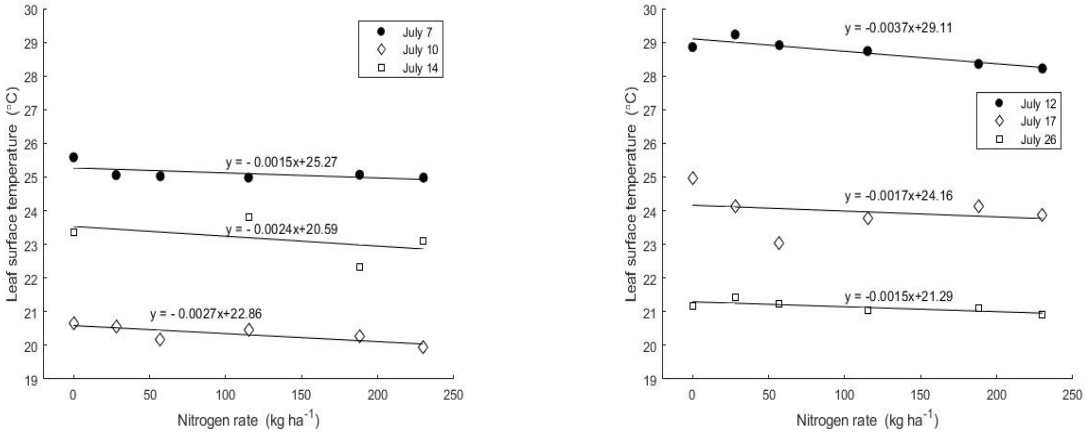

(a) 2016

(b) 2017

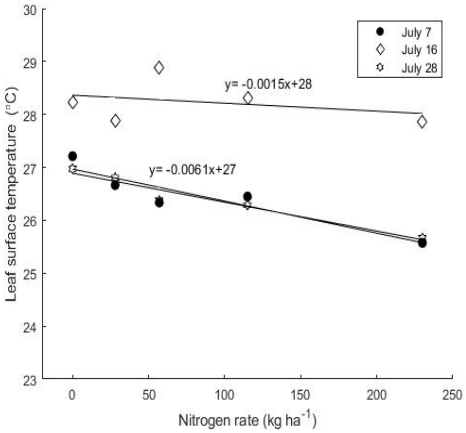

(c) 2019

Figure 6.6: The mean leaf surface temperature as influenced by nitrogen rate in July over different years.

Canopy temperature decreases with increasing nitrogen rate

Canopy temperatures decreased as the rate of nitrogen increased. A shallow but consistent negative slope was observed with increasing nitrogen rates (Figure 6.7) [34]. As an example, on July 28$^{\text{th}}$ 2019, the mean canopy temperature for corn plants that received 0 nitrogen was 26.97$\pm$0.42 °C compared to 25.66 $\pm$0.52 °C for corn that received 230 $kgN.ha^{-1}$ of nitrogen. In addition, since the relative temperatures are more important than absolute temperatures for this research, the difference in canopy temperature between stressed ($0kgN.ha^{-1}$) and non-stressed ($230kgN.ha^{-1}$) corn plants was investigated. Canopy temperature difference was calculated between the average zero nitrogen plots and the five remaining treatments (28, 57, 115, 188, 230 $kgN.ha^{-1}$) on different days in June and July 2016 and 2017 (Figure 6.8) [34]. The increasing relationship between canopy temperature difference and nitrogen rate was significant, which supports the second hypothesis that stressed plants have high temperatures compared to non-stressed plants.

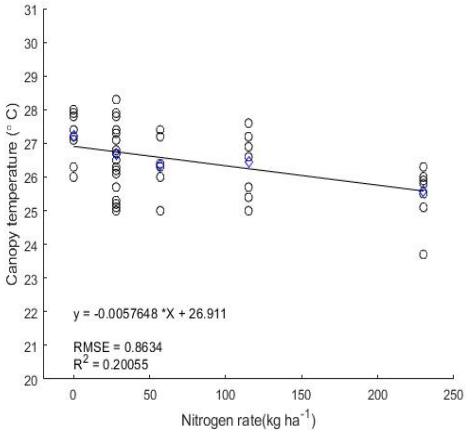

(a) On July 7$^{\text{th}}$, 2019

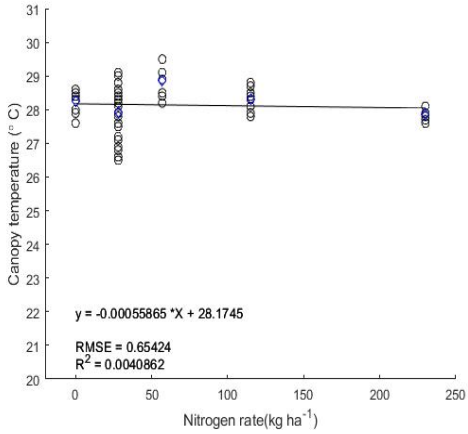

(b) On July 16$^{\text{th}}$, 2019

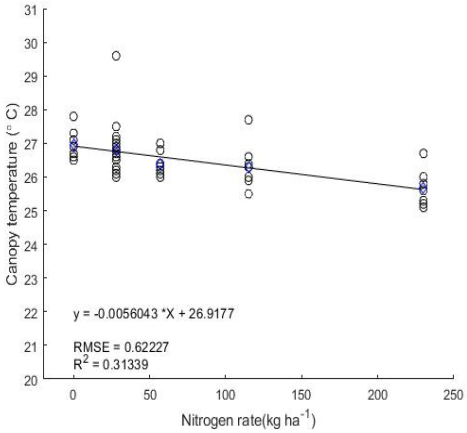

(c) On July 28$^{\text{th}}$, 2019

Figure 6.7: An inverse correlation between canopy temperature and nitrogen rate on different days in 2019.

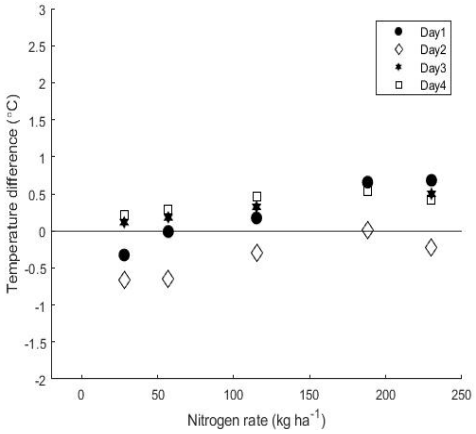

(a) June 2016 [1.14, 0.193, 0.66 °C]

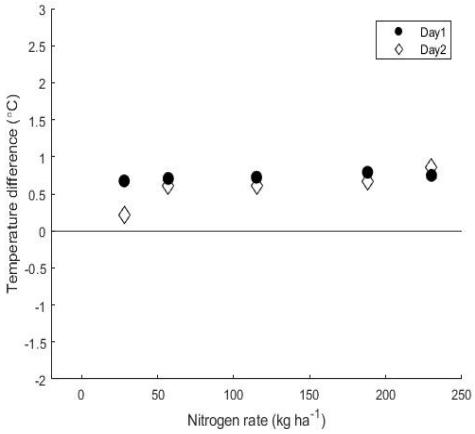

(b) July 2016 [0.967, 0.307, 0.62 °C]

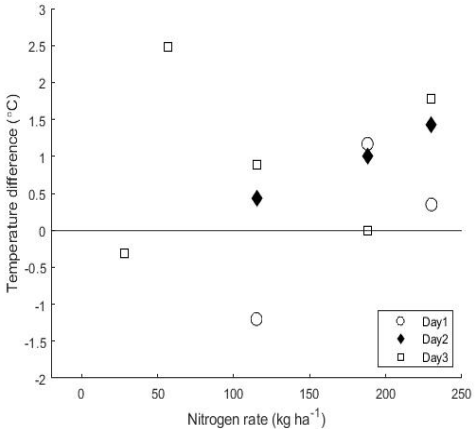

(c) June 2017 [1.84, 0.26, 1.03 °C]

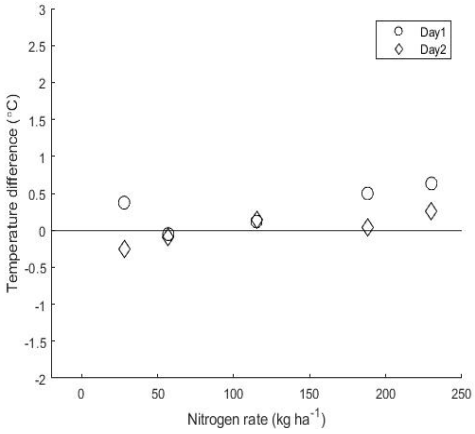

(d) July 2017 [2.45,0.27,1.28 °C]

Figure 6.8: The temperature difference between stressed and less stressed plants ($T_{LowN} - T_{HighN}$) with nitrogen, where T_{LowN} represents the temperature at low nitrogen rate and T_{HighN} represents the temperature at high nitrogen rate, and the numbers in [] are the maximum, minimum, and average standard error [max, min, avg °C].

Whorl temperatures decrease with increasing nitrogen rate

Whorl temperatures decrease as the rate of nitrogen increase. Thermocouples were inserted into the whorl of corn plants and measured on a smaller time scale (minutes and seconds), where less variability in temperature measurements would be expected. It was observed that whorl temperatures decrease with increasing rates of nitrogen for selected plots at the Elora Research Station (Figure 6.9). Temperature measurements were recorded around solar noon on a 2 minutes interval. The trend in Figure 6.9 is explained by different weather dependent variables that affects whorl temperature such as air temperature, wind speed, and solar radiation variation.

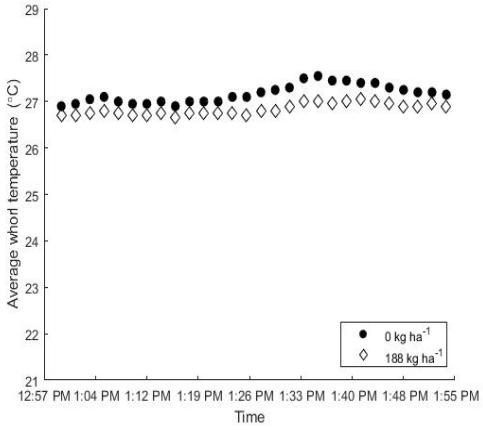

(a) On July 16$^{\text{th}}$, 2016

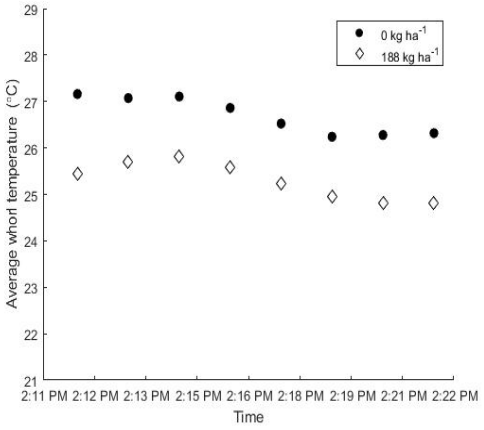

(b) On July 12$^{\text{th}}$, 2017

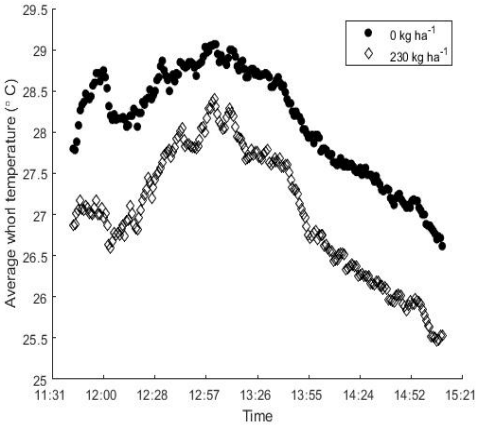

(c) On July 31$^{\text{st}}$, 2018

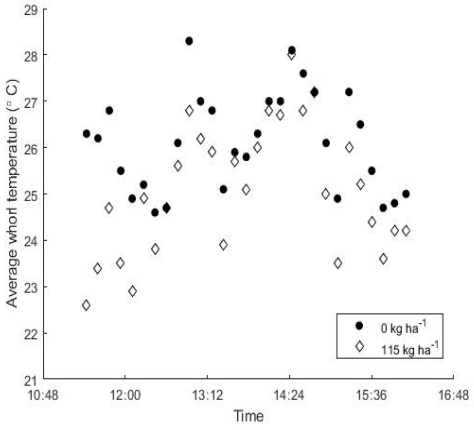

(d) On Aug 23$^{\text{st}}$, 2019

Figure 6.9: Whorl temperatures decrease with increasing nitrogen rate over different years.

For example, looking at whorl temperature data from the year of 2018 variation for three different rates of nitrogen compared on the same day (June 21$^{\text{th}}$, 2018) over different plots (Figure 6.10), it is observed that corn plants supplied with high nitrogen rate have lower whorl temperatures during the day compared to plants supplied with low or no nitrogen rate.

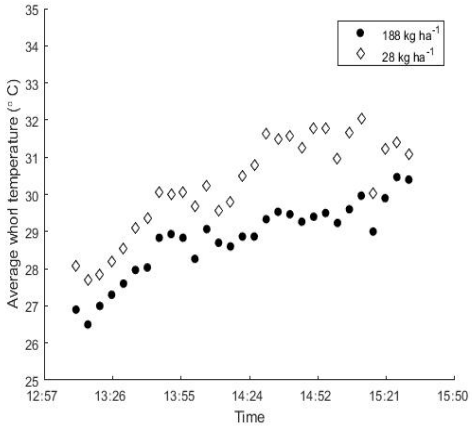

(a) Nitrogen rate of 28 and 188 $kgN.ha^{-1}$

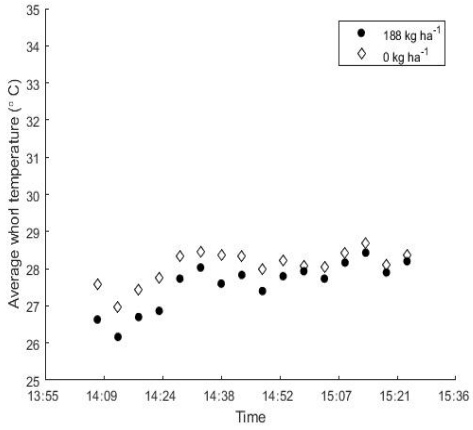

(b) Nitrogen rate of 0 and 188 $kgN.ha^{-1}$

Figure 6.10: Whorl temperature decreases with increasing nitrogen rate on June 21$^{\text{th}}$, 2018.

6.3 Crop temperature measurement sources of error

This section summarizes the potential source of errors that affect canopy temperature measurements under variable conditions. In this section, each paragraph describes one source or a group of error sources with their corresponding error minimization recommendation for the current and future canopy temperature measurements.

Crop canopy temperature is affected by the environment to which it is exposed to: growth stage[175], canopy size, canopy architecture, canopy color, root morphology, leaf orientation, leaf morphology and many other metabolic activities of crop plants [162] beside the temporal variation in environmental conditions affecting the canopy temperature. Many biochemical processes in crops are generally insensitive to temperature changes of several degrees around the optimum temperature[77]. In this research, surface temper-

atures were corrected for the variation in air and soil temperatures under variable field conditions.

Plant geometry, emissivity, inclination, and orientation of crop leaves within the canopy can also produce canopy temperature variation, therefore, an average surface temperature was calculated to minimize the crop canopy geometry related effects [176, 34]. In addition, it is expected that corn hybrid variation will affect canopy temperature [131]. If the non-nitrogen related variables can be controlled, or compensated through conditional sampling, a comparison of relative temperatures between crop plants would meet the basic needs for an experimental design to support or reject the proposed two research hypotheses. The extent of this variability was found to change day to day, further suggesting the influence of these variables on changing crop temperature. Furthermore, to minimize the error associated with the infrared camera thermal detector drift, a re-calibration is required before taking every image using the non-uniformity correction (NUC) manual button. In addition, in order to minimize the error associated with sensible heat transfer to the surrounding air there is a need for either a simultaneous measurement, or conditionally sampled measurement of air temperature.

The error in temperature difference between stressed and less stressed corn plants is related to the camera precision error, not the camera accuracy. The error in the mean temperature difference can be minimized as the sample size (# of temperature measurements) increases ($\sigma_{\text{mean}} = \frac{\sigma}{\sqrt{n}}$). For example, the average statistical error in the mean temperature for the data collected on June 24^{th} 2016 was 0.49°C, so when coupled with the precision error using Gaussian error propagation, the net error on the mean difference is 0.53°C [34].

One major piece of uncertainty affecting the accuracy, which not necessarily affecting the sensitivity, of surface temperature measurements is the uncertainty in crop plant emissivity. This research investigated the effect of varying nitrogen rate on leaf thermal emissivity in a selected waveband of the 7.5-14 μm. An average of 0.96 is proposed for corn leaves over the 7.5-14 μm as a result from laboratory based experiments being conducted, for more details please refer to Appendix B.

Air temperature, soil temperature, humidity, cloud cover, wind speed, and the amount of incoming solar radiation change regularly within a short period of time, therefore it is very important to be consistent with crop canopy temperature measurements at the same time over a short period. One of the suggested solutions to minimize the error associated with atmospheric condition variation is the normalization of canopy temperature measurements, in this research the relative canopy temperature is sufficient to distinguish between stressed and less stressed crops. In order to minimize the error associated with plant traits such as canopy size, canopy architecture, canopy color, leaf orientation, and leaf morphology average canopy temperatures need to be calculated and compared. An average of 5 m^2 containing around 40 corn plants is proposed as a reasonable sample size for field measurements.For a sample size calculation, the formula described in Kadam and Bhalerao[177] is used, which requires the assumption of type I and II errors, standard deviation and the estimated effect size. As an example, for a large field with large number of crop plants (e.g., >100,000 plants at assumed $\pm 5\%$ precision level, the proper sample size would be 400 plants located at around 40 m^2 area assuming that each plot in the field has an area of 60 m^2 with a total of 600 plants [178].

Previous studies identified the canopy thermal radiation variation with sensor view

angle [179, 180, 34]. Sensor view angle was investigated using the FLIR T620 thermal camera at different view angles (0°, 40°, -40°, and 80°) from the nadir direction. A significant difference in canopy temperature was found, at 0.05 significance level, with sensor view angle variation (Figure 6.11). The maximum and the minimum difference in canopy temperatures over two days of measurements were (27.1, 29.2)°C and (16.7, 19.8)°C when corn plants were at silking and harvest stage, respectively, therefore, it is recommended that the thermal camera images of the canopy are consistently taken perpendicular to the plant surface, that is, in the nadir direction.

(a) On August 15th, 2018 **(b)** On September 19th, 2018

Figure 6.11: Canopy temperature variation with sensor view angle at the Elora field on two days in 2018.

Chapter 7

Conclusions, recommendations and future work

7.1 Conclusions

Farmers usually over-apply nutrients, especially nitrogen fertilizer, from an agronomic perspective to achieve a target yield. The over-application of nitrogen fertilizer is a serious problem due to the cost of crop nutrients, and the harmful impact on the environment including the depletion of soil nutrients and the contamination of drinking water. Precision agriculture helps farmers to determine how much and when to apply different inputs such as herbicides, pesticides, nutrients, and water in the right location to increase yield. It is known that crop stress affects plant growth and development which, for agriculture crops, generally correlates with crop yield. When a crop plant is stressed by an external stress factor (e.g., excess heat, pests, or nutrient deficiency), its functions and processes such

as stomatal conductance, transpiration, respiration, and photosynthesis are all affected. Highly stressed crop plants experience less growth and development. This research investigates the application of the exergy destruction principle using thermal remote sensing of surface temperature to detect physiological stress in crop plants at early growth stages before any visual indicators appear on plant surface.

Two hypotheses have been developed based on previous studies supporting the inverse correlation between ecosystem development and surface temperature as predicted by the exergy destruction principle. The first hypothesis states that agricultural crops experiencing greater growth and providing greater yield will have lower surface temperatures. Given the first hypothesis and the relationship between growth, development and crop stress, the second hypothesis states that stressed crop plants will have higher surface temperature compared to less stressed plants. The two hypotheses were tested and justified under greenhouse and field conditions. The temperature data under field conditions were collected at three different scales; leaf (using a hand-held point measurement gun and a thermal camera), canopy (using a thermal camera mounted on a tripod) and over a plot area scale (using a thermal camera mounted on a drone). This research was conducted to investigate whether crop surface temperature can be used as an approach to identify crop stress in agricultural crops as predicted by the exergy destruction principle for the purpose of precision agriculture. A summary of the thesis observations and conclusions are as follows:

- It was found that relative temperatures measured across stressed and less stressed crop plants are more important than absolute temperatures, which is hard to be accurately estimated due to different variables effect on surface temperature.

- The results of this research suggest that leaf and canopy temperatures are inversely correlated with increasing nitrogen rates and increasing yield. This relationship is in support of the two proposed hypotheses. Decreasing leaf and canopy temperatures with increasing yield, supports the first hypothesis that corn experiencing greater yield will have lower surface temperatures. In addition, decreasing leaf and canopy temperatures with decreasing nitrogen stress supports the second hypothesis that corn plants supplied with optimum/high rates of nitrogen will have lower surface temperatures compared to corn grown under nitrogen stressed conditions, which increases the amount of exergy available, thus maximize its exergy utilization.

- Temperature measurements are highly variable, which is explained by many external and weather dependent variables that interact with leaf, canopy and whorl temperatures. Such variables include: variation in the incoming solar radiation, air temperature, soil temperature, soil moisture, humidity, wind speed, cloud cover, leaf angle, leaf emissivity, sensor view angle and many other factors. Therefore, if the non-nitrogen related variables can be controlled, or compensated through conditional sampling, a comparison of relative temperatures between stressed and less stressed crops would meet the basic requirements for an experimental design to support or reject the two hypotheses. Temperature variability was found to change day to day, further suggesting the influence of these variables on changing crop temperature.

- An inverse correlation between decreasing surface temperature, increasing yield and increasing nitrogen rate held true despite the large variability associated with each temperature measurement. A statistically significant difference, at 0.05 significance level, was observed in temperatures between stressed and less stressed plants. An approximate 0.5-1°C average temperature difference between corn plants that experienced different levels of development (e.g., yield and leaf stage) due to nitrogen stress to be a reasonable magnitude given that ecosystems with a wider variation in development observed 5 °C average temperature variation [91, 119], which can be explained by the small coefficient of determination (R^2) between the variables (surface temperature and nitrogen rate).

- An average leaf thermal emissivity of 0.96±0.006 over the 7.5-14 μm waveband is proposed for corn leaves based on multiple laboratory experiments involving spectral reflectance measurements.

7.2 Recommendations and future work

This research has demonstrated four years of experimental work under the greenhouse and field conditions to test the two proposed research hypotheses. Due to limited time and equipment for this research that involve the use of thermal remote sensing to detect crop stress as predicted by the exergy destruction principle, a few recommendations and proposed future work are summarized as follows:

- It is recommend to conduct conditional sampling for the temperature data collected, since it is found that the largest random error affecting canopy temperature comes from day to day variation.
- It is recommended that different corn genotypes be tested for canopy temperature variation under different stress conditions and more specifically under nitrogen stress conditions. The study of genotypic variation among corn hybrids, would enhance the breeding programs for crop stress tolerance that will increase the crop production.
- It is recommended to use another crop stress detection method (e.g., spectral reflectance, leaf transmittance,..etc) besides the thermal remote sensing, under variable field conditions, because it is hard at this stage, to identify crop stress factor that causes surface temperature variation, which might be due water stress, weed competition, or nutrient deficiency. In this research, the only stress factor that was changing is nitrogen rate, while pesticides and herbicides were applied regularly.
- It is recommended to conduct more experimental trials under controlled and uncontrolled conditions to investigate the effect of crop stress on crop emissivity and whorl

temperature.

- It is recommended to fly an Unmanned Ariel Vehicle (UAV) more frequently, under different environmental conditions and altitudes in order to investigate surface temperature variation with crop stress under variable field conditions.

- It is recommended to fly an Unmanned Ariel Vehicle (UAV) over a commercial crop field to overlay the surface temperature distribution map with a yield map to confirm the hypothesis that less stressed crop plants have lower surface temperatures and higher yield compared to highly stressed crops as predicted by the exergy destruction principle.

- It is recommended to investigate the thermal response number (TRN) [91, 118] for crop plants under different stress conditions as another proposed indicator of crop stress for precision agriculture applications. TRN is the ratio of the net total radiation to the difference in crop surface temperature over a time period. The reason for investigating TRN as a metric is because it may have greater sensitivity to nitrogen than canopy temperature measurements alone. It would, however, be more complex involving a quantified measurement of net total radiation and surface temperature at two different times of the day, such afternoon and evening.

- It is recommended to use ECOsystem Spaceborne Thermal Radiometer Experiment on Space Station (ECOSTRESS) data sets along with hyperspectral measurements if possible recognizing that the ECOSTRESS resolution is $70m \times 70m$. Furthermore, it is expected that there will be future space borne multispectral thermal data sets that

should also be considered for the use in thermal remote sensing applied to precision agriculture.

7.3 Research application

The importance of this research lies in using thermal remote sensing to detect crop stress at early growth stages before any visual indicators start to appear on crop plants (e.g., cupping, dropping, leaf yellowing and wilting). This research would enable the precise application of different nutrients, herbicides and pesticides at the right time and location under variable environmental conditions based on average relative temperatures among different plots. At this research stage, it is hard to distinguish between different types of crop stress, therefore, the use of other methods such as SPAD chlorophyll meter, spectral reflectance or leaf transmittance in the visible and near-infrared (NIR) spectrum can be proposed besides the use of thermal remote sensing through surface temperature and emissivity measurements.

The direct application of this research includes a multi channel camera with visible, NIR and mid-to far-infrared, or at least the atmospheric windows of 3-5 and 8-12 μm [181] to minimize the atmospheric attenuation, mounted on a UAV flying over a large agriculture field taking multiple images for the same location at low altitude of less than 60 m to minimize the effect of atmospheric absorption and scattering on surface temperature measurements. It is recommended to conduct flights on sunny or uniform overcast days for a uniform sky background radiation assumption around solar noon ± 2 hrs at the nadir direction. It is also recommended that each agricultural field would have a reference plot

with no nitrogen fertilizer being applied to represent the highest surface temperature value as a reference point compared to other plots/treatments within the field. On the other hand, a multi channel camera with a built-in sensor that can be mounted to a field phenotyping platform to detect immediate crop stress through temperature variation to respond by an in-crop precision treatment, such as herbicide, pesticides or nutrient addition, is recommended.

References

[1] M. Kumar, "Crop plants and abiotic stresses," *J. Biomol. Res. Ther*, vol. 3, p. e125, 2013.

[2] P. Ahmad, *Water Stress and Crop Plants: A Sustainable Approach, 2 Volume Set*. John Wiley & Sons, 2016.

[3] H. K. Lichtenthaler, "The stress concept in plants: an introduction," *Annals of the New York Academy of Sciences*, vol. 851, no. 1, pp. 187–198, 1998.

[4] T. Co., "Plant stresses: Abiotic and biotic stresses." `https://www.thoughtco.com/plant-stresses-abiotic-and-biotic-stresses-419223`.

[5] T. M. Blackmer, J. S. Schepers, and G. E. Varvel, "Light reflectance compared with other nitrogen stress measurements in corn leaves," *Agronomy Journal*, vol. 86, no. 6, pp. 934–938, 1994.

[6] P. J. Zarco-Tejada, J. R. Miller, G. Mohammed, T. L. Noland, and P. Sampson, "Vegetation stress detection through chlorophyll+ estimation and fluorescence effects

on hyperspectral imagery," *Journal of environmental quality*, vol. 31, no. 5, pp. 1433–1441, 2002.

[7] A. Chlingaryan, S. Sukkarieh, and B. Whelan, "Machine learning approaches for crop yield prediction and nitrogen status estimation in precision agriculture: A review," *Computers and Electronics in Agriculture*, vol. 151, pp. 61–69, 2018.

[8] M. Corti, D. Cavalli, G. Cabassi, P. M. Gallina, and L. Bechini, "Does remote and proximal optical sensing successfully estimate maize variables? a review," *European journal of agronomy*, vol. 99, pp. 37–50, 2018.

[9] J. Goffart, M. Olivier, and M. Frankinet, "Potato crop nitrogen status assessment to improve n fertilization management and efficiency: past–present–future," *Potato Research*, vol. 51, no. 3-4, pp. 355–383, 2008.

[10] R. Muñoz-Huerta, R. Guevara-Gonzalez, L. Contreras-Medina, I. Torres-Pacheco, J. Prado-Olivarez, and R. Ocampo-Velazquez, "A review of methods for sensing the nitrogen status in plants: advantages, disadvantages and recent advances," *sensors*, vol. 13, no. 8, pp. 10823–10843, 2013.

[11] C. Xie, C. Yang, A. Hummel Jr, G. A. Johnson, and F. T. Izuno, "Spectral reflectance response to nitrogen fertilization in field grown corn," *International Journal of Agricultural and Biological Engineering*, vol. 11, no. 4, pp. 118–126, 2018.

[12] S. Dobrowski, J. Pushnik, P. J. Zarco-Tejada, and S. L. Ustin, "Simple reflectance indices track heat and water stress-induced changes in steady-state chlorophyll fluo-

rescence at the canopy scale," *Remote Sensing of Environment*, vol. 97, no. 3, pp. 403–414, 2005.

[13] D. Xiong, J. Chen, T. Yu, W. Gao, X. Ling, Y. Li, S. Peng, and J. Huang, "Spad-based leaf nitrogen estimation is impacted by environmental factors and crop leaf characteristics," *Scientific reports*, vol. 5, p. 13389, 2015.

[14] D. Martínez and J. Guiamet, "Distortion of the spad 502 chlorophyll meter readings by changes in irradiance and leaf water status," 2004.

[15] J. Zhang, A. M. Blackmer, and T. M. Blackmer, "Reliability of chlorophyll meter measurements prior to corn silking as affected by the leaf change problem," *Communications in soil science and plant analysis*, vol. 40, no. 13-14, pp. 2087–2093, 2009.

[16] N. Vigneau, M. Ecarnot, G. Rabatel, and P. Roumet, "Potential of field hyperspectral imaging as a non destructive method to assess leaf nitrogen content in wheat," *Field Crops Research*, vol. 122, no. 1, pp. 25–31, 2011.

[17] S. Apostol, A. A. Viau, and N. Tremblay, "A comparison of multiwavelength laser-induced fluorescence parameters for the remote sensing of nitrogen stress in field-cultivated corn," *Canadian Journal of Remote Sensing*, vol. 33, no. 3, pp. 150–161, 2007.

[18] F. Padilla, M. Gallardo, M. Peña-Fleitas, R. de Souza, and R. Thompson, "Proximal optical sensors for nitrogen management of vegetable crops: a review," *Sensors*, vol. 18, no. 7, p. 2083, 2018.

[19] F. M. Padilla, R. de Souza, M. T. Peña-Fleitas, R. Grasso, M. Gallardo, and R. B. Thompson, "Influence of time of day on measurement with chlorophyll meters and canopy reflectance sensors of different crop n status," *Precision Agriculture*, pp. 1–20, 2019.

[20] H. Heege, S. Reusch, and E. Thiessen, "Prospects and results for optical systems for site-specific on-the-go control of nitrogen-top-dressing in germany," *Precision Agriculture*, vol. 9, no. 3, pp. 115–131, 2008.

[21] N. Tremblay, Z. Wang, and Z. G. Cerovic, "Sensing crop nitrogen status with fluorescence indicators. a review," *Agronomy for sustainable development*, vol. 32, no. 2, pp. 451–464, 2012.

[22] H. Yao, Y. Huang, Z. Hruska, S. J. Thomson, and K. N. Reddy, "Using vegetation index and modified derivative for early detection of soybean plant injury from glyphosate," *Computers and Electronics in Agriculture*, vol. 89, pp. 145–157, 2012.

[23] M. Diacono, P. Rubino, and F. Montemurro, "Precision nitrogen management of wheat. a review," *Agronomy for Sustainable Development*, vol. 33, no. 1, pp. 219–241, 2013.

[24] S. Khanal, J. Fulton, and S. Shearer, "An overview of current and potential applications of thermal remote sensing in precision agriculture," *Computers and Electronics in Agriculture*, vol. 139, pp. 22–32, 2017.

[25] B. Das, G. R. Mahajan, and R. Singh, "Hyperspectral remote sensing: Use in detecting abiotic stresses in agriculture," in *Advances in Crop Environment Interaction*, pp. 317–335, Springer, 2018.

[26] A. Ahmed, A. Ibrahim, and S. Hussein, "Detection of palm tree pests using thermal imaging: A review," in *Machine Learning Paradigms: Theory and Application*, pp. 253–270, Springer, 2019.

[27] R. D. Jackson, S. Idso, R. Reginato, and P. Pinter, "Canopy temperature as a crop water stress indicator," *Water resources research*, vol. 17, no. 4, pp. 1133–1138, 1981.

[28] S. Idso, R. Jackson, P. Pinter, R. Reginato, and J. Hatfield, "Normalizing the stress-degree-day parameter for environmental variability," *Agricultural Meteorology*, vol. 24, pp. 45–55, 1981.

[29] N. Abraham, P. Hema, E. Saritha, and S. Subramannian, "Irrigation automation based on soil electrical conductivity and leaf temperature," *Agricultural Water Management*, vol. 45, no. 2, pp. 145–157, 2000.

[30] C. Doulgeris, P. Georgiou, D. Papadimos, and D. Papamichail, "Water allocation under deficit irrigation using mike basin model for the mitigation of climate change," *Irrigation science*, vol. 33, no. 6, pp. 469–482, 2015.

[31] B. L. Blad, A. Bauer, J. L. Hatfield, E. T. Kanemasu, D. J. Major, R. J. Reginato, and K. G. Hubbard, "Influence of water and nitrogen levels on canopy temperatures of winter wheat grown in the north american great plains," *Agricultural and forest meteorology*, vol. 44, no. 2, pp. 159–173, 1988.

[32] D. A. Carroll, "Drought and nitrogen effects on maize canopy temperature and stress indices," 2015.

[33] N. C. Ward, "Nitrogen and water effects on canopy sensor measurements for site-specific management of crops," 2015.

[34] H. Alzaben, R. Fraser, and C. Swanton, "An inverse correlation between corn temperature and nitrogen stress: A field case study," *Agronomy Journal*, vol. 111, no. 6, pp. 1–13, 2019.

[35] M. H. Akbari, C. J. Swanton, J. J. Kay, and S. D. Murphy, *Energy-based indicators of ecosystem health.* 1996.

[36] D. Rickman, J. Luvall, J. Shaw, P. Mask, D. Kissel, and D. Sullivan, "Precision agriculture: Changing the face of farming," *Geotimes*, vol. 48, no. 11, pp. 28–33, 2003.

[37] R. Lawrence, "Thermal remote sensing and the exergy destruction principle applied to precision agriculture," 2016.

[38] H. G. Jones, "Use of infrared thermometry for estimation of stomatal conductance as a possible aid to irrigation scheduling," *Agricultural and forest meteorology*, vol. 95, no. 3, pp. 139–149, 1999.

[39] R. D. Jackson, "Canopy temperature and crop water stress," *Advances in irrigation*, vol. 1, pp. 43–85, 1982.

[40] U. Lee, C. Wie, B. O. Fernandez, M. Feelisch, and E. Vierling, "Modulation of nitrosative stress by s-nitrosoglutathione reductase is critical for thermotolerance and plant growth in arabidopsis," *The Plant Cell*, vol. 20, no. 3, pp. 786–802, 2008.

[41] T. Cools and L. De Veylder, "Dna stress checkpoint control and plant development," *Current opinion in plant biology*, vol. 12, no. 1, pp. 23–28, 2009.

[42] P. C. Scharf and V. C. Hubbard, "Method of predicting crop yield loss due to n-deficiency," May 16 2017. US Patent 9,652,691.

[43] V. Houles, M. Guerif, and B. Mary, "Elaboration of a nitrogen nutrition indicator for winter wheat based on leaf area index and chlorophyll content for making nitrogen recommendations," *European Journal of Agronomy*, vol. 27, no. 1, pp. 1–11, 2007.

[44] J. Jiyun, "Precision agriculture and its perspective in china [j]," *PLANT NATRITION AND FERTILIZEN SCIENCE*, vol. 1, 1998.

[45] R. Bongiovanni and J. Lowenberg-DeBoer, "Precision agriculture and sustainability," *Precision agriculture*, vol. 5, no. 4, pp. 359–387, 2004.

[46] P. J. Pinter Jr, J. L. Hatfield, J. S. Schepers, E. M. Barnes, M. S. Moran, C. S. Daughtry, and D. R. Upchurch, "Remote sensing for crop management," *Photogrammetric Engineering & Remote Sensing*, vol. 69, no. 6, pp. 647–664, 2003.

[47] N. Virlet, K. Sabermanesh, P. Sadeghi-Tehran, and M. J. Hawkesford, "Field scanalyzer: An automated robotic field phenotyping platform for detailed crop monitoring," *Functional Plant Biology*, vol. 44, no. 1, pp. 143–153, 2017.

[48] C. J. Bronick and R. Lal, "Soil structure and management: a review," *Geoderma*, vol. 124, no. 1, pp. 3–22, 2005.

[49] D. J. Mulla, "Twenty five years of remote sensing in precision agriculture: Key advances and remaining knowledge gaps," *Biosystems engineering*, vol. 114, no. 4, pp. 358–371, 2013.

[50] J. R. Schott, *Remote sensing: the image chain approach*. Oxford University Press on Demand, 2007.

[51] J. L. Guerrero-Rascado, F. J. Olmo Reyes, I. Avilés-Rodríguez, F. Navas-Guzmán, D. Pérez-Ramírez, H. Lyamani, L. Alados-Arboledas, *et al.*, "Extreme saharan dust event over the southern iberian peninsula in september 2007: active and passive remote sensing from surface and satellite," 2009.

[52] S. Lalwani and U. Ansari, "A new approach for increase resolution of satellite image," *IJETAE*, vol. 2, no. 5, 2012.

[53] A. Prakash, "Thermal remote sensing: concepts, issues and applications," *International Archives of Photogrammetry and Remote Sensing*, vol. 33, no. B1; PART 1, pp. 239–243, 2000.

[54] M. J. Wooster, G. Roberts, A. M. Smith, J. Johnston, P. Freeborn, S. Amici, and A. T. Hudak, "Thermal remote sensing of active vegetation fires and biomass burning events," in *Thermal Infrared Remote Sensing*, pp. 347–390, Springer, 2013.

[55] H. K. Lichtenthaler, "Vegetation stress: an introduction to the stress concept in plants," *Journal of plant physiology*, vol. 148, no. 1-2, pp. 4–14, 1996.

[56] M. Liu, A. K. Skidmore, T. Wang, X. Liu, L. Wu, and L. Tian, "An approach for heavy metal pollution detected from spatio-temporal stability of stress in rice using satellite images," *International Journal of Applied Earth Observation and Geoinformation*, vol. 80, pp. 230–239, 2019.

[57] L. Taiz and E. Zeiger, "Plant physiology, sinauer associates," 2002.

[58] W. Larcher, *Physiological plant ecology: ecophysiology and stress physiology of functional groups*. Springer Science & Business Media, 2003.

[59] S. Lenk, D. Van Der Straeten, and C. Buschmann, "Multi-sensor imaging of plant stresses: Towards the development of a stress-catalogue," 2009.

[60] G. Röll, J. Hartung, and S. Graeff-Hönninger, "Determination of plant nitrogen content in wheat plants via spectral reflectance measurements: Impact of leaf number and leaf position," *Remote Sensing*, vol. 11, no. 23, p. 2794, 2019.

[61] M. F. Buitrago, T. A. Groen, C. A. Hecker, and A. K. Skidmore, "Changes in thermal infrared spectra of plants caused by temperature and water stress," *ISPRS journal of photogrammetry and remote sensing*, vol. 111, pp. 22–31, 2016.

[62] R. D. Munson and Y. Kalra, *Principles of plant analysis*. CRC Press Boca Raton, FL, 1998.

[63] T. Blackmer and J. Schepers, "Use of a chlorophyll meter to monitor nitrogen status and schedule fertigation for corn," *Journal of production agriculture*, vol. 8, no. 1, pp. 56–60, 1995.

[64] S. Demotes-Mainard, R. Boumaza, S. Meyer, and Z. G. Cerovic, "Indicators of nitrogen status for ornamental woody plants based on optical measurements of leaf epidermal polyphenol and chlorophyll contents," *Scientia Horticulturae*, vol. 115, no. 4, pp. 377–385, 2008.

[65] M. L. Vitosh and G. H. Silva, "Factors affecting potato petiole sap nitrate tests," *Communications in Soil Science and Plant Analysis*, vol. 27, no. 5-8, pp. 1137–1152, 1996.

[66] S. E. Parks, D. E. Irving, and P. J. Milham, "A critical evaluation of on-farm rapid tests for measuring nitrate in leafy vegetables," *Scientia horticulturae*, vol. 134, pp. 1–6, 2012.

[67] N. Tremblay, E. Fallon, and N. Ziadi, "Sensing of crop nitrogen status: Opportunities, tools, limitations, and supporting information requirements," *HortTechnology*, vol. 21, no. 3, pp. 274–281, 2011.

[68] T. Blackmer, J. Schepers, and G. Meyer, "Remote sensing to detect nitrogen deficiency in corn," in *Site-specific management for agricultural systems*, no. sitespecificman, pp. 505–512, American Society of Agronomy, Crop Science Society of America, Soil Science Society of America, 1995.

[69] I. TARTACHNYK and I. RADEMACHER, "Estimation of nitrogen deficiency of sugar beet and wheat using parameters of laser induced and pulse amplitude modulated chlorophyll fluorescence," *Journal of applied botany*, vol. 77, no. 3-4, pp. 61–67, 2003.

[70] Y. Zhang and N. Tremblay, "Evaluation of the multiplex® fluorescence sensor for the assessment of corn nitrogen status," in *10th International Conference on Precision Agriculture, Denver, Colorado*, pp. 18–21, 2010.

[71] L. Li, Q. Zhang, and D. Huang, "A review of imaging techniques for plant phenotyping," *Sensors*, vol. 14, no. 11, pp. 20078–20111, 2014.

[72] J. Belasque Jr, M. Gasparoto, and L. G. Marcassa, "Detection of mechanical and disease stresses in citrus plants by fluorescence spectroscopy," *Applied Optics*, vol. 47, no. 11, pp. 1922–1926, 2008.

[73] M. Govender, P. Govender, I. Weiersbye, E. Witkowski, and F. Ahmed, "Review of commonly used remote sensing and ground-based technologies to measure plant water stress," *Water Sa*, vol. 35, no. 5, 2009.

[74] D. Krezhova, "Hyperspectral remote sensing of reflected and emitted radiation as a means for preservation of terrestrial ecosystems," in *RAD Proceedings of 1st International Conference on Radiation and Dosimetry in Various Fields of Research, Niš, Serbia*, pp. 71–74, 2012.

[75] R. Jackson, "Idso. wheat canopy temperature: a practical tool for evaluating water requirements," *W ater resourcesM anagem ent*, vol. 13, p. 6512656, 1977.

[76] N. Gontia and K. Tiwari, "Development of crop water stress index of wheat crop for scheduling irrigation using infrared thermometry," *Agricultural water management*, vol. 95, no. 10, pp. 1144–1152, 2008.

[77] H. G. Jones, "Application of thermal imaging and infrared sensing in plant physiology and ecophysiology," in *Advances in Botanical Research*, vol. 41, pp. 107–163, Elsevier, 2004.

[78] M. El-Shirbeny, A. Ali, A. Rashash, and M. Badr, "Wheat yield response to water deficit under central pivot irrigation system using remote sensing techniques," *World Journal of Engineering and Technology*, vol. 3, no. 03, p. 65, 2015.

[79] S. Irmak, D. Z. Haman, and R. Bastug, "Determination of crop water stress index for irrigation timing and yield estimation of corn," *Agronomy Journal*, vol. 92, no. 6, pp. 1221–1227, 2000.

[80] S. Siebert, F. Ewert, E. E. Rezaei, H. Kage, and R. Graß, "Impact of heat stress on crop yield—on the importance of considering canopy temperature," *Environmental Research Letters*, vol. 9, no. 4, p. 044012, 2014.

[81] S. Fahad, A. A. Bajwa, U. Nazir, S. A. Anjum, A. Farooq, A. Zohaib, S. Sadia, W. Nasim, S. Adkins, S. Saud, *et al.*, "Crop production under drought and heat stress: plant responses and management options," *Frontiers in Plant Science*, vol. 8, p. 1147, 2017.

[82] G. Arnold, P. Ozanne, K. Galbraith, and F. Dandridge, "The capeweed content of pastures in south-west western australia," *Animal Production Science*, vol. 25, no. 1, pp. 117–123, 1985.

[83] L. W. Lass, T. S. Prather, N. F. Glenn, K. T. Weber, J. T. Mundt, and J. Pettingill, "A review of remote sensing of invasive weeds and example of the early detection

of spotted knapweed (centaurea maculosa) and babysbreath (gypsophila paniculata) with a hyperspectral sensor," *Weed Science*, vol. 53, no. 2, pp. 242–251, 2005.

[84] C. Daughtry, C. Walthall, M. Kim, E. B. De Colstoun, and J. McMurtrey, "Estimating corn leaf chlorophyll concentration from leaf and canopy reflectance," *Remote sensing of Environment*, vol. 74, no. 2, pp. 229–239, 2000.

[85] P. J. Zarco-Tejada, J. R. Miller, G. H. Mohammed, T. L. Noland, and P. H. Sampson, "Chlorophyll fluorescence effects on vegetation apparent reflectance: Ii. laboratory and airborne canopy-level measurements with hyperspectral data," *Remote Sensing of Environment*, vol. 74, no. 3, pp. 596–608, 2000.

[86] P. Reiniger and B. Seguin, "Surface temperature as an indicator of evapotranspiration and soil moisture," *Remote Sensing Reviews*, vol. 1, no. 2, pp. 277–310, 1986.

[87] R. Aerts, T. Wagendorp, E. November, M. Behailu, J. Deckers, and B. Muys, "Ecosystem thermal buffer capacity as an indicator of the restoration status of protected areas in the northern ethiopian highlands," *Restoration Ecology*, vol. 12, no. 4, pp. 586–596, 2004.

[88] H. Holbo and J. Luvall, "Modeling surface temperature distributions in forest landscapes," *Remote Sensing of Environment*, vol. 27, no. 1, pp. 11–24, 1989.

[89] D. A. Quattrochi and J. C. Luvall, *Thermal remote sensing in Earth science research.* SAGE Publications Ltd.: London, UK, 2009.

[90] H. Lin, Z. Fan, L. Shi, A. Arain, H. McCaughey, D. Billesbach, M. Siqueira, R. Bracho, and W. Oechel, "The cooling trend of canopy temperature during the maturation, succession, and recovery of ecosystems," *Ecosystems*, pp. 1–10, 2016.

[91] J. Luvall and H. Holbo, "Measurements of short-term thermal responses of coniferous forest canopies using thermal scanner data," *Remote sensing of environment*, vol. 27, no. 1, pp. 1–10, 1989.

[92] D. Lieberman and M. Lieberman, "Estimation of tropical forest canopy temperatures, thermal response numbers, and evapotranspiration using an aircraft-based thermal sensor," *Photogrammetric Engineering and Remote Sensing*, vol. 56, no. 10, pp. 1393–1401, 1990.

[93] R. Fraser and J. J. Kay, "Exergy analysis of ecosystems: establishing a role for thermal remote sensing," *Thermal Remote sensing in Land Surface Processes. Quattrochi D, Luvall J (eds). CRC Press: Boca Raton, FL*, pp. 283–360, 2004.

[94] E. A. Silow, A. V. Mokry, and S. E. Jørgensen, "Some applications of thermodynamics for ecological systems," in *Thermodynamics-Interaction Studies-Solids, Liquids and Gases*, IntechOpen, 2011.

[95] Z. Rant, "Exergie, ein neues wort fur 'technische arbeitsfaehigkeit'(exergy, a new word for technical availability)," *Forschung auf dem Gebiet des Ingenieurwesens A*, vol. 22, no. 1, pp. 36–37, 1956.

[96] G. Wall and M. Gong, "On exergy and sustainable development—part 1: Conditions and concepts," *Exergy, An International Journal*, vol. 1, no. 3, pp. 128–145, 2001.

[97] Y. A. Cengel and M. A. Boles, "Thermodynamics: an engineering approach," *Sea*, vol. 1000, p. 8862, 2002.

[98] G. Wall, *Exergy-a useful concept within resource accounting*. Chalmers tekniska högskola, Göteborgs universitet, 1977.

[99] T. J. Kotas, *The exergy method of thermal plant analysis*. Elsevier, 2013.

[100] R. L. Cornelissen, "Thermodynamics and sustainable development: The use of exergy analysis and the reduction of irreversibility.," 1999.

[101] R. L. Cornelissen and G. G. Hirs, "The value of the exergetic life cycle assessment besides the lca," *Energy conversion and management*, vol. 43, no. 9-12, pp. 1417–1424, 2002.

[102] G. Wall, "Exergy conversion in the swedish society," *Resources and Energy*, vol. 9, no. 1, pp. 55–73, 1987.

[103] G. Wall, "Exergy conversion in the japanese society," *Energy*, vol. 15, no. 5, pp. 435–444, 1990.

[104] E. D. Schneider and J. J. Kay, "Life as a manifestation of the second law of thermodynamics," *Mathematical and computer modelling*, vol. 19, no. 6-8, pp. 25–48, 1994.

[105] E. D. Schneider and J. J. Kay, "Complexity and thermodynamics: towards a new ecology," *Futures*, vol. 26, no. 6, pp. 626–647, 1994.

[106] E. Schrödinger, *What is life?: With mind and matter and autobiographical sketches*. Cambridge University Press, 1992.

[107] W. Maes, T. Pashuysen, A. Trabucco, F. Veroustraete, and B. Muys, "Does energy dissipation increase with ecosystem succession? testing the ecosystem exergy theory combining theoretical simulations and thermal remote sensing observations," *Ecological modelling*, vol. 222, no. 23, pp. 3917–3941, 2011.

[108] S. E. Jørgensen and S. N. Nielsen, "Application of exergy as thermodynamic indicator in ecology," *Energy*, vol. 32, no. 5, pp. 673–685, 2007.

[109] P. N. Knudsen, *Testing and analysis of an exergetically efficient 4 K to 2 K helium heat exchanger*. Old Dominion University, 2016.

[110] J. Kay, "Ecosystems as self-organizing holarchic open systems," *Handbook of Ecosystems Theories and Management, CRS Press, Lewis Publishers*, 2000.

[111] D. Jou, J. Casas-Vázquez, and G. Lebon, "Nonequilibrium entropy and the second law of thermodynamics: A simple illustration," *International journal of thermophysics*, vol. 14, no. 4, pp. 671–683, 1993.

[112] B. Adrian, "Advanced engineering thermodynamics," 1988.

[113] K. Gaudreau, "Exergy analysis and resource accounting," 2009.

[114] I. Prigogine and P. Glansdorff, *Thermodynamic Theory of Structure, Stability and Fluctuations Structure, Stability and Fluctuations*. Wiley-Interscience, 1971.

[115] I. Prigogine and S. Ji, "Schrödinger and the riddle of life molecular theories of cell life and death," in *Conference*, Rutgers University Press, 1991.

[116] J. Kay, T. Allen, R. Fraser, J. Luvall, and R. Ulanowicz, "Can we use energy based indicators to characterize and measure the status of ecosystems, human, disturbed and natural," in *Proceedings of the international workshop: Advances in Energy Studies: exploring supplies, constraints and strategies*, pp. 121–133, SGE Editoriali Padova, 2001.

[117] I. Prigogine and J.-M. Wiame, "Biologie et thermodynamique des phénomènes irréversibles," *Experientia*, vol. 2, no. 11, pp. 451–453, 1946.

[118] J. C. Luvall and D. A. Quattrochi, "Thermal characteristics of urban landscapes," 1998.

[119] J. C. Luvall, D. Rickman, and R. Fraser, "Thermal remote sensing and the thermodynamics of ecosystem development," in *AGU Fall Meeting Abstracts*, 2013.

[120] J. J. Kay and E. D. Schneider, "Thermodynamics and measures of ecological integrity," in *Ecological indicators*, pp. 159–182, Springer, 1992.

[121] H. Lin, H. Zhang, and Q. Song, "Transition from abstract thermodynamic concepts to perceivable ecological indicators," *Ecological indicators*, vol. 88, pp. 37–42, 2018.

[122] D. A. Quattrochi and J. C. Luvall, *Thermal remote sensing in land surface processing*. CRC Press, 2004.

[123] R. J. Holdaway, A. D. Sparrow, and D. A. Coomes, "Trends in entropy production during ecosystem development in the amazon basin," *Philosophical Transactions of the Royal Society B: Biological Sciences*, vol. 365, no. 1545, pp. 1437–1447, 2010.

[124] J. T. Finn, "Re ulanowicz: Growth and development: Ecosystems phenomenology. new york, springer-verlag, 1986, 203 pp.," *Behavioral Science*, vol. 33, no. 2, pp. 158–159, 1988.

[125] W. Duncan, A. Hatfield, and J. Ragland, "The growth and yield of corn. ii. daily growth of corn kernels 1," *Agronomy Journal*, vol. 57, no. 2, pp. 221–223, 1965.

[126] R. Nunez and E. Kamprath, "Relationships between n response, plant population, and row width on growth and yield of corn 1," *Agronomy journal*, vol. 61, no. 2, pp. 279–282, 1969.

[127] Z. Ni, Z. Liu, H. Huo, Z.-L. Li, F. Nerry, Q. Wang, and X. Li, "Early water stress detection using leaf-level measurements of chlorophyll fluorescence and temperature data," *Remote Sensing*, vol. 7, no. 3, pp. 3232–3249, 2015.

[128] T. D. Havlicek, *Ecosystem responses to stress and complexity as evidenced from experiments on a small-scale vegetative system.* University of Wisconsin–Madison, 1999.

[129] J. Kay, *The ecosystem approach: complexity, uncertainty, and managing for sustainability.* Columbia University Press, 2008.

[130] T. Allen and T. W. HOEKSTRA, "Toward a unified ecology columbia university press," *New York, Chichester (West Sussex)*, 1992.

[131] B. Feng, H. Yu, Y. Hu, X. Gao, J. Gao, D. Gao, and S. Zhang, "The physiological characteristics of the low canopy temperature wheat (triticum aestivum l.) genotypes under simulated drought condition," *Acta physiologiae plantarum*, vol. 31, no. 6, pp. 1229–1235, 2009.

[132] R. Bhatt and A. Hossain, "Concept and consequence of evapotranspiration for sustainable crop production in the era of climate change," in *Advanced Evapotranspiration Methods and Applications*, IntechOpen, 2019.

[133] N. H. Abu-Hamdeh and R. C. Reeder, "Soil thermal conductivity effects of density, moisture, salt concentration, and organic matter," *Soil science society of America Journal*, vol. 64, no. 4, pp. 1285–1290, 2000.

[134] A. J. Picón, R. Vásquez, J. González, J. Luvall, and D. Rickman, "Use of remote sensing observations to study the urban climate on tropical coastal cities," *Revista Umbral*, pp. 218–232, 2009.

[135] T. Oke, "Boundary layer climates(book)," *London, Methuen and Co., Ltd.; New York, Halsted Press, 1978. 390 p*, 1978.

[136] Z. Samani, A. S. Bawazir, M. Bleiweiss, R. Skaggs, and V. D. Tran, "Estimating daily net radiation over vegetation canopy through remote sensing and climatic data," *Journal of irrigation and drainage engineering*, vol. 133, no. 4, pp. 291–297, 2007.

[137] Z. Samani, A. S. Bawazir, R. K. Skaggs, M. P. Bleiweiss, A. Piñon, and V. Tran, "Water use by agricultural crops and riparian vegetation: an application of remote

sensing technology," *Journal of Contemporary Water Research & Education*, vol. 137, no. 1, pp. 8–13, 2007.

[138] J. Nolan, "Mitigating heat island effect in the urban environment,"

[139] D. Hillel, *Introduction to environmental soil physics*. Elsevier, 2003.

[140] S. Wright, D. Scott, J. Haddow, and M. Rosen, "On the entropy of radiative heat transfer in engineering thermodynamics," *International journal of engineering science*, vol. 39, no. 15, pp. 1691–1706, 2001.

[141] A. Bejan, *Advanced engineering thermodynamics*. John Wiley & Sons, 2016.

[142] A. Stefanescu, "Energy conversion and entropy production in open systems," 1996.

[143] R. Feistel, "Entropy flux and entropy production of stationary black-body radiation," *Journal of Non-Equilibrium Thermodynamics*, vol. 36, no. 2, pp. 131–139, 2011.

[144] M. Planck, *Theorie der Wärmestrahlung*. JA Barth, 1966.

[145] S. Kabelac, "Thermodynamik der strahlung, braunschweig," 1994.

[146] Z. Chen, S. Mo, P. Hu, S. Jiang, G. Wang, and X. Cheng, "Entropy flow, entropy generation, exergy flux, and optimal absorbing temperature in radiative transfer between parallel plates," *Frontiers of Energy and Power Engineering in China*, vol. 4, no. 3, pp. 301–305, 2010.

[147] G. Stephens and D. O'brien, "Entropy and climate. i: Erbe observations of the entropy production of the earth," *Quarterly Journal of the Royal Meteorological Society*, vol. 119, no. 509, pp. 121–152, 1993.

[148] R. Petela, "Exergy of heat radiation," 1964.

[149] P. Landsberg and G. Tonge, "Thermodynamics of the conversion of diluted radiation," *Journal of Physics A: Mathematical and General*, vol. 12, no. 4, p. 551, 1979.

[150] S. Kabelac, "A new look at the maximum conversion efficiency of black-body radiation," *Solar Energy*, vol. 46, no. 4, pp. 231–236, 1991.

[151] H. Ozawa, A. Ohmura, R. D. Lorenz, and T. Pujol, "The second law of thermodynamics and the global climate system: A review of the maximum entropy production principle," *Reviews of Geophysics*, vol. 41, no. 4, 2003.

[152] W. H. Press, "Theoretical maximum for energy from direct and diffuse sunlight," *Nature*, vol. 264, no. 5588, pp. 734–735, 1976.

[153] P. Landsberg and J. Mallinson, "Thermodynamic constraints, effective temperatures and solar cells," in *International Conference on Solar Electricity*, pp. 27–42, 1976.

[154] M. Israel, *Entwicklung eines UAV-basierten Systems zur Rehkitzsuche und Methoden zur Detektion und Georeferenzierung von Rehkitzen in Thermalbildern: Der Fliegende Wildretter*. PhD thesis, Universität Osnabrück, 2016.

[155] F. Niklaus, C. Vieider, and H. Jakobsen, "Mems-based uncooled infrared bolometer arrays: a review," in *MEMS/MOEMS technologies and applications III*, vol. 6836, p. 68360D, International Society for Optics and Photonics, 2008.

[156] X. Sui, Q. Chen, and G. Gu, "Nonuniformity correction of infrared images based on infrared radiation and working time of thermal imager," *Optik-International Journal for Light and Electron Optics*, vol. 124, no. 4, pp. 352–356, 2013.

[157] H. G. Jones, M. Stoll, T. Santos, C. d. Sousa, M. M. Chaves, and O. M. Grant, "Use of infrared thermography for monitoring stomatal closure in the field: application to grapevine," *Journal of Experimental Botany*, vol. 53, no. 378, pp. 2249–2260, 2002.

[158] W. Maes and K. Steppe, "Estimating evapotranspiration and drought stress with ground-based thermal remote sensing in agriculture: a review," *Journal of Experimental Botany*, vol. 63, no. 13, pp. 4671–4712, 2012.

[159] F. Di Felice, A. Mazzini, G. Di Stefano, and G. Romeo, "Drone high resolution infrared imaging of the lusi mud eruption," *Marine and Petroleum Geology*, vol. 90, pp. 38–51, 2018.

[160] K. Subedi and B. Ma, "Assessment of some major yield-limiting factors on maize production in a humid temperate environment," *Field crops research*, vol. 110, no. 1, pp. 21–26, 2009.

[161] L. Echarte, S. Rothstein, and M. Tollenaar, "The response of leaf photosynthesis and dry matter accumulation to nitrogen supply in an older and a newer maize hybrid," *Crop Science*, vol. 48, no. 2, pp. 656–665, 2008.

[162] M. Bhandari *et al.*, *Use of Infrared Thermal Imaging for Estimating Canopy Temperature in Wheat and Maize*. PhD thesis, 2016.

[163] D. Song and B. Bhushan, "Bioinspired triangular patterns for water collection from fog," *Philosophical Transactions of the Royal Society A*, vol. 377, no. 2150, p. 20190128, 2019.

[164] M. E. SAFTY, "Use and organization of domestic space in the arab world," *International Journal of Sociology of the Family*, pp. 179–199, 1981.

[165] C. E. Greub, T. L. Roberts, N. A. Slaton, J. P. Kelley, and E. E. Gbur, "Evaluating tissue tests to improve nitrogen management in furrow-irrigated mid-south corn production," *Agronomy Journal*, vol. 110, no. 4, pp. 1580–1588, 2018.

[166] K. L. Sahrawat, "Plant nutrients: sufficiency and requirements," *Encyclopedia of soil science*, pp. 1306–1310, 2006.

[167] A. P. Mallarino, A. Pagani, and J. E. Sawyer, "Corn and soybean response to soil ph level and liming," 2011.

[168] A. McCauley, C. Jones, and J. Jacobsen, "Soil ph and organic matter," *Nutrient management module*, vol. 8, no. 2, pp. 1–12, 2009.

[169] D. Bullock and D. Anderson, "Evaluation of the minolta spad-502 chlorophyll meter for nitrogen management in corn," *Journal of Plant Nutrition*, vol. 21, no. 4, pp. 741–755, 1998.

[170] J. M. L. Corte, A. M. Ruiz, A. O. Hernandez, E. J. V. Ramirez, M. E. M. Beltran, J. F. L. de la Rocha, P. H. Herrera, and E. D. Lopez, "Effect of nitrogen on agronomic yield, spad units and nitrate content in roselle (hibiscus sabdariffal.) in dry weather," *International Journal of Environment, Agriculture and Biotechnology*, vol. 1, no. 4.

[171] Z. Yuan, Q. Cao, K. Zhang, S. T. Ata-Ul-Karim, Y. Tian, Y. Zhu, W. Cao, and X. Liu, "Optimal leaf positions for spad meter measurement in rice," *Frontiers in plant science*, vol. 7, p. 719, 2016.

[172] L. F. Ratliff, J. T. Ritchie, and D. K. Cassel, "Field-measured limits of soil water availability as related to laboratory-measured properties 1," *Soil Science Society of America Journal*, vol. 47, no. 4, pp. 770–775, 1983.

[173] G. Dovrat, T. Masci, H. Bakhshian, E. Mayzlish Gati, S. Golan, and E. Sheffer, "Drought-adapted plants dramatically downregulate dinitrogen fixation: Evidences from mediterranean legume shrubs," *Journal of Ecology*, vol. 106, no. 4, pp. 1534–1544, 2018.

[174] R. E. Neild and J. E. Newman, *Growing season characteristics and requirements in the Corn Belt*. Cooperative Extension Service, Iowa State University, 1987.

[175] S. Taghvaeian, L. Comas, K. C. DeJonge, and T. J. Trout, "Conventional and simplified canopy temperature indices predict water stress in sunflower," *Agricultural water management*, vol. 144, pp. 69–80, 2014.

[176] B. S. Chauhan and J. L. Opeña, "Effect of plant geometry on growth and yield of corn in the rice-corn cropping system," *American Journal of Plant Sciences*, vol. 4, no. 10, p. 1928, 2013.

[177] P. Kadam and S. Bhalerao, "Sample size calculation," *International journal of Ayurveda research*, vol. 1, no. 1, p. 55, 2010.

[178] G. D. Israel, "Determining sample size," 1992.

[179] D. S. Kimes, S. Idso, P. Pinter Jr, R. Reginato, and R. Jackson, "View angle effects in the radiometric measurement of plant canopy temperatures," *Remote Sensing of Environment*, vol. 10, no. 4, pp. 273–284, 1980.

[180] M. K. Nanda, U. Giri, and N. Bera, "Canopy temperature-based water stress indices: Potential and limitations," in *Advances in Crop Environment Interaction*, pp. 365–385, Springer, 2018.

[181] H. Schneider, T. Maier, J. Fleissner, M. Walther, P. Koidl, G. Weimann, W. Cabanski, M. Finck, P. Menger, W. Rode, *et al.*, "Dual-band qwip focal plane array for the second and third atmospheric windows," *Infrared physics & technology*, vol. 47, no. 1-2, pp. 53–58, 2005.

[182] M. Mancuso and F. Bustaffa, "A wireless sensors network for monitoring environmental variables in a tomato greenhouse," in *IEEE International Workshop on Factory Communication Systems*, vol. 10, 2006.

[183] D. Hamby, "A review of techniques for parameter sensitivity analysis of environmental models," *Environmental monitoring and assessment*, vol. 32, no. 2, pp. 135–154, 1994.

[184] F. Pianosi, K. Beven, J. Freer, J. W. Hall, J. Rougier, D. B. Stephenson, and T. Wagener, "Sensitivity analysis of environmental models: A systematic review with practical workflow," *Environmental Modelling & Software*, vol. 79, pp. 214–232, 2016.

[185] Z.-y. Zheng, Z.-g. Wei, Z.-p. Wen, W.-j. Dong, Z.-c. Li, X.-h. Wen, X. Zhu, C. Chen, and S.-s. Hu, "A study of variation characteristics of gobi broadband emissivity based

on field observational experiments in northwestern china," *Theoretical and applied climatology*, vol. 131, no. 3-4, pp. 1357–1368, 2018.

[186] C. Chen, "Determining the leaf emissivity of three crops by infrared thermometry," *Sensors*, vol. 15, no. 5, pp. 11387–11401, 2015.

[187] L. González-Fernández, E. Risueño, R. Pérez-Sáez, and M. Tello, "Infrared normal spectral emissivity of ti–6al–4v alloy in the 500–1150 k temperature range," *Journal of alloys and compounds*, vol. 541, pp. 144–149, 2012.

[188] F. Jabbari, A. Aziz, S. Saedodin, and M. Torabi, "Transient thermal analysis of a rectangular radiation heat shield with spatially dependent emissivities," *Arabian Journal for Science and Engineering*, vol. 38, no. 12, pp. 3495–3504, 2013.

[189] A. López, F. Molina-Aiz, D. Valera, and A. Peña, "Determining the emissivity of the leaves of nine horticultural crops by means of infrared thermography," *Scientia Horticulturae*, vol. 137, pp. 49–58, 2012.

[190] Y. Zhuang, *Thermal Properties of Leaf Traits*. University of Twente Faculty of Geo-Information and Earth Observation (ITC), 2014.

[191] M. Fuchs and C. Tanner, "Infrared thermometry of vegetation 1," *Agronomy Journal*, vol. 58, no. 6, pp. 597–601, 1966.

[192] C. Coll, V. Caselles, E. Rubio, E. Valor, and F. Sospedra, "Field emissivity measurements during the reseda experiment," *Physics and Chemistry of the Earth (Part B)*, 2000.

[193] J. W. Salisbury, "Preliminary measurements of leaf spectral reflectance in the 8-14 μm region," *International Journal of Remote Sensing*, vol. 7, no. 12, pp. 1879–1886, 1986.

[194] E. Rubio, V. Caselles, and C. Badenas, "Emissivity measurements of several soils and vegetation types in the 8–14, μm wave band: Analysis of two field methods," *Remote Sensing of Environment*, vol. 59, no. 3, pp. 490–521, 1997.

[195] C. Wong and W. Blevin, "Infrared reflectances of plant leaves," *Australian Journal of Biological Sciences*, vol. 20, no. 3, pp. 501–508, 1967.

[196] P. Kolattukudy, "Enzymatic penetration of the plant cuticle by fungal pathogens," *Annual review of phytopathology*, vol. 23, no. 1, pp. 223–250, 1985.

[197] B. R. da Luz and J. K. Crowley, "Spectral reflectance and emissivity features of broad leaf plants: Prospects for remote sensing in the thermal infrared (8.0–14.0 μm)," *Remote sensing of environment*, vol. 109, no. 4, pp. 393–405, 2007.

[198] A. Van de Griend and M. OWE, "On the relationship between thermal emissivity and the normalized difference vegetation index for natural surfaces," *International Journal of remote sensing*, vol. 14, no. 6, pp. 1119–1131, 1993.

[199] M. Gerhards, G. Rock, M. Schlerf, and T. Udelhoven, "Water stress detection in potato plants using leaf temperature, emissivity, and reflectance," *International journal of applied Earth observation and geoinformation*, vol. 53, pp. 27–39, 2016.

[200] P. Pampaloni and S. Paloscia, "Microwave emission and plant water content: A comparison between field measurements and theory," *IEEE Transactions on Geoscience and Remote Sensing*, no. 6, pp. 900–905, 1986.

[201] E. Neinavaz, R. Darvishzadeh, A. K. Skidmore, and T. A. Groen, "Measuring the response of canopy emissivity spectra to leaf area index variation using thermal hyperspectral data," *International journal of applied Earth observation and geoinformation*, vol. 53, pp. 40–47, 2016.

[202] S. Ullah, M. Schlerf, A. K. Skidmore, and C. Hecker, "Identifying plant species using mid-wave infrared (2.5–6 μm) and thermal infrared (8–14 μm) emissivity spectra," *Remote Sensing of Environment*, vol. 118, pp. 95–102, 2012.

[203] L. Kirkland, K. Herr, E. Keim, P. Adams, J. Salisbury, J. Hackwell, and A. Treiman, "First use of an airborne thermal infrared hyperspectral scanner for compositional mapping," *Remote Sensing of Environment*, vol. 80, no. 3, pp. 447–459, 2002.

[204] H. Buddenbaum, G. Rock, J. Hill, and W. Werner, "Measuring stress reactions of beech seedlings with pri, fluorescence, temperatures and emissivity from vnir and thermal field imaging spectroscopy," *European Journal of Remote Sensing*, vol. 48, no. 1, pp. 263–282, 2015.

[205] A. N. Watson, "Preliminary study of the relation between thermal emissivity and plant temperatures," 1933.

[206] L. T. Wang and T. L. De Liberty, "Landsat atmospheric correction: The good, the bad, and the ugly," in *2005 ESRI International User Conference Proc*, 2005.

[207] W. Minkina and S. Dudzik, *Infrared thermography: errors and uncertainties*. John Wiley & Sons, 2009.

[208] J. J. Picotte, D. M. Rosenthal, J. M. Rhode, and M. B. Cruzan, "P lastic responses to temporal variation in moisture availability: consequences for water use efficiency and plant performance," *Oecologia*, vol. 153, no. 4, pp. 821–832, 2007.

[209] A. Sansom, *Water in Texas: an introduction*. University of Texas Press, 2008.

[210] P.-L. Lizotte, P. Savoie, and A. De Champlain, "Ash content and calorific energy of corn stover components in eastern canada," *Energies*, vol. 8, no. 6, pp. 4827–4838, 2015.

[211] S. S. Anapalli, T. R. Green, K. N. Reddy, P. H. Gowda, R. Sui, D. K. Fisher, J. E. Moorhead, and G. W. Marek, "Application of an energy balance method for estimating evapotranspiration in cropping systems," *Agricultural Water Management*, vol. 204, pp. 107–117, 2018.

[212] "Measuring the temperature of the sky and clouds." `https://mynasadata.larc.nasa.gov`. Accessed: 2020-04-20.

[213] J. H. McIntyre, "Photovoltaic potential in the city of guelph," *Guelph Eng J*, vol. 1, no. 1, pp. 24–26, 2008.

[214] J. De Beer, *Potential for industrial energy-efficiency improvement in the long term*, vol. 5. Springer Science & Business Media, 2013.

[215] B. A. Qureshi and S. M. Zubair, "Application of exergy analysis to various psychrometric processes," *International Journal of Energy Research*, vol. 27, no. 12, pp. 1079–1094, 2003.

[216] M. Salazar-Pereyra, M. Toledo-Velázquez, G. T. Eslava, R. Lugo-Leyte, C. R. Rosas, *et al.*, "Energy and exergy analysis of moist air for application in power plants," *Energy and Power Engineering*, vol. 3, no. 3, pp. 376–381, 2011.

APPENDICES

Appendix A

Crop temperature sensitivity analysis

Different variables affect crop canopy temperature either directly or indirectly. Such variables include: applied nitrogen rate (N), variation in solar irradiance ($\dot{\phi}_{Solarinput}$), air temperature (T_{air}), soil temperature (T_{soil}), vapor pressure deficit (VPD), soil moisture ($Soil_{moist}$), humidity (RH), wind speed (V), time of the day (t), cloud cover(CC), crop genetics (G), leaf angle (θ_{Leaf}), leaf emissivity (ε), sensor view angle (θ), and many other variables. Canopy temperature can be expressed as a function of those variables as presented in Equation A.1

$$T_{Canopy} = f(N, \dot{\phi}_{Solar\_input}, T_{air}, T_{soil}, T_{VPD}, S_{moist}, RH, V, t, CC, G, \theta_{Leaf}, \varepsilon, \theta_{Sensor}) \quad \text{(A.1)}$$

Sensitivity and uncertainty analyses usually run in tandem, sensitivity analysis extends the uncertainty analysis by describing how the uncertainty in the output variable (T_{Canopy}) can be apportioned to different sources of uncertainty in the input variables (e.g., N,

$\dot{\phi}_{Solarinput}$,T_{air} . . . ,etc). The general error or uncertainty propagation equation as a function of two variables x and y is given in Equation A.2.

$$\sigma_u{}^2 = \sigma_x{}^2\left(\frac{\partial u}{\partial x}\right)^2 + \sigma_y{}^2\left(\frac{\partial u}{\partial y}\right)^2 + 2\sigma^2{}_{xy}\left(\frac{\partial u}{\partial x}\right)\left(\frac{\partial u}{\partial y}\right) \tag{A.2}$$

Where: x and y are independent variables, σ_{xy} is the correlation between the two input variables, also referred to as a cross-correlation,$\sigma_x$and σ_y are the standard deviations in the input variables. It is common to assume the independence of input variables, in which case a cross-correlation, σ_{xy} is zero, so Equation A.2 can be re-written as follows:

$$\sigma_u{}^2 = \sigma_x{}^2\left(\frac{\partial u}{\partial x}\right)^2 + \sigma_y{}^2\left(\frac{\partial u}{\partial y}\right)^2 \tag{A.3}$$

The partial derivatives ($\frac{\partial u}{\partial x}$, $\frac{\partial u}{\partial y}$), which are often referred as sensitivity coefficients and the uncertainties (σ_x,σ_y ,σ_{xy}) are to be calculated from the collected data. It is typical to use either one standard deviation (1σ) or two standard deviations (2σ) for the uncertainties σ_x,σ_y,σ_{xy}. 1σ captures 68.26% of the data and 2σ captures 95.44% of the data for a Gaussian distributed random data. It is assumed for T_{canopy} that all the variables are independent except air temperature and humidity, which are known to have a direct positive correlation [182]. Therefore, the T_{canopy} uncertainty propagation equation can be

written as in Equation A.4:

$$\sigma^2{}_{T_{canopy}} = \sigma^2{}_N\left(\frac{\partial T_{canopy}}{\partial N}\right)^2 + \sigma^2{}_{\dot{\phi}_{solar\_input}}\left(\frac{\partial T_{canopy}}{\partial \dot{\phi}_{solar\_input}}\right)^2 + \sigma^2{}_{T_{air}}\left(\frac{\partial T_{canopy}}{\partial T_{air}}\right)^2 + \sigma^2{}_{T_{soil}}\left(\frac{\partial T_{canopy}}{\partial T_{soil}}\right)^2 + \sigma^2{}_{soil_{moist}}\left(\frac{\partial T_{canopy}}{\partial soil_{moist}}\right)^2 + \sigma^2{}_{RH}\left(\frac{\partial T_{canopy}}{\partial RH}\right)^2 + \sigma^2{}_V\left(\frac{\partial T_{canopy}}{\partial V}\right)^2 + \sigma^2{}_G\left(\frac{\partial T_{canopy}}{\partial G}\right)^2 + \sigma^2{}_{\theta_{leaf}}\left(\frac{\partial T_{canopy}}{\partial \theta_{leaf}}\right)^2 + \sigma^2{}_{\varepsilon}\left(\frac{\partial T_{canopy}}{\partial \varepsilon}\right)^2 + \sigma^2{}_{\theta_{Sensor}}\left(\frac{\partial T_{canopy}}{\partial \theta_{Sensor}}\right)^2 \quad \text{(A.4)}$$

Where the uncertainty contribution from the dependence of humidity on air temperature is captured in the cross-correlation term of Equation A.4. In order to understand how the T_{canopy} uncertainty change for the changes in the input variables, a sensitivity coefficient is commonly calculated and quantified. A sensitivity coefficient is defined as the ratio of the output to the input variable ($\frac{\partial y}{\partial x}$) and is calculated to observe how much the output variable changes for a given change in the input variable under the assumption that independent variables are uncorrelated, and the effect of humidity variation is negligible given the short distance from the camera sensor to the plant surface, and that the partial derivative is to be taken at a fixed value. Given those assumptions, it follows that the variable that has the highest sensitivity coefficient will have a greater impact in the output change (T_{canopy}). The sensitivity coefficients (S) for Equation A.4 are as follows:

$$S_N = \left(\frac{\partial T_{Canopy}}{\partial N}\right), S_{\dot{\phi}_{solar\_input}} = \left(\frac{\partial T_{Canopy}}{\partial \dot{\phi}_{solar\_input}}\right), S_{T_{air}} = \left(\frac{\partial T_{Canopy}}{\partial T_{air}}\right), S_{T_{Soil}} = \left(\frac{\partial T_{Canopy}}{\partial T_{Soil}}\right)$$
$$, S_{Soil_{moist}} = \left(\frac{\partial T_{Canopy}}{\partial Soil_{moist}}\right), S_{RH} = \left(\frac{\partial T_{Canopy}}{\partial T_{RH}}\right), S_V = \left(\frac{\partial T_{Canopy}}{\partial V}\right), S_G = \left(\frac{\partial T_{Canopy}}{\partial G}\right)$$
$$, S_{\theta_{Leaf}} = \left(\frac{\partial T_{Canopy}}{\partial \theta_{Leaf}}\right), S_{\varepsilon_{Leaf}} = \left(\frac{\partial T_{Canopy}}{\partial \varepsilon_{Leaf}}\right), S_{\theta_{Sensor}} = \left(\frac{\partial T_{Canopy}}{\partial \theta_{Sensor}}\right) \quad \text{(A.5)}$$

As an example, the proposed economic optimum rate of nitrogen is between 150 to 170 kg.ha^{-1} (personal communication, C. Swanton).The sensitivity coefficient with respect to nitrogen can be calculated by taking the difference in the highest and lowest nitrogen rates (the input variable x) and the difference in their corresponding mean surface temperature values (the output variable y) at a specific day.Then, diversion of the difference in y over the difference in x provides the desired result. For this example the data collected from the Elora Research Station on July 6$^{\text{th}}$, 2016 is used.

- The highest N rate is 230 kg.ha^{-1} and the corresponding mean canopy temperature is 24.98 °C.
- The lowest N rate is 0 kg.ha^{-1} and the corresponding mean temperature is 25.73°C.

The partial derivative that is referred to the sensitivity coefficient can be approximated as a finite difference and output values can be calculated for small changes in the input variables[183, 184]. Thus, the partial derivative can be approximated as in Equation A.6. After substituting the given data in the example into Equation A.7, the sensitivity coefficient for nitrogen variation is 0.003 °C/ kg.ha^{-1}, which is significantly small due to the

variability from other variables that affect canopy temperature, which explains the shallow decreasing slope between applied nitrogen rate and surface temperature.

$$\frac{\partial y}{\partial x} = \frac{\Delta y}{\Delta x} \tag{A.6}$$

$$\frac{\Delta y}{\Delta x} = \frac{\Delta T_{Canopy}}{\Delta N} = \frac{24.9833 - 25.733}{230 - 0} = 0.003^{o}C/kg.ha^{-1} \tag{A.7}$$

The direct measurement of 1σ in T_{Canopy} is 0.5°C, and in the mean surface temperature is 0.1 °C. Given the direct measure of T_{Canopy}, Equation A.4 can be used to determine the other variables sensitivities to canopy temperature. For example, T_{Canopy} is known to be a strong function of $(\dot{\phi}_{Solarinput})$, so if $\dot{\phi}_{Solarinput}$ was to be measured enabling $\sigma_{\dot{\phi}_{Solarinput}}$ to be calculated then the sensitivity coefficient for solar radiation can be calculated assuming negligible uncertainty contributions from all the other variables except the nitrogen fertilizer variation. Therefore, the non-nitrogen related variables need to be controlled, or compensated through conditional sampling for more accurate investigation of the relationship between nitrogen rate and surface temperature under variable conditions, please refer to Section 6.3 for more detail.

Appendix B

Corn leaf thermal emissivity experiments

The knowledge of emissivity is very important for accurate surface temperature measurements. This chapter discusses different experiments that were conducted on leaves extracted from corn plants grown under different greenhouse and field conditions to investigate the emissivity variation with nitrogen stress using the Surface Optics Corporation (SOC 400T) infrared reflectometer and the Bruker Fourier transform infrared spectrometer. This chapter has three specific objectives: (1) to propose an average leaf emissivity for corn plants over the 7.5- 14 μm spectral waveband. (2) to confirm the emissivity spectral shape for corn leaves over a chosen waveband of the 7.5- 14 μm compared to geranium leaves spectral shape, which was found to have a higher average spectral emissivity compared to corn leaves. (3) to propose further investigation in spectral wavebands as observed in the emissivity spectra for corn plants supplied with different nitrogen rates.

B.1 Introduction

Emissivity is defined as a measure of a surface's ability to emit energy. It is the ratio between the actual emitted energy from a surface at a given temperature to the energy emitted by a blackbody at the same temperature [185, 186]. Its value ranges from 0 (perfect reflector) to 1 (perfect emitter or a blackbody). Emissivity is a function of wavelength, material type, thickness, roughness, and direction [187, 188]. Spectral absorptance (α) is calculated through $\alpha = 1 - \rho$, where ρ is the spectral reflectance, then Kirchhoff's Law and the Stefan-Boltzmann equation are used to calculate the spectral emittance (ϵ).

Thermal remote sensing requires emissivity as an input for accurate surface temperature measurements. Spectral emissivity has been assumed as a constant over selected wavebands, for example, the average spectral emissivity over the 8-14 μm waveband is assumed to be 0.98 [189], which affects surface temperature measurements. Emissivity is different for various surfaces and species, for instance, one study observed that older leaves have different emissivities compared to newer leaves [190, 186]. The emissivity of vegetation is generally high compared to other objects because of its complex structure, low spectral contrast, and high water content [191, 192]. Small variation in emissivity of 0.002 to 0.006 can induce a temperature difference of 0.1 °C to 0.3 °C between the upper and lower sides of the leaf [193]. Little attention has been given to crop characteristics in the thermal infrared waveband due to the complexity of spectral variations in crop plants, which include both biophysical and biochemical variations [194]. It was found that plant cuticle, which is a protective film covering the external wall of plant epidermal cells, and the underlying cell wall, are the principal cause of spectral emissivity variation in crop

plants [195, 196, 197]. An emissivity of 0.98 is recommended by Lopez et al.[189] as a reference value when measuring surface temperature of horticultural crops and vegetables. It is found that a small difference in emissivity for some crops may induce errors in surface temperature up to 1.0 °C [198, 186] when the set emissivity is between 0.05 and 0.07 of the actual emissivity at 22 °C temperature, which indicates the importance of emissivity setting for accurate surface temperature measurement using infrared thermography [186].

Most of the one channel thermal cameras assume a constant emissivity of 0.97 for vegetation [199], which limits the accuracy of surface temperature measurements. Jonas [77] observed an average leaf spectral emissivity of 0.95 over the 8-14μm band compared to plant canopies of 0.98-0.99. The variation between leaf and canopy average emissivity is due the internal reflections among different leaves. The focus of this research is on spectral emissivity instead of spectral reflectance because thermal remote sensing is associated with surface emitted radiation, not surface reflected radiation. However, little attention has been given in the past to spectral emissivity for different reasons including the low and complex spectral emissivity variations due to plant physiological changes, leaf structure traits, biochemical changes besides plant structural effects, and low signal-to-noise ratio of the thermal infrared sensors, which fail to detect minor variations in crop thermal spectral fingerprints[199]. Under variable field conditions, spectral emissivity which depend on leaf structure and water content is affected by leaf cuticle thickness that depends on the environmental conditions, growth stage, and crop hybrid [200].

Negative correlations were observed by Zhuang [190] between thermal emissivity with stomata size, vein length, vein area, and top cuticular membrane thickness. Neinavaz et al.[201] investigated the effect of leaf area index (LAI) variation on spectral emissivity

[201]. A positive correlation was found between canopy emissivity and LAI, which indicated that plants with high LAI have higher spectral emissivities compared to plants with lower LAI. Ullah et al.,[202] used the mid and far infrared spectrum to investigate the difference among plant species at a laboratory level. A statistically significant difference was observed in thermal emissivity at selected wavebands. The emissivity signature of plant leaves is dominated by a feature related to cellulose of the epidermis cells [202].

The relationship between spectral emissivity and crop stress was investigated in previous studies involving water stress effect on spectral emissivity [176]. It was observed that stress increases the emissivity due to cavity effects (loss of spectral contrast due to multi scattering [203]), as a result of cuticle thickness increase. On the other hand, emissivity spectra decreases with stress as observed in beech and potato leaves [61, 176]. It is still unclear how the emissivity spectra interact with vegetation biophysical and biochemical properties in the thermal infrared spectrum [201]. It was found that leaf thermal emissivity increases with water content increase [190]. Buddenbaum et al.[204] used a passive emissive imaging spectrometer to differentiate between water stressed and non-stressed European beeches. However, no solid conclusions were drawn regarding at which stage the water stress can be detected using spectral emissivity [199]. Watson [205] investigated the relationship between thermal emissivity and plant temperature, it was concluded that thermal emissivity not the transpiration process prevents overheating of plant tissue. In addition, it was found that the presence of Vaseline on the plant surface decreases the emissivity of that surface.

The main objective of investigating the possibility of emissivity variation with nitrogen stress came from the small temperature difference observed between stressed and less

stressed corn plants under greenhouse and variable field conditions. In addition, an emissivity variation was observed in previous studies involving crop species variation ([189, 186]).

B.2 Materials and methods

Corn leaves (Zea mays) were collected from the Elora Research Station operated and owned by the University of Guelph, ON, Canada in the year of 2018 and 2019. For 2018, three experiments were conducted on the third fully expanded leaf counting from the top, and for 2019 two experiments were conducted in August on ear leaves collected from corn plants. For the experiments conducted in 2018, corn plants were at different growth stages when leaves were collected for the spectral reflectance measurements; in July 2018 corn plants were at 11-12 leaf tip stage, in August 2018 plants were at the silking stage and in September 2018 plants were at the maturity stage. For the experiment conducted in September 2018 three ear leaves were collected from different corn plants from a plot supplied with 188 $kgN.ha^{-1}$ nitrogen, the main objective was to observe the effect of repeated measurements on spectral emissivity variation. Three leaf samples from different plants were collected per nitrogen treatment of 0, 28, 57, 115, 188, and 230 $kgN.ha^{-1}$. The hemispherical reflectance was consistently measured using Surface Optics Corporation infrared reflectometer (SOC 400T) under laboratory conditions.

In addition, corn leaves were collected from the University of Waterloo greenhouse, ON, Canada in 2019. Spectral reflectance was measured on the top side of a corn leaf for 3-4 fully expanded corn leaves. The spectral reflectance was measured using two devices under laboratory conditions. The spectral reflectance was measured using a Surface Optics

Corporation infrared reflectometer (SOC 400T) for Expt 1, and the spectral reflectance with 10 nm resolution was measured using a Bruker Fourier transform infrared spectrometer for Expt 4. Both devices cover the mid-infrared spectrum (2-25 μm). The chosen spectral waveband of interest was the infrared (IR) band from 7.5 to 14 μm, which matches the thermal camera waveband spectral range. The spectral emissivity in the infrared region (ε_λ) was calculated from the spectral reflectance (ρ_λ) via ε_λ=1- ρ_λ under the assumption of zero leaf transmissivity in the IR (7.5 to 14 μm) waveband [195, 193, 202]. When the transmissivity is zero, which is the case for crop plants plus the soil, emissivity is simply one minus the reflectance. This research reports emissivity instead of reflectance because thermal remote sensing involves surface emitted radiation, not surface reflected radiation.

Furthermore, in order to investigate the spectral emissivity variation for different plant species, the spectral reflectance for geranium leaves was measured in the two experiments conducted for plants grown under greenhouse conditions in the year of 2019 (Expts 1 and 4) where healthy, clean and green geranium leaves were chosen for spectral reflectance measurements. In both experiments one geranium plant was selected with multiple leaves. The geranium plant was chosen due to its availability in the greenhouse at the time of spectral reflectance measurements were conducted.

B.3 Data analysis

Statistical data analysis was conducted to investigate the significance of the difference in leaf thermal emissivity among nitrogen treatments. Analysis of variance (ANOVA) and F-test were applied. In addition, a paired t-test with an equal variance assumption, at

a 0.05 significance level, was used to investigate if there is a difference in leaf emissivity between the two nitrogen extremes (high and low nitrogen supply rates).

B.4 Results and Discussion

The very first experiment was conducted for leaves extracted from corn plants grown at the University of Guelph greenhouse. Corn plants were supplied with a high rate of nitrogen (160 $kgN.ha^{-1}$) at different timings; at the beginning (Zone 1 and 4), middle (Zone 2 and 5) and close to the end of the experiment (Zone 3 and 6). A non-significant difference was observed between stressed plants (supplied with nitrogen before the end of the experiment) and less stressed plants (supplied with nitrogen from the beginning of the experiment). Stressed plants had an average spectral emissivity over the 7.5-14 μm range of 0.966$\pm$0.01 and less stressed plants had an average of 0.967$\pm$0.01 as presented in Figure B.1.

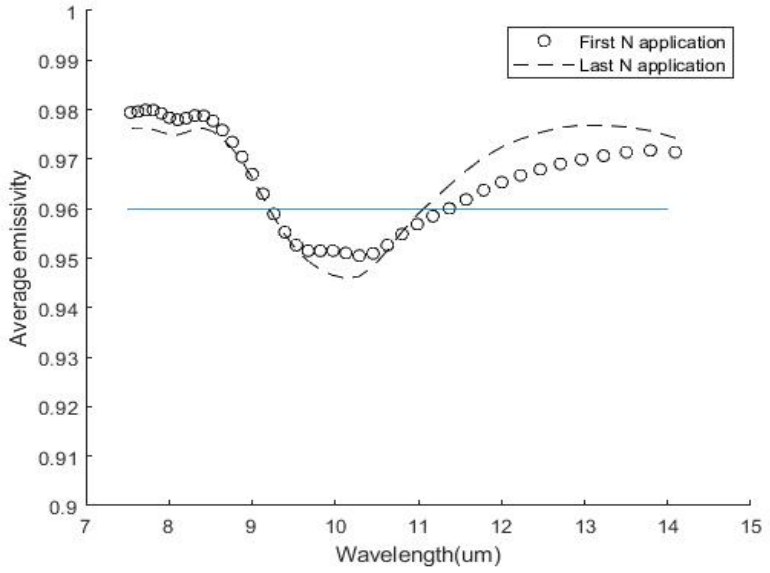

Figure B.1: Spectral emissivity variation for stressed and less stressed corn leaves extracted from plants grown at the University of Guelph greenhouse

B.4.1 Corn leaves collected from the Elora Research Station

Four experiments were conducted to measure the spectral reflectance of corn plants grown under variable field conditions; two experiments were conducted in 2018 and two experiments were conducted in 2019 (Figure B.2). Under variable field conditions, corn plants were supplied with 6 different rates of nitrogen (i.e., 0, 28, 57, 115, 188, 230 $kgN.ha^{-1}$).A non-significant difference was observed among nitrogen treatments over the selected thermal infrared waveband (7.5-14 μm). The mean and one standard deviation variability for the average spectral emissivity among the six supplied nitrogen treatments on different days in 2018 and 2019 is summarized in Table B.1. The spectral reflectance measurements were conducted on three leaves at three selected measurement points per leaf (a total of

nine measurements) for a given supplied nitrogen rate using the surface optics Fourier transform reflectometer(SOC-400T).

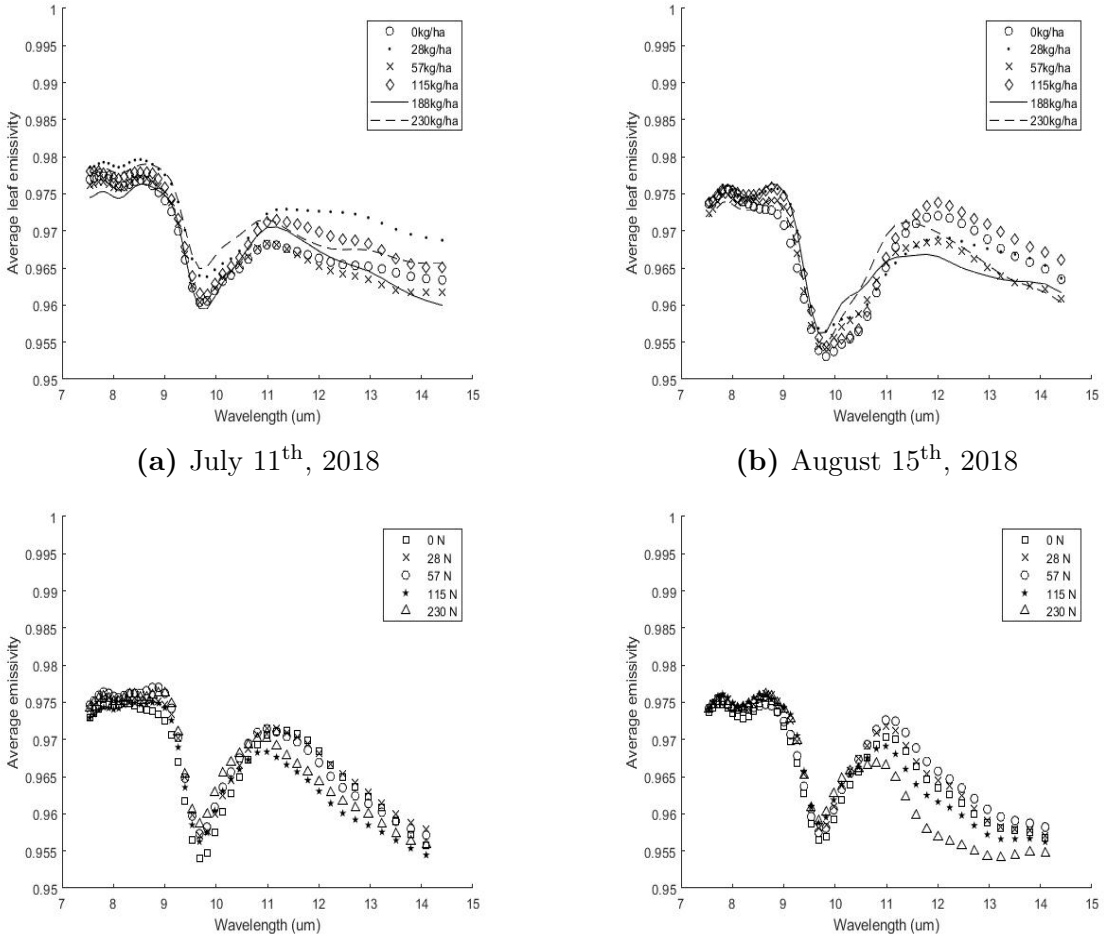

(a) July 11$^{\text{th}}$, 2018

(b) August 15$^{\text{th}}$, 2018

(c) August 15$^{\text{th}}$, 2019

(d) August 22$^{\text{th}}$, 2019

Figure B.2: Average spectral emissivity variation with supplied nitrogen rate for corn leaves collected from the Elora field on different days in 2018 and 2019.

Table B.1: The mean spectral emissivity over the 7.5-14 μm waveband for different supplied nitrogen rates

Date	$0 kgN.ha^{-1}$	$28 kgN.ha^{-1}$	$57 kgN.ha^{-1}$	$115 kgN.ha^{-1}$	$230 kgN.ha^{-1}$
July 11th, 2018	0.969± 0.006	0.973± 0.005	0.969± 0.006	0.971± 0.005	0.972±0.005
August 15th, 2018	0.967± 0.007	0.968± 0.006	0.968± 0.006	0.969± 0.007	0.968± 0.006
August 15th, 2019	0.968± 0.0067	0.969± 0.0063	0.969± 0.0068	0.9669± 0.0069	0.968± 0.0068
August 22th, 2019	0.967± 0.0065	0.968± 0.0066	0.968± 0.0062	0.967± 0.007	0.966± 0.008

In order to quantify the spectral reflectance measurement error, the measurements were repeated five times at each of the selected two measurement points (i.e., near the leaf base and on the leaf tip) for three corn leaf samples collected from one plot in the Elora field where the corn plants were supplied with 188 $kgN.ha^{-1}$ of nitrogen. The average and one standard deviation variability of spectral emittance for each set of five repeated measurements over the 8-14 μm waveband is presented in Figure B.3. The notation on the x-axis includes the sample leaf number (i.e., S1, S2 or S3) with a corresponding selected measurement point (i.e., p1 and p2). As an example, S1p1 refers to leaf sample 1 and measurement point 1 near the leaf base. One-factor ANOVA was conducted on the repeated spectral reflectance measurements to investigate the significance of the difference between repeated measurements. A non-significant difference was observed between repeated spectral measurements at a 0.05 significance level.

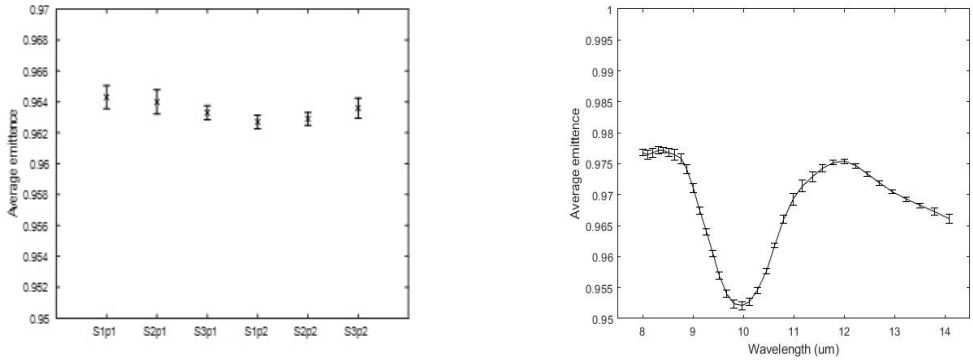

(a) The average emissivity and variability for selected measurement points

(b) An example of spectral emissivity for leaf sample 2 and measurement point 1

Figure B.3: An average leaf emissivity over the 8-14μm waveband for five repeated measurements

The variation in spectral emissivity among multiple leaves per corn plant was investigated (Figure B.4). For example, the average spectral emissivity for two ear leaves per corn plant collected from a plot supplied with 230 $kgN.ha^{-1}$ of nitrogen are 0.9669± 0.006 and 0.9686± 0.006, respectively.

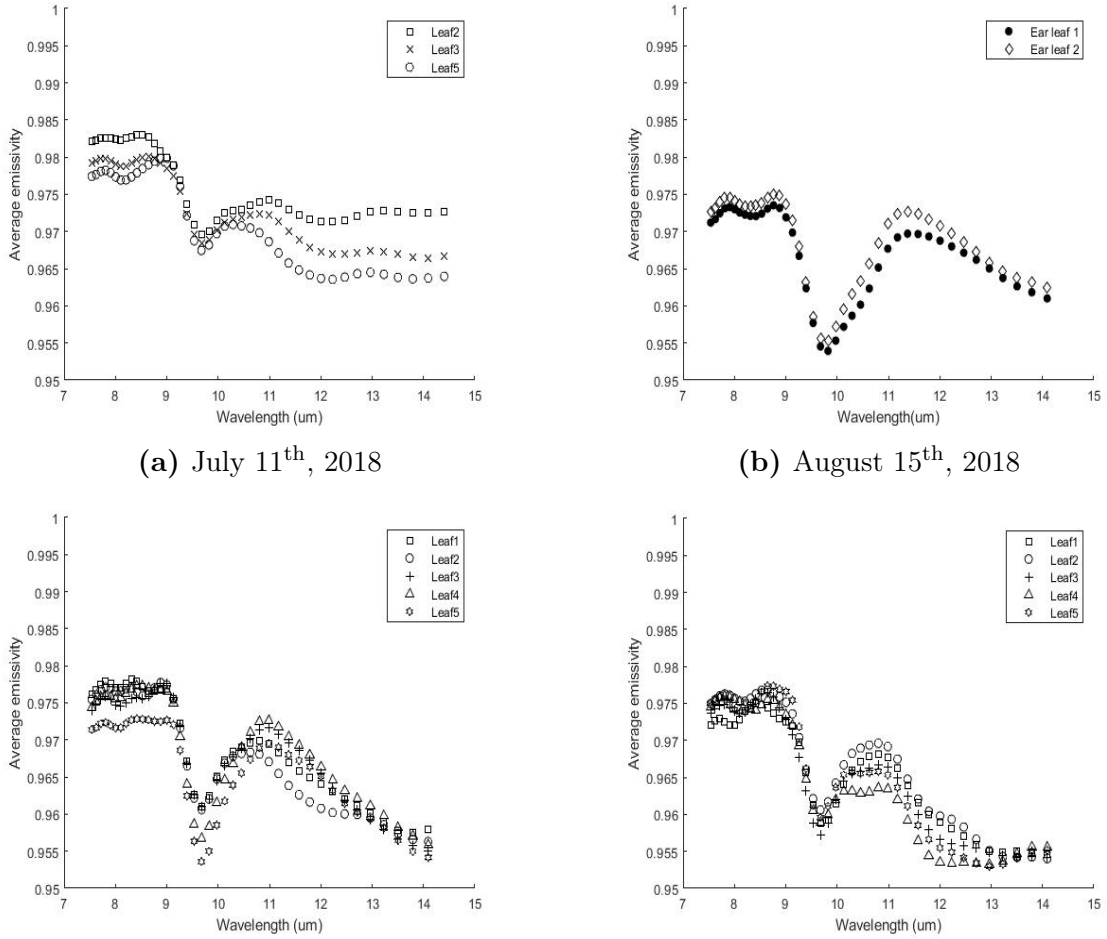

(a) July 11$^{\text{th}}$, 2018

(b) August 15$^{\text{th}}$, 2018

(c) August 15$^{\text{th}}$, 2019

(d) August 22$^{\text{th}}$, 2019

Figure B.4: Average spectral emissivity variation for the same supplied nitrogen rate (230 $kgN.ha^{-1}$) for different corn leaves in 2018 and 2019.

The variation in spectral emissivity for the same corn leaf with three different measurement locations on the leaf (i.e., near the leaf tip, middle, near the leaf base) was investigated as presented in Figure B.5. The average emissivity over the 8-14 μm waveband and standard deviation for the three selected points on ear leaf 1 were 0.9687 $\pm$ 0.0088, 0.9720 $\pm$

0.0078, and 0.9695 ± 0.0085, in addition, for ear leaf 2 the average emissivity were 0.9675 ± 0.0071, 0.9696 ± 0.0082, and 0.9707 ± 0.0070, respectively. A slight variation in the spectral emissivity per measurement point per leaf was observed, which was not significant. The maximum difference in the average emissivity over the 8-14 μm waveband between the three selected points were 0.0033 and 0.0032 for the two presented corn ear leaves (ear leaf 1 and 2), respectively.

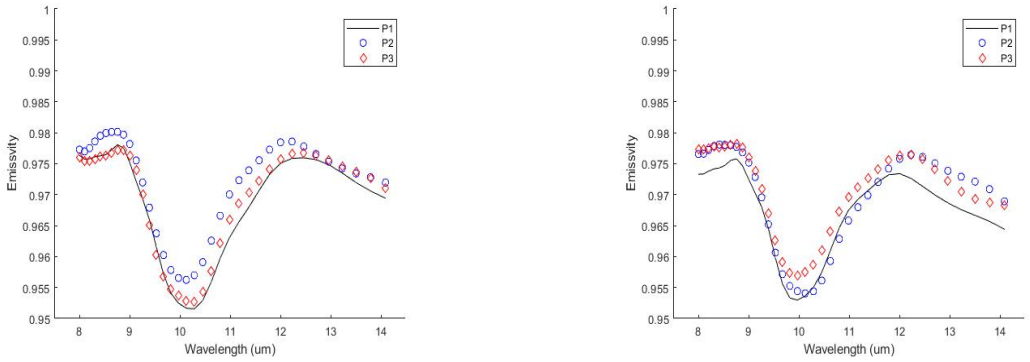

(a) Corn ear leaf 1 **(b)** Corn ear leaf 2

Figure B.5: Spectral emissivity variation on three selected measurement points per corn ear leaf

B.4.2 Corn leaves collected from the University of Waterloo greenhouse experiments

Spectral reflectance (ρ_λ) was measured for corn leaves extracted from Expt 1 (Apr-May, 2019) using a surface optics Fourier transform infrared reflectometer, and a spectral reflectance (ρ_λ) was measured for corn leaves extracted from Expt 4 (Oct-Nov, 2019) using a Bruker Fourier transform infrared spectrometer. The spectral reflectance was converted to spectral emissivity (ε_λ), respectively, using the formula of ε_λ=1- ρ_λ. A non-significant

difference in leaf emissivity among nitrogen treatments over the 7.5-14 μm waveband was observed in both Expts 1 and 4, at a 0.05 significance level, whereas the spectral shape remained unchanged.

In Expt 1, the average leaf emissivity was calculated for 20 measurement points per corn sample for both high and low N rates. In Expt 4, two sub-experiments were conducted on two different days; on Oct 25$^{\text{th}}$ and on Nov 19$^{\text{th}}$, 2019 where the spectral reflectance was measured using a Bruker Fourier transform infrared spectrometer. For the experiment conducted on Oct 25$^{\text{th}}$, 2019 the average leaf emissivity was calculated for two corn samples and four measurement points per sample, which represents four selected leaves per N treatment. For the experiment conducted on Nov 19$^{\text{th}}$, 2019, the average leaf emissivity was calculated for three corn plants. For the high N rate 13 measurement points were selected from three corn plants, and for the low N rate 10 measurement points were selected from three corn plants. It was observed that corn plants supplied with a low nitrogen rate has higher emissivity over the 7.5-11 μm waveband compared to corn plants supplied with a high nitrogen rate (Figure B.6). The error bars represent the error in the mean ($\frac{\sigma}{\sqrt{n}}$), therefore the greater the number of measurement points (n) selected, the smaller the calculated error in the mean for a given standard deviation (σ).

The average leaf emissivity of 0.96 ± 0.017, 0.968 ± 0.015, and 0.963 ± 0.015 for corn plants supplied with a high N rate for Expt 1, Expt 4-Oct 25$^{\text{th}}$, and Expt 4-Nov 19$^{\text{th}}$ over the 7.5- 14 μm waveband, respectively. Due to the non-significant difference among nitrogen treatments, the average emissivity of 0.96 can be used as a user input to a one channel thermal camera that requires emissivity input for accurate surface temperature measurements.

A spectral peak for corn plants is observed at a 9.67 μm wavelength. This peak is related to surface scattering response due to the presence of xylan found in corn hulls and leaves [197]. Xylan is a major component of plant biomass and hemicellulose. A variation in plant cuticle thickness is reported in previous studies for different leaves within a plant canopy [61].

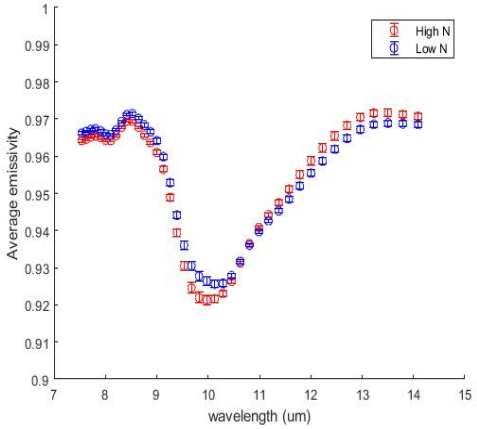

(a) Expt 1- June 5$^{\text{th}}$, 2019

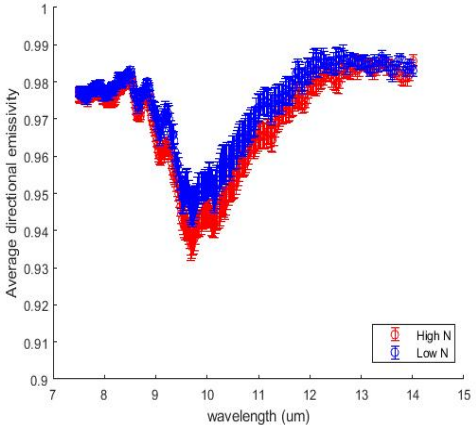

(b) Expt 4- Oct 25$^{\text{th}}$, 2019

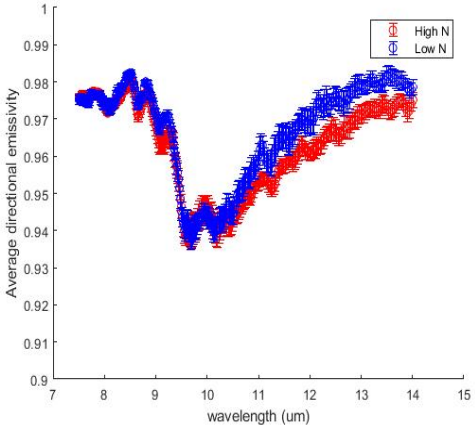

(c) Expt 4- Nov 19$^{\text{th}}$, 2019

Figure B.6: The average leaf emissivity for corn plants from the greenhouse experiments conducted in 2019 supplied with high and low N rates.

In addition, the spectral reflectance was measured for geranium leaves in Expts 1 and 4. A geranium plant was selected due to its availability at the greenhouse on the time of growing corn plants for reflectance measurements and because it has a large round leaves that are easy to attach to the small spectrometer and reflectometer aperture. It was observed that germanium leaves have higher average spectral emissivity of 0.987 ± 0.004 and 0.983 ± 0.003 over the 7.5-14 μm waveband in Expts 1 and 4, respectively, compared to corn leaves (Figures B.7 and B.8). One possible explanation for this average emissivity variation between corn and geranium leaves is that the two crop plants have different cuticle thickness, therefore, different emissivity spectra would be expected. The average leaf thermal emissivity for geranium plant is based on 7 leaves for Expts 1 and 4. In both Figures B.7 and B.8 the error bars represent the error in the mean.

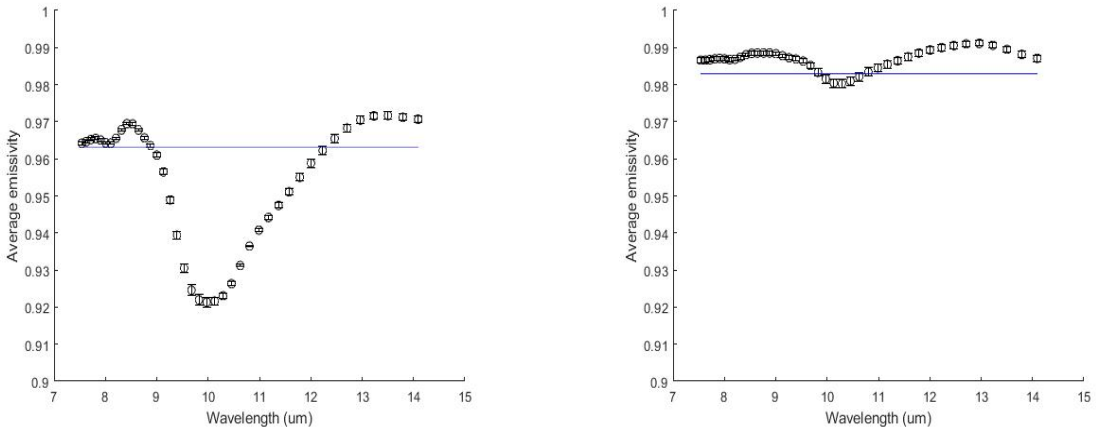

(a) Corn supplied with high N rate **(b)** Geranium

Figure B.7: An average spectral emissivity over the 7.5-14 μm waveband from Expt 1.

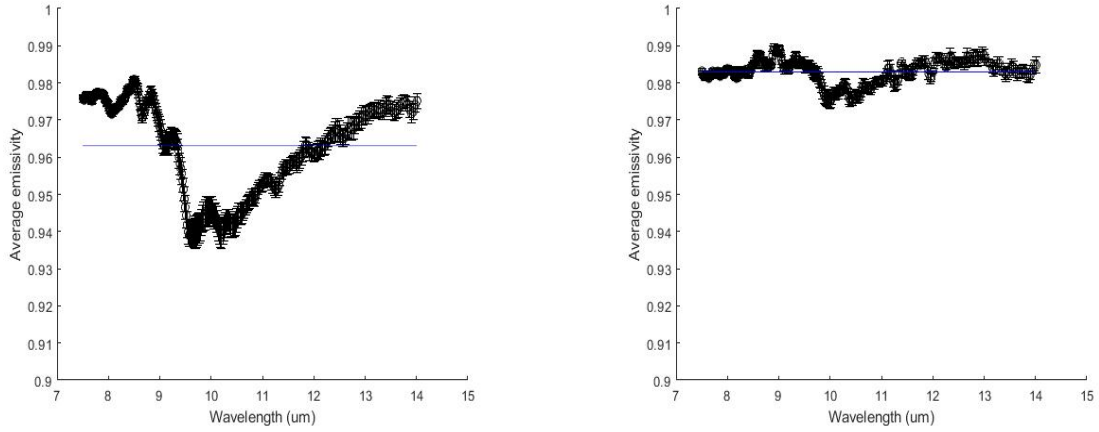

(a) Corn supplied with high N rate **(b)** Geranium

Figure B.8: An average spectral emissivity over the 7.5-14 μm waveband from Expt 4.

One experiment was conducted on June 13th, 2019 using the SOC400T reflectrometer to study the spectral emissivity variation with measurement time with the need of SOC400T reflectrometer calibration every hour before collecting the spectral reflectance measurements. The same leaf location was selected every time a reflectance measurement was conducted. A non-significant difference was observed between spectral emissivity and time variation, which is expected since the only variable that was changing is time and after every hour of reflectance measurement, the SOC 400T reflectrometer was calibrated before collecting spectral reflectance data to reduce the error associated with the accuracy of the device.

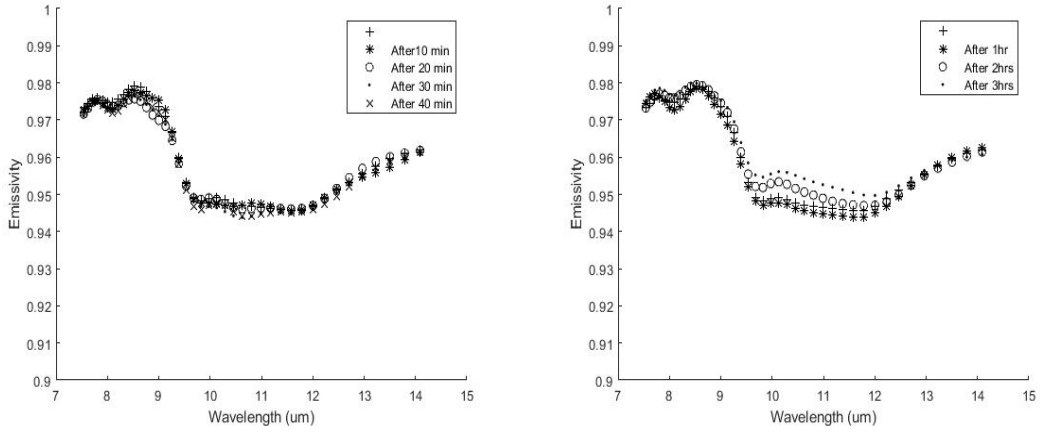

(a) 10 minutes time interval between measurements

(b) 1 hour time interval between measurements

Figure B.9: Spectral emissivity variation with time, while holding other variables constant

B.5 Experimental sources of error

The potential sources of error in the spectral reflectance measurements for crop plant leaves include the following:

- **Number of scans and runs selected for the spectral reflectance measurements.** The more number of measurements is selected the less error expected in the experiment.
- **Systematic error from the device itself.** This can be tested through conducting multiple reflectance measurement for the same measurement point/location while holding all other variables as constant.

- **Leaf randomization.** In order to minimize the systematic error, spectral reflectance needs to be measured while alternating between stressed and less stressed leaves to ensure that the data are random for statistical analysis purpose.

- **Holding leaves in a good shape until the spectral measurements are conducted.** Leaves were removed along with 4 cm of stem. Leaf stems were wrapped in a wet tissue paper until the spectral reflectance was measured to prevent leaf wilting and rapid changing of leaf properties. Leaves need not to be wet due to spectral emissivity variations between dry and wet leaves[77].

- **The variation in operating conditions.** Spectral reflectance measurements were conducted under laboratory conditions due to device sensitivity to outdoor conditions, area, and software set up limitations.

- **Device calibration and correction for atmospheric attenuation.** Calibration was conducted using a gold plate reference (high reflectively of 0.986) when the reflectrometer was left without operation for more than 2 hours to minimize the errors associated with accuracy.

- **Leaf tissue analysis.** It is recommended to conduct leaf tissue analyses before conducting spectral reflectance measurements and emissivity calculation in order to investigate if the difference in the leaves nitrogen content under study is significant. The previously mentioned experiments in this work are based on the variation of supplied nitrogen rate to corn plants under different greenhouse and field conditions.

B.6 Conclusion

The results obtained previously by Ullah [202] and Neinavaz [201] confirm that crop plants have relatively high emissivity compared to other objects. This research investigated the effect of varying nitrogen rate on leaf thermal emissivity under laboratory conditions. An average leaf emissivity of 0.96 ± 0.006 for corn leaves over the 7.5-14 μm waveband is proposed as an input for one channel thermal cameras, which can be used as a reference value for future studies involving surface temperature measurements of corn plants. A slight increase was observed in the average emissivity over the 7.5-14μm waveband with nitrogen deficiency, which was expected given the previous studies involving increasing emissivity in the infrared waveband with water stress [199]. Finally, it is recommended that extensive studies be conducted under more controlled conditions such as greenhouse growth chambers to investigate the effect of nitrogen stress on leaf spectral emissivity in the infrared band.

Appendix C

Whorl temperature measurements

Whorl temperatures were proposed in this research as a proxy for crop surface temperature, because the exergy destruction principle involves surface temperature measurements. Whorl temperature is measured using thermocouple to provide longer time duration measurements from a consistent single location as the leaves are small to support the thermocouple weight without causing tissue damage, therefore, thermocuples were placed into the corn whorl at 4-5 leaf tip stage, when the whorl was big enough to keep the thermocouple in its place. In addition, a wooden stake was used for an additional thermocouple support. The main objective of this chapter is to investigate the variation of whorl temperature with nitrogen rate under controlled greenhouse conditions.

Whorl temperatures were measured using a type T, ungrounded with FEP-Insulated thermocouple. The chosen thermocouples were manufactured by Digi-Sense, Canada, with $T_{max} = 400$ °C, 0.51 mm in diameter, and ± 2 °C accuracy. Thermocouples were attached through a mini connector to a 12 channel data-logger with an SD card (Extech DT4208SD,

Cole-Parmer, Canada) for continuous temperature measurements, with a selected sampling rate of 30 minutes. Whorl temperature averages were recorded. Thermocouples were placed directly into the whorl of corn plants as the leaf surface is very small to support the thermocouple weight without causing tissue damage, and to minimize the error associated with heat radiation.

An expected mid-day and mid-night relative whorl temperature reversal trend was observed at the University of Guelph greenhouse and the Elora field conditions between stressed and less stressed corn plants. The results for some whorl temperature measurements have been shown in this thesis in previous greenhouse and field results sections. It was observed that less stressed plants were cooler in the day and warmer at night compared to highly stressed plants as predicted by the exergy destruction principle. During the night, there is no energy input and less stressed plant system should be more conservative to use energy, thus it has higher surface temperature at night. However, a non-consistent relationship was observed between whorl temperature and nitrogen stress under greenhouse and field conditions. Therefore, the need was realized to conduct more experiments in a more controlled environment such as growth chambers.

C.1 University of Waterloo growth chamber experiments

Two experiments were conducted at the University of Waterloo growth chamber from November 2019 to February 2020 under semi controlled conditions to investigate the effect of nitrogen deficiency on whorl temperature during the day and night cycle. Corn plants were grown using the same methodology described previously in the "greenhouse

experiments at the university of Waterloo material and methods section". Whorl temperature data were collected starting at V3 growth stage. The growth chamber maintained semi controlled conditions for growing corn plants. The conditions were day/night temperature of 25°C/18°C, a day/night photo-period of 16/8 hours, and light intensity of 600 $umol/m^2/s$ at a distance of 50 cm and 430 $umol/m^2/s$ at 100 cm. The lights were off from 9:00 pm to 5:00 am. The growth chamber has an area of 1.4 m^2, therefore, due to space limitations only 9 pots were chosen (Figure C.1); 5 pots with corn plants were supplied with high nitrogen rate of 1.4 g/L and 4 pots were supplied only with tap water from the beginning of the experiment. The experiment was conducted in a randomized order to minimize the systematic error. *It was expected that nitrogen stressed corn plants will have higher whorl temperatures during the day and lower temperatures during the night compared to less stressed plants.*

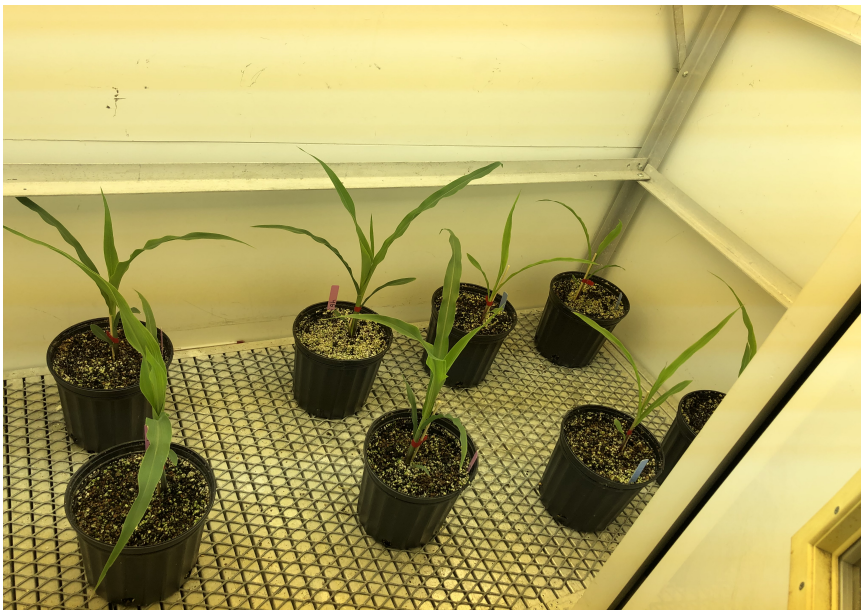

Figure C.1: Corn plants grown under growth chamber conditions at the University of Waterloo

Two experiments were conducted under the growth chamber conditions. The first experiment was conducted in Nov 2019, during which it was observed that two less stressed corn plants, supplied with a high nitrogen rate, out of five plants had lower whorl temperatures (day/night average temperature of 21.5°C/14.5°C) during the days compared to the average day/night surrounding measured air temperature in the growth chamber of (22.4°C/14.4°C), and the other three corn plants supplied with higher rate of nitrogen had higher temperatures during the days compared to stressed corn plants (supplied with only tap water from the beginning of the experiment). A significant visual difference was observed between stressed and less stressed corn plants. Less stressed plants grew faster and had green leaves with strong stems compared to stressed plants. One of the limitations of using thermocouples is that wires were falling from the stem and measuring the soil or surrounding air temperature depending on where they fell, therefore, it was important to check the plants daily to make sure that the wires were inside the stem. The days when the wires were off were excluded from whorl temperature analysis. Figure C.2 represents the non-consistency in the results, which showed the opposite of what was expected regarding the correlation between whorl temperature and nitrogen stress during the day and night cycle. For example, on Dec 20th, 2019, it was observed that 3 out of 4 corn plants supplied with high nitrogen rate had higher whorl temperatures during the day compared to stressed plants that were supplied with only water from the beginning of the experiment. Otherwise, four plants supplied with a high nitrogen rate had very close whorl temperatures during the night of 14.7±0.96°C, 14.86±0.98°C, 14.66±0.78°C, and 14.95±0.98°C, respectively. A corresponding average air temperature of 22.4±0.08°C and 14.4±0.12°C and surface soil temperature of 22.7±0.08°C and 15±0.25°C was recorded on that day

during the day and night cycle, respectively.

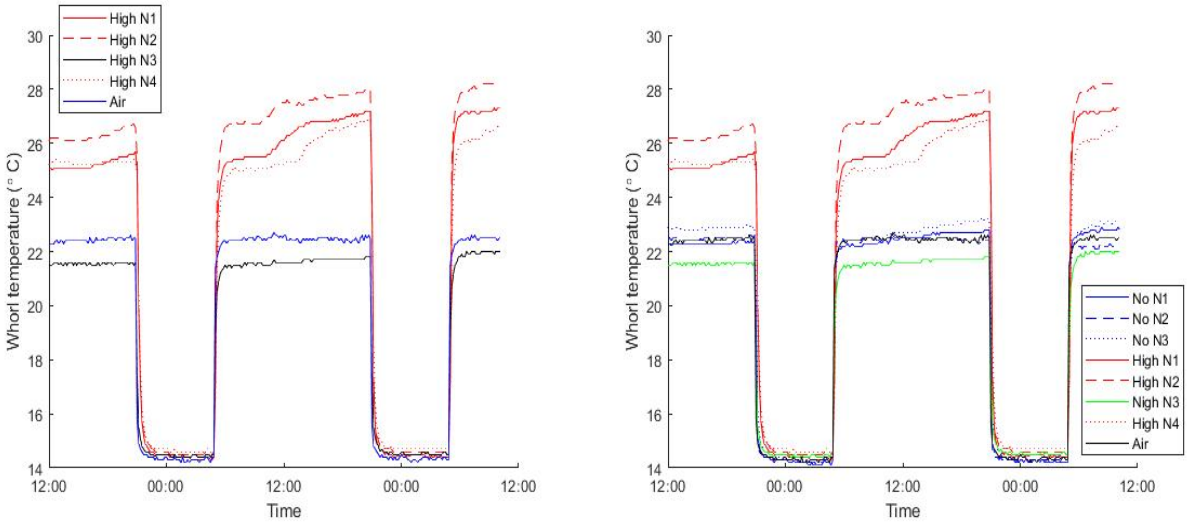

(a) Comparison of the four high nitrogen treatments with air temperature measurements

(b) Comparison in whorl temperature between high and no nitrogen supplied corn plants

Figure C.2: Corn plants supplied with a high nitrogen rate are hotter compared to stressed plants on Dec 20^{th}, 2019.

The second experiment was conducted in Jan 2020 for approximately 6 weeks, five plants were supplied with only tap water from the beginning of the experiment and four plants were supplied with a high nitrogen rate ($1.4g/L$) after seed emergence. Whorl temperature data were recorded every 1 minute. A slight temperature difference was observed in the surrounding air temperature during the day of 1°C difference between the two ends in the growth chamber at 1 m height, which introduced an additional source of error to whorl temperature measurements. It was observed that less stressed plants had higher temperatures during the day compared to stressed plants. As an example, the average temperature during the day and night on Feb 4^{th}, 2020 for plants supplied with a high rate

of nitrogen was 24.47±0.14 and 17.07±0.21 compared to stressed plants of 22.97±0.075 and 17.056±0.334, respectively.

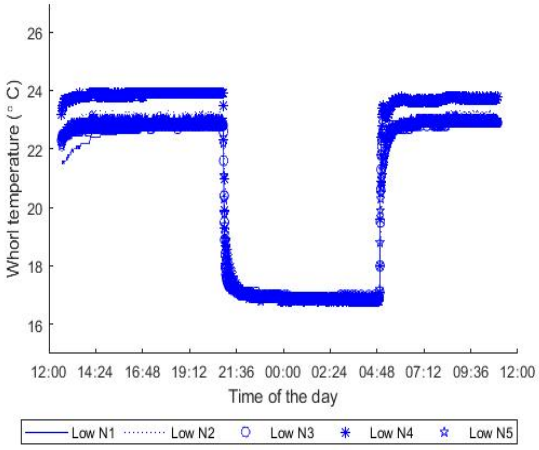

(a) Whorl temperature for stressed corn on Jan 31- Feb 1th, 2020

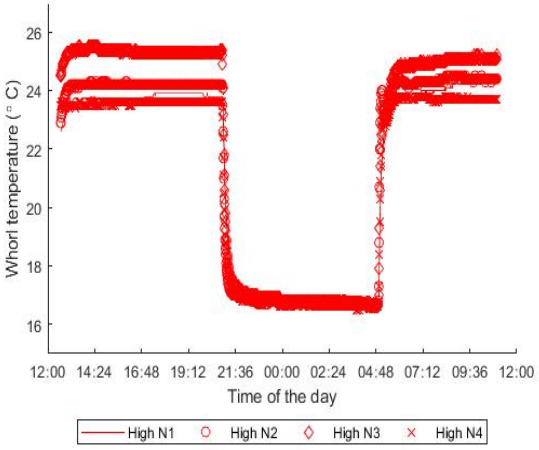

(b) Whorl temperature for less stressed corn on Jan 31- Feb 1th, 2020

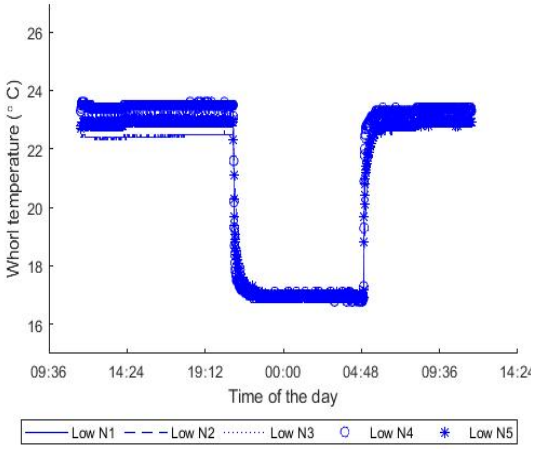

(c) Whorl temperature for stressed corn on Feb 4-5th, 2020

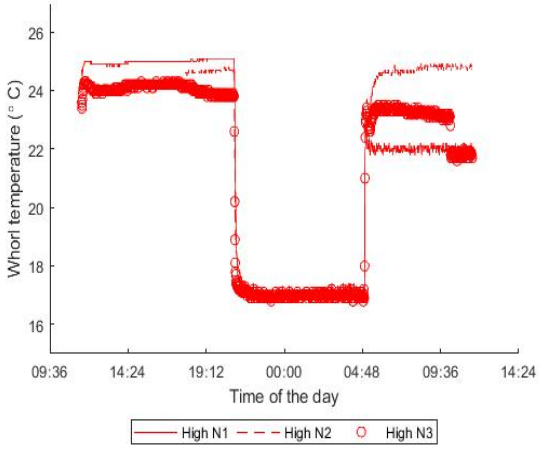

(d) Whorl temperature for less stressed corn on Feb 4-5th, 2020

Figure C.3: Whorl temperature variation between day and night for stressed and less stressed corn plants grown in a growth chamber

Finally, there were many issues associated with growing corn plants under growth cham-

ber conditions, despite it being a semi controlled environment. Some of the issues are described as follows:

- A non-uniform air temperature distribution in the growth chamber, despite it being set to 25°C during the day and 18°C during the night. There were two holes in the growth chamber walls for air input and air output. As an example, Figure C.4 shows the temperature difference in the two thermocouple measurements collected on two days in February at the same height (1 m). The location from where the thermocouple used to measure air temperature 2 was very close to the air input, therefore, a cooler temperature would be expected compared to air temperature 1.

- Corn plants supplied with high nitrogen rate were growing faster and sprouting more leaves compared to stressed plants that were weak and mostly covered with yellow leaves. It was observed that corn plants supplied with high nitrogen rate were experiencing water stress due to high light intensity (personal communication, C. Swanton, 2019) that affected whorl temperatures. Water stress was detected visually through leaf wilting, which explained the sudden increase in temperature.

- Uneven light intensity distribution. At the beginning of the experiment, each pot was placed under one light bulb to ensure that all plants had even light distribution.

- Using whorl temperature as a proxy for surface temperature is very unpredictable since it depends on which depth the thermocouple was inserted and what the tip of the wire measures, which introduced much error while conducting data analysis and comparing treatments.

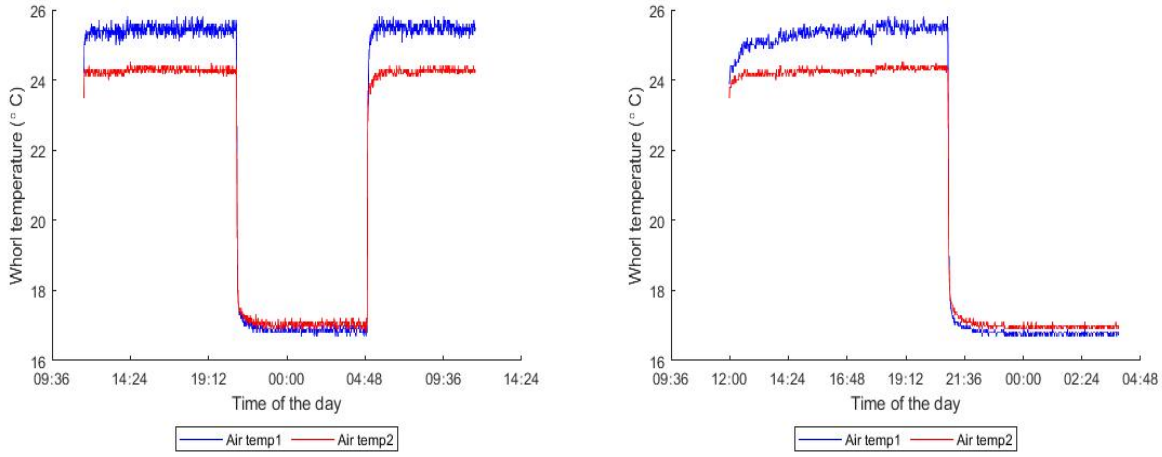

(a) On Feb 5$^{\text{th}}$, 2020 **(b)** On Feb 6$^{\text{th}}$, 2020

Figure C.4: Air temperature variation in the growth chamber during the day and night cycle

Therefore, more controlled experiments are required to collect 24 hours continuous surface temperature measurements using a thermal camera, because whorl temperature is found to be a not good proxy for surface temperature.

Appendix D

Corn canopy temperature extracted from a thermal camera mounted on a drone

Canopy temperature measurements were conducted using a high resolution thermal camera mounted on a drone over the Elora field in 2019 to capture a large study area including one plot (approximately 60 m^2 in area with 600 corn plants). In this chapter, relative temperatures are compared for different plots supplied with different nitrogen rates.

D.1 Materials and methods

Thermal images were collected using the DJI Zenmuse XT2 dual camera that has a good stabilization system. The thermal camera has 640× 512 pixel resolution, spectral range of

7.5-13.5 μm, 17μm pixel pitch, 45° horizontal field of view (FOV) and 37° vertical FOV, 13 mm diameter lens, a thermal sensitivity of 50 mk, and it is less than 1 kg in weight.

Thermal images were collected on five different days in July and August 2019, when corn plants growth stage range from V7 to tassling stage. Canopy temperatures were collected at 40 m above ground level, which reduced the image distortion caused by atmospheric effects. Three flights were conducted at morning (11 am), around noon (12 pm) and afternoon time (2 pm). Each flight included two reverse flights (back to back flights) to investigate the variation in canopy temperature with nitrogen stress over large scale area when the time between measurements varies. The flights were conducted over the first two rows in the field with their corresponding reverse flights which took approximately 20 minutes of flying time. Three thermal images were collected per location and approximately 100 thermal images were recorded in a morning or noon or afternoon flight. Thermal images were taken perpendicular on the field, in the nadir direction. The temperature data collection was conducted under clear sky or uniform overcast days for uniform sky background radiation assumption. Thermal images were collected from the first two rows, each row containing 20 plots supplied with different rates of nitrogen, however, 60% of plots per row were supplied with $28 kgN.ha^{-1}$ nitrogen in order to investigate if there is any residual nitrogen that could be accounted for after 10 years of repeated nitrogen treatments (from 2009 through 2019). A manual flight path was used for thermal image acquisition. In addition, wooden stakes covered with aluminum foil were used to identify plot borders in the thermal images.

D.1.1 Thermal image processing

Thermal images were processed using FLIR ResearchIR software (version 3.5, FLIR), and Matlab software R2018B (Mathworks Inc., Natick, MA, USA). Thermal images were obtained in a JPG format. Multiple images were collected for the same plot to calculate the error in canopy temperature measurements. The pixel value in each image represents the temperature of that pixel. Thermal images were analyzed in Matlab using the image processing toolbox.

The atmospheric correction was not conducted for the collected thermal images using the DJI Zenmuse XT2 dual camera because the images were taken under clear sky or uniform overcast days and the drone was flying at relatively low altitude of 40 m above the ground level. However, atmospheric correction is important for accurate temperature estimation of satellite and airborne sensors to account for atmospheric absorption, scattering and emission. It was found that surface temperature variations in satellite image analysis without conducting atmospheric correction can range from 1-5°C temperature difference [206]. Atmospheric transmission (τ), which is a function of relative humidity, air temperature, and the distance between the object and the camera sensor was calculated using equations described in Di Felice et al. [159] and in Minkina and Dudzik [207]. It is assumed that all crop plants are exposed to approximately the same atmospheric conditions [208]. For leaf and canopy temperature measurements the maximum distance between crop surface and the thermal camera sensor was set to 5 m, and for the temperature measurements acquired using the DJI Zenmuse XT2 dual camera, the altitude was no more than 40 m above the ground level, therefore, atmospheric correction was not necessary because

of low altitude, short time duration, and uniform weather conditions. It is found that atmospheric transmittance at 5 m distance is 0.986, and at 40 m distance is 0.953, which was calculated using equations presented in Di Felice et al. [159] with an assumed atmospheric temperature of 300 K and 50% humidity. The effect of distance variation on atmospheric transmission is presented in Figure D.1. It is observed that increasing the thermal camera distance from the crop surface decreases the atmospheric transmission.

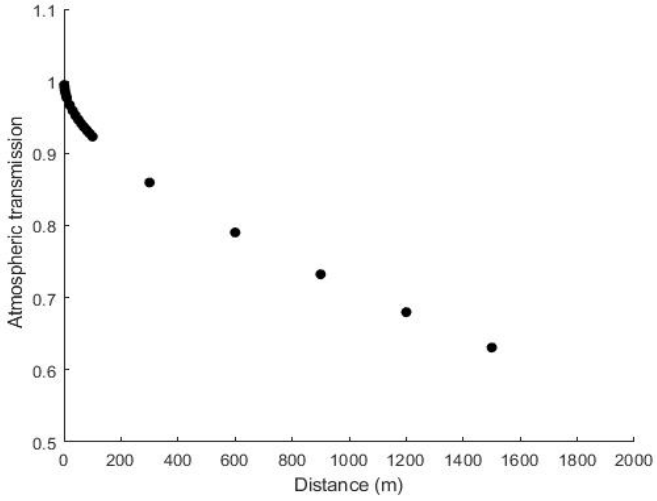

Figure D.1: Atmospheric transmission decreases with object to camera sensor distance increase.

D.2 Result and Discussions

Three flights were conducted each day for temperature data collection, including two reverse flights (back to back flights) at selected times (morning, noon and afternoon) to investigate crop temperature variation during a small time duration. It was observed that corn plants supplied with the highest rate of nitrogen (230 $kgN.ha^{-1}$) consistently

had the lowest surface temperature compared to other plots (Figure D.2). In addition, it was observed that plots supplied with the same rate of nitrogen ($28 kgN.ha^{-1}$) scattered throughout the field had a temperature difference up to 1 °C. The possible explanation is the existence of residual nitrogen in the soil from the previous years which cause nitrogen variation across plots supplied with the same amount of nitrogen, which is not detected during soil nitrate sampling due to limited samples collected from the whole field. The temperature variability for the same plot in two reverse flights was between 0.2-0.8°C. From the first row in the field corn plants supplied with high nitrogen rate (230 $kgN.ha^{-1}$) had consistently lower crop temperatures compared to corn supplied with lower nitrogen rate on different days in July and August 2019 for the second flight conducted around noon time (12 pm) as presented in Figure D.3. The error bars represent the error in the temperature measurements.

Variations in canopy average temperature was observed during different days conducted in July and August 2019, the temperature range for plants supplied with a high rate of nitrogen was from 14°C to 28°C. A significant temperature difference was observed between the two plots supplied with high and low nitrogen rates, respectively, in the three flights conducted per day as summarized in Table D.1. The error calculated is the standard error from three measurements points per nitrogen rate.

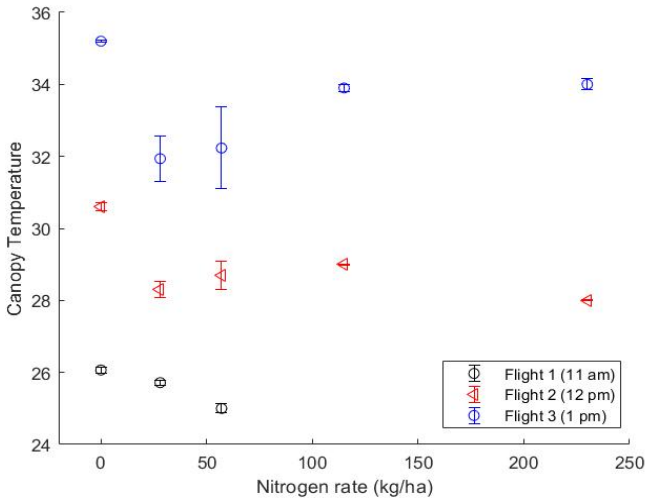

Figure D.2: Corn plants supplied with high nitrogen rate had lower temperatures compared to plants supplied with low nitrogen rate(data collected on July 18th, 2019)

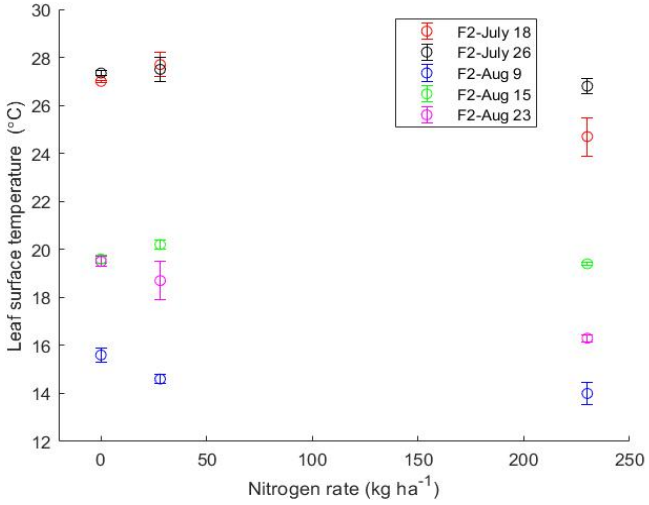

Figure D.3: Corn plants supplied with high nitrogen rate had consistently lower temperatures compared to plants supplied with low nitrogen rate on different days in 2019 for the second flight (F2) conducted around noon time.

Table D.1: The average surface temperature for two N extremes plots in three flights acquired on different days in 2019.

Date	Flight	T_{HighN}	T_{lowN}
18-Jul	at 11 am	25±0.13	26.07±0.09
	at 12 pm	28±0.01	30.6±0.12
	at 1pm	34±0.15	35.2±0.03
26-Jul	at 11 am	32.38±0.15	33.37±0.2
	at 12 pm	30.4±0.057	34.8±0.01
	at 2pm	29.6±0.5	29.97±0.06
9-Aug	at 11 am	19.57±0.057	19.89±0.7
	at 12:30 pm	14±0.45	15.64±0.3
	at 2pm	18.3±0.3	18.7±0.3
15-Aug	at 12 am	22.67±0.057	22.9±0.9
	at 1 pm	19.47±0.0578	19.6±0.17
	at 2pm	22±0.2	22.6±0.1
23-Aug	at 11 am	20±0.7	22.3±0.0577
	at 12 pm	22.2±0.1	25.23±0.057
	at 1pm	21.47±0.7	24.2±0.057

Crop temperature variation on Aug 15$^{\text{th}}$, 2019 over the same plot supplied with 230 $kgN.ha^{-1}$ nitrogen located in the first row (i.e., first plot in the field) at different times of the day is presented in Figure D.4. An average crop temperature of 20.8±1.2°C, 19.5±0.8°C, and 20.8±0.9°C with selected rectangular box of 19000 pixels for flights conducted at 12:00 pm, 1:00 pm, and 2:00 pm, respectively. An approximate average crop temperature difference of 1°C is observed across the three flights for the same plot at different times on Aug 15$^{\text{th}}$, 2019. A possible explanation of temperature variation over a short period of time $\pm 2hrs$ is the variation in the cloud cover, despite conditional sampling of uniform overcast days, which sequentially change the incoming solar radiation.

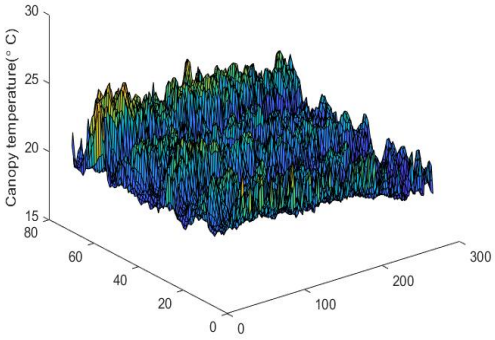

(a) at 12 pm

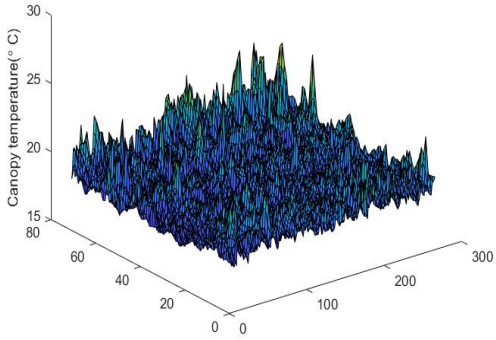

(b) at 1 pm

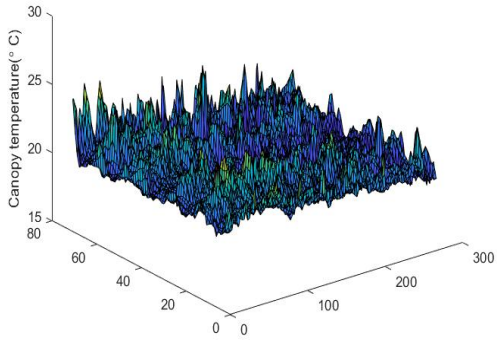

(c) at 2 pm

Figure D.4: Temperature variation of one selected plot supplied with a high rate of nitrogen at different times on Aug 15$^{\text{th}}$, 2019.

As a conclusion, for an accurate crop temperature data collection it is recommended to be conducted under the same atmospheric conditions and the same time of the day and more preferably around solar noon, for the maximum incoming solar radiation assumption, in order to be able to compare different plots and draw more solid conclusions regrading the relationship between crop surface temperature and crop stress. However, further experiments are required under different variable conditions to test and justify the two proposed hypotheses on a large scale area not only on selected plots within the field but also over a whole field scale.

Appendix E

Order of magnitude estimates for energy equation terms

This appendix describes order of magnitude estimates for energy related components described in the energy Equation 3.3.

E.1 Air expansion

Consider the 2 m high volume above ground shown for the system in Figure E.1. This system boundary volume by definition is fixed, however, as the air warms during the day it will expand forcing some air to leave the system carrying with it some energy. For an order of magnitude estimate of the energy loss by expanding air flow it can be assume that all the air exits in the vertical direction as shown in Figure E.1. For simplicity of calculation we can consider a 1 m^2 surface area as shown in Figure E.1b.

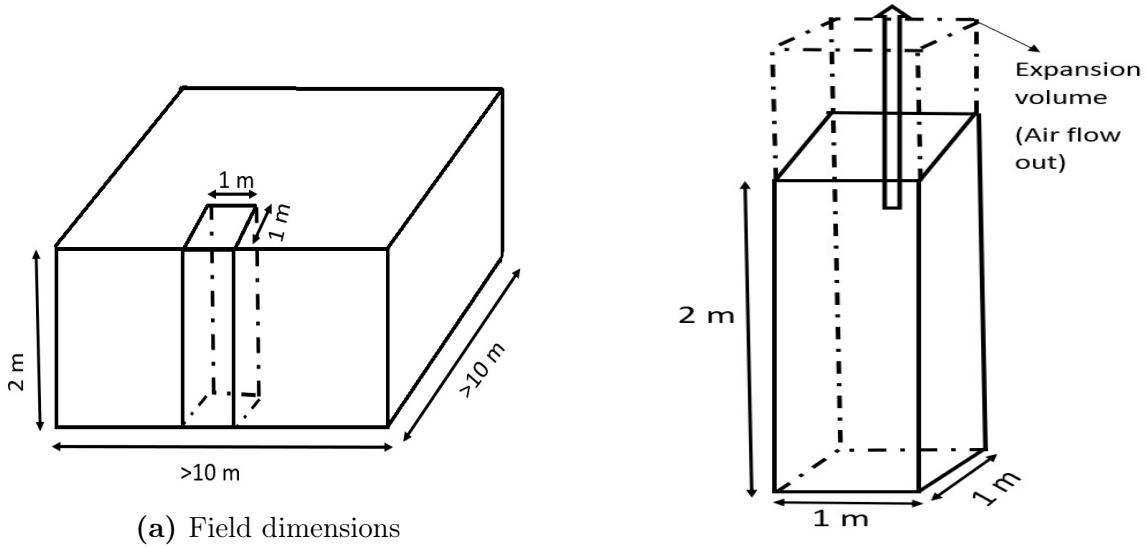

(a) Field dimensions

(b) Expansion volume, air flow out

Figure E.1: The air expansion model

For a conservative estimate of the energy flow out due to air expansion the entire volume will be considered to be filled with air. Now consider an initial volume of 2 m^3 of air (Figure E.1b) at 10 °C. If the pressure is taken as constant at P = 100 kPa, and the temperature increases by a conservative 20 °C resulting in an end temperature of 30 °C, then by the ideal gas law, the air density will decrease causing the air to expand resulting in 0.14 m^3 of air exiting the system due to air expansion.

$$\Delta V = V(30C) - V(10C) = \frac{T(30C)V(10C)}{T(10C)} - 2 = 2.14 - 2.00 = 0.14\ m^3 \qquad \text{(E.1)}$$

The energy transported outside the system is $(E_{out}) = m_{out}C_p\Delta T$, where the mass is calculated using an ideal gas law with R (individual gas constant) of 286.9 J/kgK for air,

as follows:

$$m_{out} = \frac{PV}{RT} = \frac{100000(0.14)}{286.9(293)} = 0.167 \text{ kg} \tag{E.2}$$

so the energy output from the system is $E_{out} = m_{out} C_p \Delta T$=(0.167 kg) (1.003 $kJ/kg.k$) (20°C) = 3.35 kJ, therefore, the energy output rate during a 4 hour period as the air heats from 10 °C to 30 °C is then given by

$$\text{E}_{\text{outrate}} = \frac{3.35kJ}{4hr \times \frac{60\,\text{min}}{1hr} \times \frac{60s}{1\,\text{min}}} = 0.00023\ kW \tag{E.3}$$

This $\dot{E}_{out}$ of 0.23 W is negligible compared to the observed mid-day radiation components of incoming solar radiation of 400-900 W/m^2, reflected radiation of 80-120 W/m^2, background radiation of 350-500 W/m^2, and emitted radiation of 400-700 W/m^2. These radiation values were measured using a net radiometer at the Elora field on clear sky conditions under different days in the summer of 2019.

E.2 Water expansion

Following the same method detailed in section E.1 used to estimate the contribution of air expansion to the energy balance (Equation 3.3), however, the contribution of water expansion is also negligible. For example, if the entire 2 m^3 volume shown in Figure E.1b is now assumed completely filled with water vapour at 100 kPa, and experiencing a temperature change from 10 °C to 30 °C, the ideal gas volume expansion remains the

same at $\Delta V = 0.14\ m^3$, with R (individual gas constant) of 461.4 J/kgK for water vapor, whereas m_{out}=0.104 kg, and with a C_p= 1.872 kJ/kgK, the energy output is

$$\dot{E}_{out} = \dot{m}_{out} C_p \Delta T = (0.104kg)(1.872kJ/kg.k)(20^{\mathrm{O}}C) = 3.89\ kJ \tag{E.4}$$

$$\mathrm{E}_{\mathrm{out\_rate}} = \frac{3.89kJ}{4hr \times \frac{60\,\mathrm{min}}{1hr} \times \frac{60s}{1\,\mathrm{min}}} = 0.00027\ kW \tag{E.5}$$

This $\dot{E}_{out}$ of 0.27 W is negligible compared to the observed mid-day radiation components.

E.3 Water transport due to transpiration

Different studies investigated how much water is output for a corn crop per day [138, 209, 132] and the maximum value is taken for water energy output calculation of 15100 liter per day per acre [132]. Assuming an output mass flow of 3.7 $L/day/m^2$ which is equivalent to $4.3 \times 10^{-5}\ kg/s$ [138]. In the transpiration process the water enters as a liquid and leave the plant surface as a water vapor, the change in enthalpy can be estimated as follows

$$\Delta h = h_{in} - h_{out} \tag{E.6}$$

$$\Delta h = c_{p_{liquid}}(T_{in} - T_{leaf}) + h_{fg}(T_{leaf}) + c_{p_{vapor}}(T_{leaf} - T_{out}) \tag{E.7}$$

Where h_{in}, h_{output} are the input and output enthalpy in and out of the system measured in kJ/kg. Assuming T_{in}=10 °C, T_{leaf}=25 °C, T_{out}=30 °C. Where $c_{p_{liquid}}$ is 4.18 kJ/kgK and $c_{p_{water\_vapor}}$ is 1.996 kJ/kgK, h_{fg} for water at 25 °C is 2442.3 kJ/kg, so Δh=2369.62 kJ/kg.

$$\dot{\mathrm{E}}_{\mathrm{net\_water\_out}} = \dot{m}_{out}\Delta h \tag{E.8}$$

The energy water output due to transpiration is 0.102 kW. $\dot{E}_{water\_out}$ of 102 W is significant.

E.4 Biomass output

The energy associated with biomass output before harvest is zero when temperature measurements were conducted. After harvest, there is an effect of biomass output on the total energy for a crop plant system. As an example, the corn cob and stalk has a high calorific energy of 17.72 $MJ.kg^{-1}$ and corn leaves have a calorific energy of 16.99 $MJ.kg^{-1}$ [210].

Assuming that 5 corn plants have a 6 kg biomass (given the biomass data collected from the greenhouse and field experiments), so per field plot area of 60 m^2 containing 600 corn plants over a growing season of 3 months, the total biomass per plot can be estimated as 720 kg. Multiplying the total biomass per plot area of 60 m^2 with specific energy, so the biomass energy output after harvest is 26 W.

$$720kg \times \frac{1}{60\ m^2} \times 17\ \frac{MJ}{kg} = 204\ \frac{MJ}{m^2} \tag{E.9}$$

$$\dot{E}_{biomass\_out} = 204\ \frac{MJ}{m^2} \times \frac{1}{3months} \times \frac{1month}{30days} \times \frac{1day}{24hrs} \times \frac{1hr}{3600s} = 26\ W \qquad \text{(E.10)}$$

This $\dot{E}_{biomass\_out}$ of 26 W is small compared to radiation components. The fraction of biomass output compared to the incoming solar radiation (assuming the maximum incoming radiation energy of 900 W/m^2 under clear sky conditions) is 3% ((26/900) $\times$ 100%).

In addition, there is no net energy gain or loss due to heat storage changes in the biomass because, on a daily basis, biomass energy stored in the morning and early afternoon will be returned to the air in the late afternoon and evening hours [211].

Appendix F

Order of magnitude estimates for exergy terms compared to the solar exergy

This appendix describes order of magnitude estimates for exergy related components compared to the solar exergy.

F.1 Solar exergy

As explained in Section 3.9, Model 1 from Kabelac [150] which assumes zero entropy production and finite area is used to determine the solar exergy.

$$\frac{X_{solar}}{\phi_{Solar}} = \left[1 - \frac{4}{3}\frac{T_{Surface}}{T_{Solar}} + \frac{1}{3}\frac{{T^4}_{Surface}}{{T^4}_{Solar}}\right] \tag{F.1}$$

Assuming a crop surface temperature, $T_{Surface}$, of 25 °C (298 K) and a solar temperature of 5762 K [93], the solar exergy ($\frac{X_{solar}}{\phi_{Solar}}$) then is given by

$$\frac{X_{solar}}{\phi_{Solar}} = \left[1 - \frac{4}{3}\frac{(298k)}{(5762k)} + \frac{1}{3}\frac{(298k)^4}{(5762k)^4}\right] = 0.931 \tag{F.2}$$

Where the incoming solar energy (ϕ_{Solar}), as measured using a net radiometer on different days in 2019 at the Elora field, is in the range of 400-900 W/m^2. Therefore, the solar exergy (X_{solar}) is in this range of

$$X_{Solar} = [400 - 900\ W/m^2] \times 0.931 = 370\ W/m^2\ to\ 838\ W/m^2 \tag{F.3}$$

By definition, the relative solar exergy is 1 as given by

$$\frac{X_{solar}}{X_{solar}} = 1 \tag{F.4}$$

F.2 Background exergy

The exergy associated with background radiation is estimated assuming a crop surface temperature, $T_{Surface}$, of 25 °C (298 K), and background temperatures of $T_{Background}$=1 °C (274 K) for clear sky conditions and $T_{Background}$ = 18 °C (291 K) for cloudy conditions [212]. The exergy of background radiation using Model 1 from Section 3.9 is given in the following equation

$$\frac{X_{Background}}{\phi_{Background}} = \left[1 - \frac{4}{3}\frac{T_{Surface}}{T_{Background}} + \frac{1}{3}\frac{T^4{}_{Surface}}{T^4{}_{Background}}\right] \tag{F.5}$$

For $T_{Background}$=1°C and 18°C, the background exergy ($\frac{X_{Background}}{\phi_{Background}}$) is given by

$$\begin{aligned}
&\rightarrow For\ T_{Background} = 1\ ^{\circ}C\ (274\ K)\\
&\tfrac{X_{Background}}{\phi_{Background}} = \left[1 - \tfrac{4}{3}\tfrac{(298k)}{(274K)} + \tfrac{1}{3}\tfrac{(298k)^4}{(274k)^4}\right] = 0.0163\\
&\rightarrow For\ T_{Background} = 18\ ^{\circ}C\ (291\ K)\\
&\tfrac{X_{Background}}{\phi_{Background}} = \left[1 - \tfrac{4}{3}\tfrac{(298K)}{(291k)} + \tfrac{1}{3}\tfrac{(298K)^4}{(291K)^4}\right] = 1.173 \times 10^{-3}
\end{aligned} \tag{F.6}$$

The background energy ($\phi_{Background}$), as measured using a net radiometer on different days in 2019 at the Elora field, is in the range of 350-500 W/m^2. Therefore, the background exergy ($X_{Background}$) for $T_{Background}$=1 °C and 18 °C is in this range of

$$\begin{aligned}
&\rightarrow For\ T_{background} = 1\ ^{\circ}C\ (274\ k)\\
&X_{Background} = [350 - 500\ W/m^2] \times 0.0163 = 5.7\ W/m^2\ to\ 8.2\ W/m^2\\
&\rightarrow For\ T_{background} = 18\ ^{\circ}C\ (291\ k)\\
&X_{Background} = [350 - 500\ W/m^2] \times 1.173 \times 10^{-3} = 0.4\ W/m^2\ to\ 0.6\ W/m^2
\end{aligned} \tag{F.7}$$

The relative background exergy ($\frac{X_{Background}}{X_{solar}}$) for $T_{Background}$=1°C and 18°C is as follows

$$
\begin{aligned}
&\rightarrow For\ T_{background} = 1\ ^{\circ}C\ (274\ k) \\
&\frac{X_{Background}}{X_{solar}} = \frac{[5.7-8.2\ W/m^2]}{[370-838\ W/m^2]} = \frac{6.95\ W/m^2}{604\ W/m^2} = 0.012 \\
&\rightarrow For\ T_{background} = 18\ ^{\circ}C\ (291\ k) \\
&\frac{X_{Background}}{X_{solar}} = \frac{[0.4-0.6\ W/m^2]}{[370-838\ W/m^2]} = \frac{0.5\ W/m^2}{604\ W/m^2} = 8.28 \times 10^{-4}
\end{aligned}
\tag{F.8}
$$

Therefore, the exergy contribution from background radiation is small (1.2 %) to negligible (0.0828 %).

F.3 Fertilizer input

The exergy associated with input fertilizer is calculated using the following assumptions: The average solar plus background flux in Elora, ON, Canada is 1325 W/m2 [213], $1m^2$ surface area, 3 months of growing season, 10 hours sunlight per day, and the fertilizer is Ammonium Nitrate. The total solar energy is calculated as follows

$$
Total solar energy = 1325W \times 3month \times \frac{30days}{month} \times \frac{10hr}{day} \times \frac{60\,\mathrm{min}}{1hr} \times \frac{60s}{1\,\mathrm{min}} = 4.29\ GJ \tag{F.9}
$$

The total fertilizer sprayed, assuming an optimum nitrogen rate of 150 $kgN.ha^{-1}$ over $1m^2$ surface area can be estimated of 0.015 kg

$$
150\frac{kg}{ha} \times \frac{1ha}{10^4 m^2} \times 1m^2 = 0.015\ kg \tag{F.10}
$$

The Gibbs free energy is 2.3 $GJ/tonne$ [214]. The total exergy associated with fertilizer is then

$$2.3\frac{GJ}{1ton} \times \frac{1ton}{1000kg} \times 0.015 = 0.0000345\ GJ \tag{F.11}$$

Comparing the Gibbs free energy (which is equal to a substance's chemical exergy) to the solar exergy yields

$$\frac{X_{Fertilizer}}{X_{Solar}} = \frac{0.0000345GJ}{4.29GJ} = 0.8 \times 10^{-5} \approx 0 \tag{F.12}$$

Therefore, the fertilizer exergy is negligible compared to the solar exergy.

F.4 Air expansion

Following the same example of air expansion discussed previously in Appendix E with the same assumptions of: 1 m^2 area, P_0 = 100 kPa, soil input temperature of T=10 °C, and the reference environment temperature of T_0=30 °C, the exergy of the air within the system boundaries (Figure 3.2) can be calculated as follows:

$$X_{Air\_expansion} = m_{air\_out} \times [(u_{in} - u_0) + P_0(v - v_0) - T_0(S_{in} - S_0)] \tag{F.13}$$

Assuming an ideal gas, the internal energy and entropy terms in Equation F.13 can be expanded as follows:

$$X_{Air\_expansion} = m_{air\_out} \times \left[C_v(T - T_0) + P_0(v - v_0) - T_0 \left(C_v \ln\left(\frac{T}{T_0}\right) - R \ln\left(\frac{V_0}{V}\right)\right)\right] \tag{F.14}$$

Where $X_{Air\_expansion}$ is the exergy associated with air expansion, u_{in} is the input internal energy and s_{in} is the input entropy at the input soil temperature of T=10 °C. u_0 is the internal energy and s_0 is the entropy at the reference environment temperature T_0=30 °C. P_0 is the assumed environment pressure, v is the specific volume at T=10 °C and v_0 is the specific volume at the environment temperature T_0=30 °C.

For Equation F.14, $P_0 = 100\ kPa$, $V_0 = 2\ m^3$, V(from Appendix E calculations)=2.14 m^3, C_v for the air is 0.718 $kJ/kg.K$, T=10 °C, T_0=30 °C, and R for the air=0.2870 $kJ/kg.K$. The mass of air that exits the system due to expansion was calculated in Appendix E to be m_{air_out}=0.167 kg, and also recall the volume change of air exiting the system is 0.14 m^3, therefore,

$$X_{Air\_expansion} = 0.167\ kg \times \left[0.718\ \frac{kJ}{kg.k} \times (283\ k - 303\ k) + 100\ kPa \times (\frac{0.14}{2.46}\ \frac{m^3}{kg})\right]$$
$$-0.167\ kg \times 303\ k \left[\left(0.718\ \frac{kJ}{kg.k} \times \ln\left(\frac{283\ k}{303\ k}\right) - 0.287\ \frac{kJ}{kg.k} \times \ln\left(\frac{2\ m^3}{2.14\ m^3}\right)\right)\right] = 0.05\ kJ \tag{F.15}$$

Then, the exergy associated with air expansion during a 4 hour period is

$$X_{Air\_expansion} = \frac{0.05\ kJ}{4\ hr \times 3600\frac{s}{hr}} = 3.5 \times 10^{-6}\ kW = 3.5 \times 10^{-3}\ W \tag{F.16}$$

Therefore, the relative exergy associated with air expansion ($\frac{X_{Air\_expansion}}{X_{solar}}$) is

$$\frac{X_{Air\_expansion}}{X_{solar}} = \frac{0.0035\ W/m^2}{604\ W/m^2} = 5.8 \times 10^{-6} \approx 0 \tag{F.17}$$

This is negligible compared to the solar exergy.

F.5 Water expansion

Following the example of water expansion discussed previously in Appendix E with the same assumptions of: 1 m^2 area, P_0 = 100 kPa, soil input temperature of T=10 °C, and the reference environment temperature of T_0=30 °C, the total flow exergy per kilogram of air and water vapor can be calculated as described in Bejan [141], which is given by

$$X_{water\_vapor\_mixture} = (C_{p,a} + wC_{p,v})\, T_0 \left(\frac{T}{T_0} - 1 - \ln\frac{T}{T_0}\right) + (1+\tilde{w})\, R_a T_0 \ln\frac{P}{P_0} + R_a T_0 \left(\ln\frac{1+\tilde{w}_0}{1+\tilde{w}} + \tilde{w}\ln\frac{\tilde{w}}{\tilde{w}_0}\frac{1+\tilde{w}_0}{1+\tilde{w}}\right) \tag{F.18}$$

Now, $X_{water\_vapor\_mixture}$ is the exergy associated with water expansion, $C_{p,a}$ is the specific heat capacity of the air of 1.003 $kJ/kg.K$, w is the specific humidity ($kg_{water}kg_{air}^{-1}$), w_0 is the specific humidity at the reference environment conditions ($kg_{water}kg_{air}^{-1}$), $C_{p,v}$ is the specific heat capacity of the water vapor of 1.872 $kJ/kg.K$, T_0 is the assumed environment temperature of 30°C (303 K), T is the assumed water input temperature of 10 °C (283 K),

$\tilde{w}$ is the mole fraction ratio ($kmol_{water}kmol_{air}^{-1}$), P_0 is the environment pressure of 100 kPa, and R_a is the gas constant for air of 0.2871 $kJ/kg.K$

The proportionality between specific humidity ratio (w) and specific humidity ratio on a mole basis ($\tilde{w}$) is given by [215]

$$\tilde{w} = 1.608w \tag{F.19}$$

Where the specific humidity ratio is given by [216]

$$w = 0.622 \times \frac{p_v}{P_{atm} - P_v},\ p_v = \phi \times P_{sat@dbT} \tag{F.20}$$

And P_{atm} is the atmospheric pressure, p_v is the partial pressure, and ϕ is the relative humidity which is assumed to be 60%. Therefore, using Equation F.20, w at 10 °C is 4.62×10^{-3} and w_0 at the environment temperature of 30 °C is 0.0163.

In addition, Equation F.18, can be re-written as follows

$$\begin{aligned} X_{water\_vapor\_mixture} = (C_{p,a} + wC_{p,v})\, T_0 \left(\frac{T}{T_0} - 1 - \ln\frac{T}{T_0}\right) + (1 + 1.608w)\, R_a T_0 \ln\frac{P}{P_0} \\ + R_a T_0 \left((1 + 1.608w) \ln\left[\frac{1 + 1.608w_0}{1 + 1.608w}\right] + 1.608w \ln\frac{w}{w_0}\right) \end{aligned} \tag{F.21}$$

After using all the values discussed above the $X_{water\_vapor\_mixture}$ is given by

$$X_{water\_vapor\_mixture} = \left(1.003\frac{kJ}{kg.K} + (4.62\times10^{-3})\times 1.872\frac{kJ}{kg.K}\right)\times(303K)\times\left(\frac{283K}{303K} - 1 - \ln\frac{283K}{303K}\right)$$
$$+\left[\left(1+1.608\times(4.62\times10^{-3})\right)\right]\times(0.287\frac{kJ}{kg.K})\times(303K)\times\ln[1]$$
$$+(0.287\frac{kJ}{kg.K})\times(303K)\times\left(\left[(1+1.608\times(4.62\times10^{-3}))\right]\times\ln\left[\frac{(1+1.608\times(0.0163))}{(1+1.608\times(4.62\times10^{-3}))}\right]\right.$$
$$\left.+1.608\times(4.62\times10^{-3})\times\ln\left[\frac{4.62\times10^{-3}}{0.0163}\right]\right. = 1.486\ \frac{kJ}{kg} \quad \text{(F.22)}$$

With $X_{water\_vapor\_mixture}$ calculated to be 1.49 kJ/kg, and with the mass of water that exits the system due to expansion being m_{water_out}= 0.104 kg as determined in Appendix E, then the exergy associated with water expansion,$X_{Water\_expansion}$, is given by

$$X_{Water\_expansion} = m_{Water\_out}\times X_{Water\_expansion} = 0.104\ kg\times 1.49\ \frac{kJ}{kg} = 0.154\ kJ \quad \text{(F.23)}$$

Correspondingly, the exergy associated with water expansion during a 4 hour period is

$$\dot{X}_{Water\_expansion} = \frac{0.154\ kJ}{4\ hr\times 3600\ \frac{s}{hr}} = 0.011\ W \quad \text{(F.24)}$$

Therefore, the relative exergy associated with water expansion ($\frac{X_{Water\_expansion}}{X_{solar}}$) is

$$\frac{X_{Water\_expansion}}{X_{solar}} = \frac{0.011\ W/m^2}{604\ W/m^2} = 1.77\times10^{-5} \approx 0 \quad \text{(F.25)}$$

This is negligible compared to the solar exergy.

F.6 Water transport due to transpiration

Assuming steady state flow, the water transpired is equal to the water flowing in from the ground, and assuming an environment temperature,T_0, of 30 °C, and input temperature, T_{Soil_in}, of 10 °C, the exergy associated with water transpiration then is given by

$$\dot{X}_{water\_transpiration} = \dot{m}_{out} \times X_{water\_transpiration} = \dot{m}_{out} \times [(h_{in} - h_{out}) - T_0(S_{in} - S_{out})] \quad \text{(F.26)}$$

Where $X_{water\_transpiration}$ is the exergy associated with water transpiration, h_{in} is the input enthalpy and s_{in} is the input entropy at the input soil temperature of T_{Soil_in}=10 °C, and h_0 is the enthalpy and s_0 is the entropy at the reference environment temperature T_0=30 °C. The specific enthalpy (h) and entropy (s) for water for the reference environment temperature,T_0, of 30 °C and soil temperature, T_{Soil_in}, of 10 °C are as described in detail in Bejan [141]:

$$\begin{aligned} h_{in} &= h_f(T) + (P - P_{sat}(T))\, v_f(T) \\ h_{out} &= h_g(T_0) \\ S_{in} &= S_f(T) \\ S_{out} &= S_g(T_0) - R_v \left(\ln \tfrac{P_0}{P_{sat}(T_0)}\right) \end{aligned} \quad \text{(F.27)}$$

Using the thermodynamics tables for saturated water of T_0= 30 °C, and T_{Soil_in}= 10 °C,

where the subscription in front of enthalpy (h) and entropy (s) of f and g denotes to fluid and gas status. Therefore, $h_{in} = 42.12\ kJ/kg$, $S_{in} = 0.1511\ kJ/kg.K$, $h_{out} = 2555.6\ kJ/kg$, and $S_{out} = 7.1332\ kJ/kg.K$. The environment temperature T_0 is 303 K. The water mass output flow of $4.3 \times 10^{-5}\ kg/s$ [138]. Therefore, the exergy associated with water transpiration ($\dot{X}_{water\_transpiration}$) is

$$\dot{X}_{water\_transpiration} = \dot{m}_{out} \times X_{water\_transpiration} = 4.3 \times 10^{-5}\ \frac{kg}{s} \times \left(42.12\ \frac{kJ}{kg} - 2555.6\ \frac{kJ}{kg}\right) - (303\ K)\left(0.1511\ \frac{kJ}{kg.K} - 7.1332\ \frac{kJ}{kg.K}\right) = 0.0171\ kW = 17.1\ W \quad \text{(F.28)}$$

The relative exergy associated with water expansion ($\frac{X_{Water\_transpiration}}{X_{solar}}$) is then given by

$$\frac{X_{Water\_transpiration}}{X_{solar}} = \frac{17\ W/m^2}{604\ W/m^2} = 0.028 \quad \text{(F.29)}$$

Therefore, the exergy contribution from water transpiration is small (2.8 %).